UNIVERSITÉ DE NANTES

Chimie Et Interdisciplinarité Synthèse, Analyse, Modélisation
UMR CNRS 6230
UNIVERSITÉ DE NANTES

UNIVERSITÉ DE NANTES
FACULTÉ DES SCIENCES ET DES TECHNIQUES

ÉCOLE DOCTORALE • 3MPL

Année 2013

N° attribué par la bibliothèque

Methodological developments in ultrafast 2D NMR for metabolic studies

THÈSE DE DOCTORAT

Discipline : Chimie

Spécialité : Chimie analytique

Présentée
et soutenue publiquement par

Meerakhan PATHAN

Le 12 décembre 2013, devant le jury ci-dessous

Rapporteurs	M. Jean-Marie BONNY, *Directeur de recherche • INRA, Clermont-Ferrand*
	M. Denis MERLET, *professeur • Université Paris-Sud*
Examinateur	M. Stefano CALDARELLI, *professeur • Aix-Marseille Université*
Directeur de thèse	M. Serge AKOKA, *professeur • Université de Nantes*
Co-directeur de thèse	M. Patrick GIRAUDEAU, *maître de conférences • Université de Nantes*

With the blessings of "HAZARAT KHWAJA SYED SHAH ARIFULLAH HUSSAIN" (Asthana-e-Magdoom'ullahi Dargah, Kadapa, India).

First and foremost I would like to thank and express my heartfelt gratitude to the Director of the lab ***Dr. Bruno Bujoli*** *for providing me the opportunity to complete my PhD thesis within EBSI team (Elucidation de Biosynthèse par Spectrométries Isotopiques), at the laboratory CEISAM (Chimie Et Interdisciplinarité : Synthèse, Analyse, Modélisation, UMR-CNRS 6230), University de Nantes.*

I must say that finding the right words to thank both my supervisors is the hardest task in this thesis. ***Prof. Serge Akoka*** *is one of the most interesting and lovely characters that one would ever meet; he always kept his door open to me, any time for the last three years with no complaints. His expertise in NMR as well as his advanced knowledge in spatial encoding has made this work possible. My sincerest and deepest thanks go to him for his endless support during these years of research.*

I am in great debt to ***Dr. Patrick Giraudeau****, my co-supervisor, who made me love NMR applying his unique self-motivating technique. He has been an inspirational role model for me and I truly appreciate his continuous support, unflinching encouragement and invaluable guidance that have helped me to accomplish successfully my research work. Through the years his enthusiasm and sheer passion towards research has left on me a deep impression, have inspired me to see things positively and gave me confidence to trust my abilities. I am deeply indebted to him and hope that I will in turn pass on the research values and dreams that he has given me.*

I would also extend my humble gratitude to ***Prof. Denis Merlet*** *and* ***Dr. Jean-Marie Bonny*** *for considering my request to review my thesis work. Thanks are also due to my examiner* ***Prof. Stefano Caldarelli*** *for accepting to be a member of the jury.*

I would also like to express my sincere thanks to ***Dr. Richard Robins****, and* ***Prof. Gérald Remaud*** *for their worthy advice and helpful suggestions. I appreciate their ever ready helping attitude and also the knowledge that they imparted over the scientific discussions which always motivated me as a researcher.*

My gratitude extends to, ***Dr. Illa Tea*** *and* ***Benoît Charrier****, who have been very closely associated to my research work.*

My sincerest thanks go to ***Dr. Estelle Martineau****, for her supportive encouragements, and constant co-operation. I gratefully acknowledge* ***Dr. Manoj Nimbalkar*** *for providing fantastic four pulses.*

I would also like to thank my fellow labmates ***Dr. Evelyne Baguet****,* ***Dr. François Kouamé Bi-Koffi, Kevin Bayle, Didier Diomandé Gbè Gondo, Maxime Julien, Adrien Le Guennec,***

Renaud Boisseau, *and* ***Laetitia Rouger*** *for their valuable support and their skills in spreading happiness and fun during the days I have spent in the lab. I am also thankful to* ***Dr. Virginie Silvestre*** *NMR instrumentation engineer and,* ***Denis Loquet*** *Lab research assistant, for their co-operative assistance in the lab.*

I am indebted to ***Johann Hendrickx****,* ***Dr. David Teze, Swapnil Mahajan*** *and* ***Sharat*** *for their generous friendship and ever sustaining encouragement during the completion of my thesis.*

Finally, I wish to express my love and deepest gratitude to all my family members. I would particularly like to thank my parents, ***Ammi*** *and* ***Baba*** *for always motivating and inspiring me to continue, even in the most difficult times I have gone through. They always had the confidence and faith in me and completely trusted my abilities. Many thanks are going to my brothers* ***Yousafkhan*** *and* ***Masthankhan****, for their lovely encouragements and supports. Wholehearted thanks to my Wife* ***Dr. Nusrat Ali*** *who has been very encouraging and supportive through the completion of my thesis.*

Above all, I would give my highest gratitude to our ***Almighty Allah*** *for being a constant strength during the weak times, and for surrounding me with such great people, who never failed to help me in all my endeavors.*

Thank you all for everything!!

Meerakhan Pathan

NOTATIONS AND ABBREVIATIONS

O_f^{π} ; $O_f^{\pi/2}$	Final frequencies of π and π/2 chirp pulses
O_i^{π} ; $O_i^{\pi/2}$	Initial frequencies of π and π/2 chirp pulses
γ	Gyromagnetic ratio
$\Delta\nu^{1/2}$	Half-height peak width in the ultrafast dimension
Ω_1	Precession frequency in the rotating frame
ΔO	Chirp pulse band width
Δt	Dwell time
1D, 2D, nD NMR	One, two, multi-dimensional NMR
BEST	Band-Selective Excitation Short-Transient
C	Spatial encoding Constant
COSY	COrrelation SpectroscopY
CPMG	Carr–Purcell–Meiboom–Gill
CT- COSY	Constant–time COrrelation SpectroscopY
D	Diffusion coefficient
DNP	Dynamic Nuclear Polarisation
DQF-COSY	Double Quantum Filtered COrrelation SpectroscopY
EPI	Echo-Planar Imaging
EPSI	Echo-Planar Spectroscopic Imaging
fb	Receiver band width
FID	Free Induction Decay
FMQ	Fast Metabolite Quantification
FT	Fourier Transformation

G_a	Amplitude of acquisition gradient
G_e	Amplitude of excitation gradient
GFT	G-matrix Fourier Transform
HMBC	Hetero-nuclear Multiple Bond Correlation
HMQC	Hetero-nuclear Multiple Quantum Coherence
HSQC	Hetero-nuclear Single Quantum Correlation
INADEQUATE	Incredible Natural Abundance Double Quantum Transfer Experiment
INEPT	Insensitive Nuclei Enhanced by Polarization Transfer
k	Wave number
L	Length of the radio frequency coil
LP	Linear Prediction
MER	Maximum Entropy Reconstruction
MLEV	Malcom LEVitt's composite pulse decoupling sequence
N_1	Number of t_1 values in the F_1 dimension
nOe	Nuclear Overhauser effect
NS	Number of Scans
NUS	Non-Uniform Sampling
Q-HSQC	Quantitative HSQC
qNMR	Quantitative NMR
Q-OCCAHSQC	Quantitative, Offset-Compensated, CPMG-Adjusted HSQC
RD	Reduced Dimension
rf	radio frequency
RSD	Relative Standard Deviation
SMART NMR	Small Recovery Time NMR
SNR	Signal–to-Noise Ratio

SOFAST	Selective Optimized-Flip-Angle Short-Transient
SW_1	Spectral width in the F_1 dimension
SW_2	Spectral width in the F_2 dimension
t_1	Evolution period
T_1	Longitudinal relaxation time
T_2	Transverse relaxation
T_a	Duration of acquisition gradient
T_d	Number of complex points in the ultrafast dimension
T_e	Time of Spatial encoding
TOCSY	Total COrrelation SpectroscopY
TPPI	Time Proportional Phase Incrementation
TR	Repetition Time
ufJCOSY	UltraFast J-resolved COSY
ZQC	Zero Quantum Coherence
$\delta^{\pi/2}$; δ^{π}	Duration of $\pi/2$ and π chirp pulses

CONTENTS

INTRODUCTION

Chimie Et Interdisciplinarité
Synthèse, Analyse,
Modélisation
CEISAM
UMR CNRS 6230
UNIVERSITÉ DE NANTES

Introduction

Nuclear magnetic resonance (NMR) is a highly accomplished spectroscopic technique, which is extensively used for its quantitative potentialities in a variety of application in a large range of disciplines, such as pharmaceutical analysis [1, 2], metabolic studies [3-5] or the authentication of natural products [6-8]. ^{1}H NMR is a versatile tool to provide quantitative information for small molecules or simple mixtures of low molecular weight substances. However, this technique is limited in the case of complex molecules due to the peak overlapping. Quantitative ^{13}C NMR [9] is an interesting alternative, as it provides a better discrimination of resonances due to its much larger chemical shift range. However, its use in metabolomics is generally limited to ^{13}C-labeled metabolites [10] because of its inherent low sensitivity. Therefore, in order to address this limitation, it is important to spread out to higher dimensions. In the last ten years an exponential increase of quantitative approaches have been perceived based on two-dimensional (2D) NMR for solving the overlap problem inherent to one-dimensional (1D) spectroscopy, mainly for mixture analysis [11-13]. However, the use of 2D NMR for quantitative purposes is far from being trivial, not only because of the associated experiment time, but also due to its subsequent high sensitivity to hardware instabilities. The latter highly affects the analytical performance of 2D experiments (repeatability, linearity), consequently altering the accuracy and precision of quantitative analysis. Recent papers have described the development and optimization of 2D NMR experiments for quantitative analysis of metabolic samples [12, 14-16]. Reducing the experiment duration appears as indispensable to reach a high quantitative performance. Therefore, in order to drastically reduce the duration of 2D NMR experiments, the NMR community has developed a number of methodologies, which are different from the classical parametric incrementation scheme of 2D NMR. Ultrafast (uf) 2D NMR is a very promising methodology enabling the acquisition of 2D spectra in a single scan. The analytical performances of uf 2D NMR have highly increased in the last few years [17-19], and the potentialities of ultrafast 2D NMR for precise and accurate quantitative analysis have been demonstrated [17]. The ambition of my project is to develop a complete methodology to set ultrafast 2D-NMR as a standard tool for fast and precise quantitative analysis of complex metabolic mixtures.

In the introductory Part A, the quantitative applications of 1D, 2D NMR and their disadvantages are reviewed. A special attention is paid towards the metabolic mixtures. This part also provides

an overview of the current fast NMR techniques. In addition we focus on ultrafast NMR and its recent developments.

In Part B, we discuss about the development of practical tools to run the ultrafast experiments and for the implementation on spectrometers. We demonstrate the efficiency of this tool with different samples by recording ufCOSY and ufHSQC spectra.

Part C deals with the quantitative applications of ufNMR. In order to compare with its conventional counterpart in terms of sensitivity, we introduce a "Multi-Scan-Single-Shot" (M3S) approach. Its analytical performance is evaluated by applying it to breast cancer cell extracts. In addition to this we introduce the M3S approach in ufHSQC and discussed different strategies for improving its performance.

Part D portrays the measurement of site specific ^{13}C-enrichment in fluxomics. We present two novel techniques called ultrafast hetero-nuclear *J*-resolved and ultrafast *J*-resolved COSY for these studies. These methods are applied to the measurement of ^{13}C-enrichments on a biomass hydrolysate obtained from *E. coli* cells.

To conclude, Part E briefly summarizes the findings of the research described in this thesis, followed by some perspectives on future research.

Part A

LITERATURE REVIEW

Chimie Et Interdisciplinarité
Synthèse, Analyse,
Modélisation
CEISAM
UMR CNRS 6230
UNIVERSITÉ DE NANTES

1. Quantitative NMR

NMR is a powerful, non-destructive technique that gives a comprehensive structural and conformational analysis of simple and complex molecules. Since its invention, NMR spectroscopy has been used routinely as a qualitative technique. It offers several advantages when compared to other analytical techniques: it can provide selectivity without separation, it is independent of analyte polarity, and does not require sample derivatization prior to analysis which makes it a non-destructive technique. Theoretically, the peak intensity of NMR signal accurately reflects the molar ratio of the nuclei, making this technique conceptually simple for the quantification. Based on this, the first quantification measurements were performed in 1963 by Jungnickel and Forbes [20] and Hollis [21]. Since then, various articles have been reported demonstrating the potential of qNMR [2, 22-24].

1.1 1D qNMR

Nowadays ^{1}H-qNMR is a well-established technique in many domains such as pharmaceutical analysis [1], natural products [6], *in vivo* spectroscopy [25], metabolomics [3] and plants studies [26]. Most of the quantitative studies are performed on ^{1}H due to its high frequency and sensitivity, relatively short spin lattice relaxation times, no nOe (nuclear Overhauser effect) and nearly 100% natural abundance and low gyromagnetic ratio. Quantitative ^{13}C NMR is less sensitive due to the low natural abundance. In spite of this, quantitative ^{13}C NMR has been widely described [27-29] and applied in a variety of domains from food science [30-32] to the isotopic analysis of natural or synthetic molecules [9, 33, 34]. Apart from this, quantitative applications of other nuclei have also been reported such as ^{31}P [35],^{15}N [36], ^{17}O [37] and ^{19}F [38] NMR. Moreover hetero-nuclei exhibit high potentialities for quantification owing to the larger spectral widths which offer a high degree of discrimination between the peaks.

^{13}C, ^{15}N and ^{17}O NMR are inherently less sensitive than ^{1}H, ^{31}P and ^{19}F due to their low natural abundance. To overcome this drawback, either more concentrated samples are needed or the experimental time needs to be extended. In case of metabolic mixtures, since it is very difficult to get such a high concentration of sample, long experiments are run to get a good sensitivity. Obviously, with such long experimental times quantitative measurements are not practical for

routine qNMR applications. However, the experimental time can be decreased by using paramagnetic agents [9] or by employing time-shortening acquisition strategies [39] or introducing polarisation-transfer [40]. Nevertheless, with the recent introduction of higher magnetic field and cryogenically cooled probes, the issue of sensitivity is of less concern.

1.2 Limitations of 1D NMR

1D NMR is a well-established platform as a quantitative tool. However, this technique still suffers from several limitations. In the case of complex mixtures such as metabolic mixtures, quantification and assignment are made difficult by the high degree of spectral overlap. Discrimination is difficult even at a high magnetic field, mainly due to two major reasons. Firstly, the metabolic mixtures contain a high number of similar metabolites; therefore they give peaks nearly at the same positions. Another reason is the high number of metabolites generally present in the biological sample. This is well illustrated in Figure 1A on a model metabolic mixture. In this ^{1}H spectrum of a metabolic mixture resonances are overlapped. In such type of spectrum it is difficult to precisely assign the peaks and measure their area.

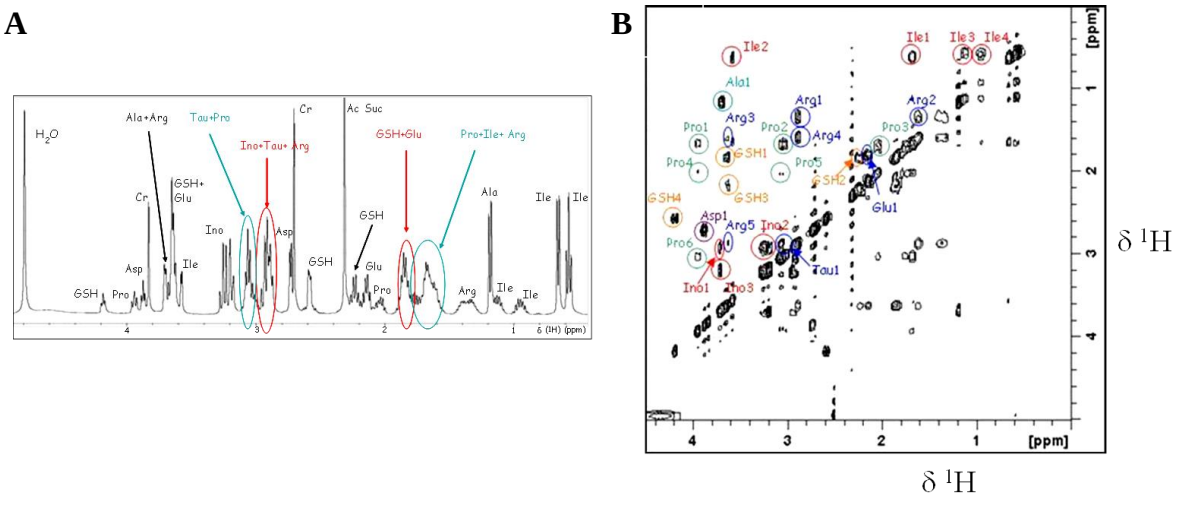

Figure 1: 1D ^{1}H (A) and 2D TOCSY (B) spectra of a model metabolic mixture, recorded at 298 K on a 400 MHz spectrometer [41].

1.3 Why quantitative 2D NMR?

2D NMR appears as an attractive solution to the problems of overlapping signals in quantitative 1D NMR based quantitative measurements, because it allows a better discrimination of resonances by spreading them in two orthogonal dimensions [11, 42]. It is clearly explained in Figure 1B. On the 1D spectrum of the model metabolic mixture it is very difficult to assign the peaks due to the overlap, whereas on the 2D TOCSY spectrum peaks are well discriminated in two dimensions and all are easily assigned. Figure 2 highlights the potentiality of quantitative 2D NMR in two different cases. Figure 2A shows the 2D DQF-COSY spectrum of a model mixture of tropine and nortropine, two tropane alkaloids that are members of a group of compounds with important pharmaceutical activity. The 1D spectra of these two compounds present a large degree of overlap, while the resonances arising from tropine and nortropine are clearly separated on the homo-nuclear 2D spectrum The mixtures of metabolites are another example, as illustrated in Figure 2B. The 2D HSQC spectrum provides a good discrimination between these resonances, thus avoiding overlap.

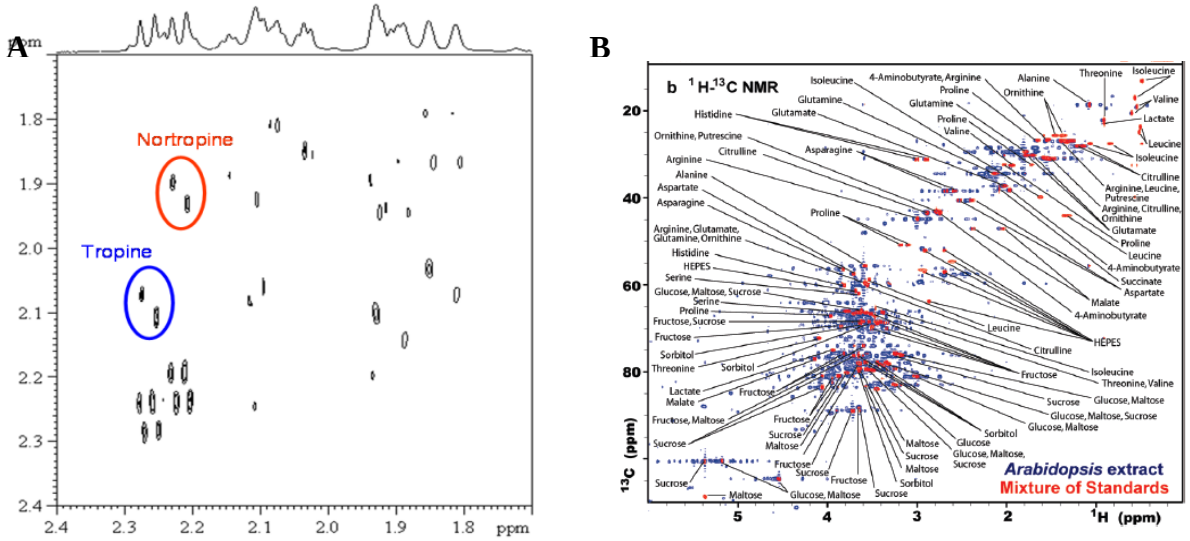

Figure 2: 2D DQF-COSY spectrum (A) of an equimolar mixture of tropine and nortropine recorded in 12 min. Only the positive components are plotted [43]. 2D 1H−13C HSQC NMR spectra (B) of a synthetic metabolic mixture (red) overlaid onto a spectrum of aqueous whole-plant extract from A.thaliana (blue) recorded in 12 minutes [15]. These examples point out the limitations of 1D NMR and the potential of 2D NMR for quantitative analysis.

1.4 Challenges of 2D qNMR

In 1D NMR spectroscopy, the peak intensity is directly proportional to the concentration of the metabolites. In 2D NMR cross peak intensities are affected by various factors. Firstly, 2D NMR sequences are always multi-pulse and therefore much more sensitive to pulse imperfections, which is contrary to the single-pulse sequence commonly used in quantitative 1D NMR. These pulse imperfections affect precision. However, they can be reduced by introducing composite [44-47] or adiabatic pulses [48-51] in place of hard pulses. Prior reports on 1D and 2D proved this by introducing such pulses in multi-pulse experiments which improved the quantitative performance [16, 40, 52-54].

In addition to the pulse imperfections many other factors affect the peak volumes, such as the relaxation times, homo or hetero-nuclear couplings etc [11, 53]. These aspects should be taken into account when considering using 2D NMR for quantitative analysis.

There are mainly two different approaches proposed to take these factors into account and obtain reliable quantitative results. The first one is the measure the peak volumes and then correct them by a correlation factor [42]. This correlation factor depends on relaxation, *J*-couplings and mixing time. This approach requires measuring all coupling constants and relaxation time with a high precision which again leads to long experimental durations. Moreover it is probably an utopia in the case of biological samples. The second approach is based on calibration curves. It consists in recording spectra of model mixtures at different concentrations and plotting the peak volumes versus the concentrations for each peak of interest [15, 43, 55-57]. These plots can then be used for measuring unknown concentrations. In addition to this, a few more approaches are proposed for quantification by using 2D NMR [58, 59]. However all these experiments lead to long experimental durations.

1.5 Principle of 2D NMR

The concept of two-dimensional NMR (2D NMR) was first proposed by the Belgian physicist J. Jeener in 1971 [60]. However it was experimentally implemented by R.R.Ernst and his co-workers [61-63]. The pulse sequence of a 2D NMR experiment in general may be divided into the following blocks: preparation –evolution (t_1) – mixing – detection (t_2) as described in Figure 3. The trick of 2D NMR spectroscopy is that a second time variable, the evolution time t_l, is

introduced after preparation. It is followed by a mixing period, which makes it possible to exchange information between spins.

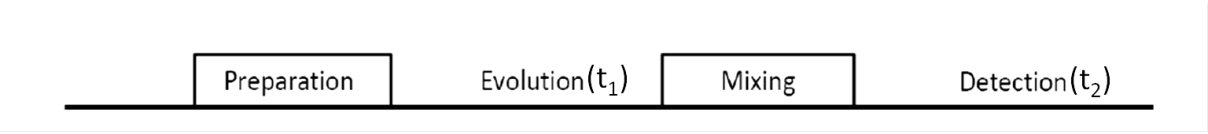

Figure 3 : Schematic representation of 2D NMR principle

The detection period corresponds exactly to the one for 1D NMR spectroscopy. The time t_2 provides, after Fourier transformation, the Ω_2 frequency axis of a 2D NMR spectrum. The evolution time t_l is made stepwise longer, i.e. incremented, in analogy to the detection time t_l. For each t_l increment a separate FID is detected in t_2. This process is repeated N_1 times until the desired resolution is obtained. A signal is therefore obtained which is a function of two time variables, t_l and t_2: S (t_1, t_2). A series of Ω_2 spectra is then obtained upon Fourier transformation of each of the FIDs. They differ from one another in the intensities and/or phases of the individual signals, according to the different t_1 increments. A second Fourier transformation over t_1 "orthogonal" to the Ω_2 dimension, results in a spectrum as a function of two frequencies (Ω_2 horizontal, $\Omega_1$vertical).

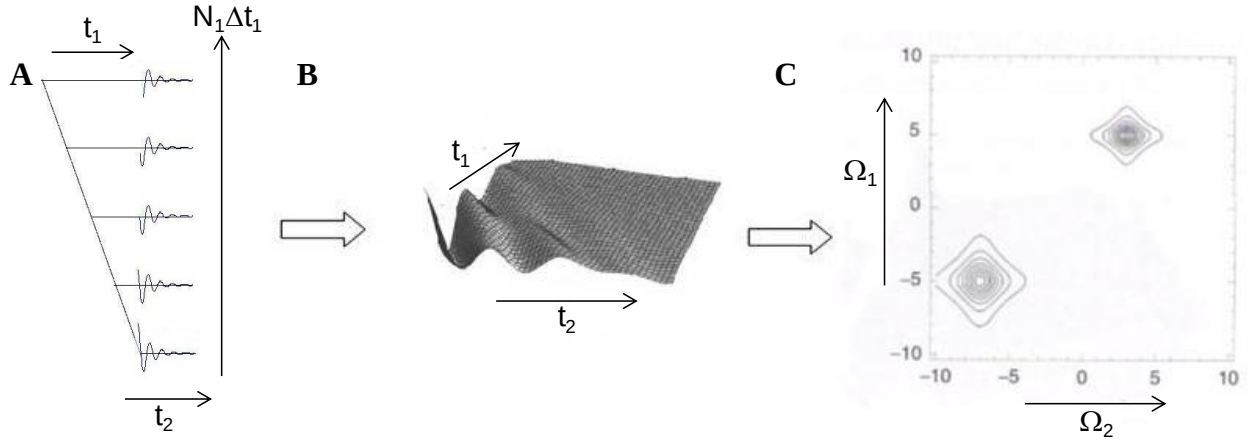

Figure 4: Construction of a 2D NMR experiment (A), FID representation in 2D Matrix (B), and 2D spectrum after Fourier Transformation (C).

The principles of 2D NMR spectroscopy are demonstrated in Figure 4. The acquisition of N transients is necessary to obtain a 2D-FID with $N = N_1 \cdot NS$. Here, N_1 is the number of t_1 values in the F_1 dimension and NS is the number of transients accumulated in order to increase the SNR of each 1D-FID and to perform the phase cycling. The experiment duration (T_{exp}) is given by

$$T_{exp} = N_1 \times NS \times TR$$

Where TR is the repetition time, i.e. the interval between two consecutive transient. TR is set as typically 5 times the highest longitudinal relaxation time T_1.

1.6 Previous Work on 2D qNMR

1.6.1 Homo-nuclear *J*-resolved

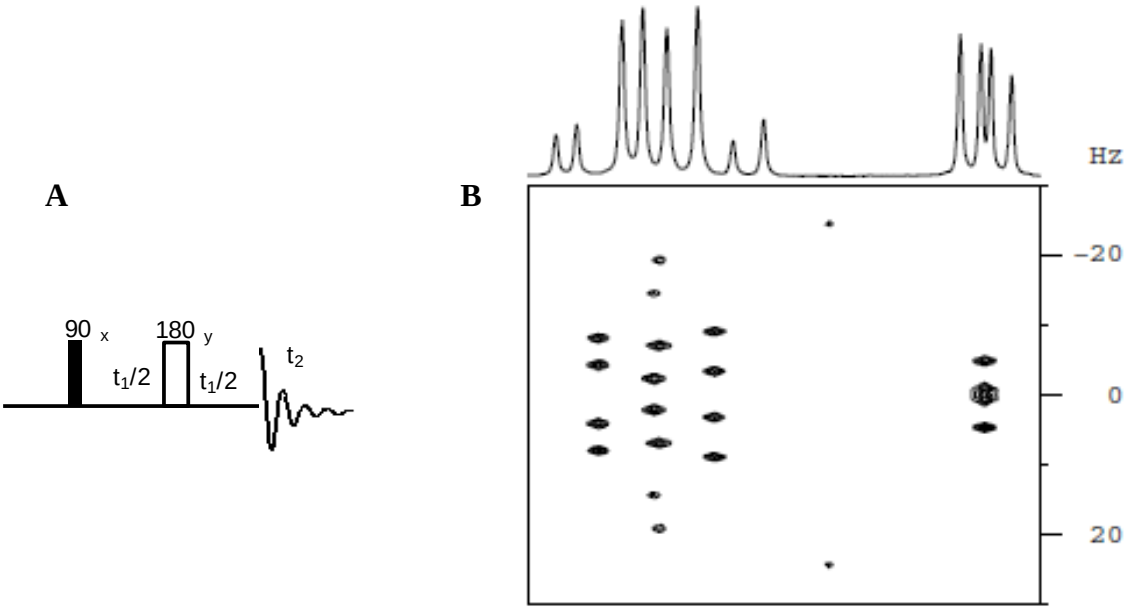

Figure 5: *J*-resolved pulse sequence (A), *J*-resolved spectrum (B) of serine [64]. Proton chemical shifts are expressed in the horizontal dimension whereas $J_{H\text{-}H}$ are expressed in the vertical dimension.

The *J*-resolved sequence (Figure 5A) was proposed by Ernst and his coworkers in 1971 [65]. It offers chemical shifts and *J*-couplings in two orthogonal dimensions. As shown in Figure 5B, chemical shifts (^1H) are expressed in the horizontal dimension (F_2) and *J*-couplings (J_{HH}) are expressed in the vertical dimension (F_1). From the quantitative point of view Viant et al. [66] used 2D *J*-resolved in the study of fish extracts. They established the correlation between

the concentrations calculated from the 2D spectra and those calculated from the 1D spectrum for the quantification of metabolites. They also reported a significant quantitation error of up to 33%. An approach quite akin to this one has also been used by other groups in the analysis of liver tissues [67] and plant metabolism studies [68-70].

1.6.2 Correlation SpectroscopY (COSY & DQF COSY)

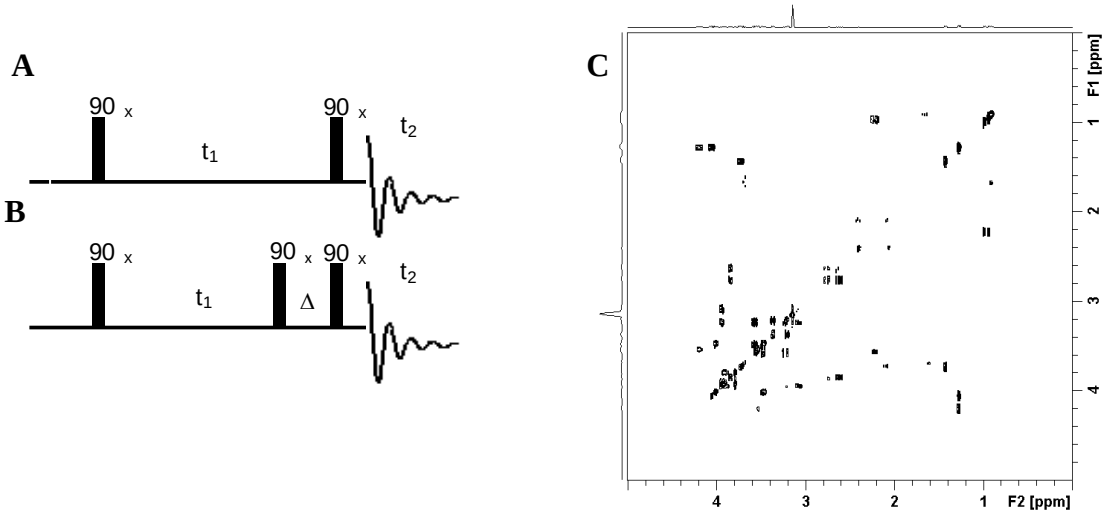

Figure 6: Pulse sequences of COSY (A) and DQF-COSY (B). COSY spectrum (C) of a 100 mM model metabolic mixture.

The first and most popular two-dimension NMR experiment is the homo-nuclear correlation spectroscopy (COSY) [61]. This experiment allows determining which protons are coupled by scalar *J*-couplings. The sequence is made of two 90° pulses which are separated by an evolution period (t_1) (Figure 6A). In the spectrum we can see two types of peaks: diagonal peaks and correlation peaks. Diagonal peaks correspond to the peaks in a 1D-NMR experiment, while the cross peaks indicate couplings between pairs of chemical shifts. Chemical shifts and couplings are obtained in both dimensions. Alonso et al. calculated the metabolite concentrations in frog muscles from COSY spectra [71]. They performed the quantification of the lactate levels on the basis of lactate cross peak volumes. The group

reported a good linear correlation (R^2-0.996) for the cross peaks of lactate at various concentrations with respect to an internal reference cross peak. The normal COSY experiments are measured in magnitude mode. The dispersive nature of the diagonal peaks (broad tails) makes it very difficult to observe the COSY cross peaks that are close to the diagonal. A variant of COSY, the DQF-COSY technique (COSY with Double Quantum Filter) [72] has been proposed to overcome these drawbacks.

The DQF-COSY sequence (Figure 6 B) differs from the COSY by an additional 90° pulse adjoining the detection pulse. This pair of pulses represents a filter for passing through the double-quantum coherence [73], whereby the diagonal peaks and non-diagonal ones have the same amplitude modulation and the same anti-phase character. It also eliminates diagonal peaks from uncoupled nuclei. These all have the advantage that they give a cleaner spectrum in which the diagonal peaks are prevented from obscuring the cross peaks. Nouaille et al. identified and quantified maltodextrin-1-phosphate in a strain of *Fibrobacter succinogenes* (rumen bacterium) using the DQF-COSY sequence [74].

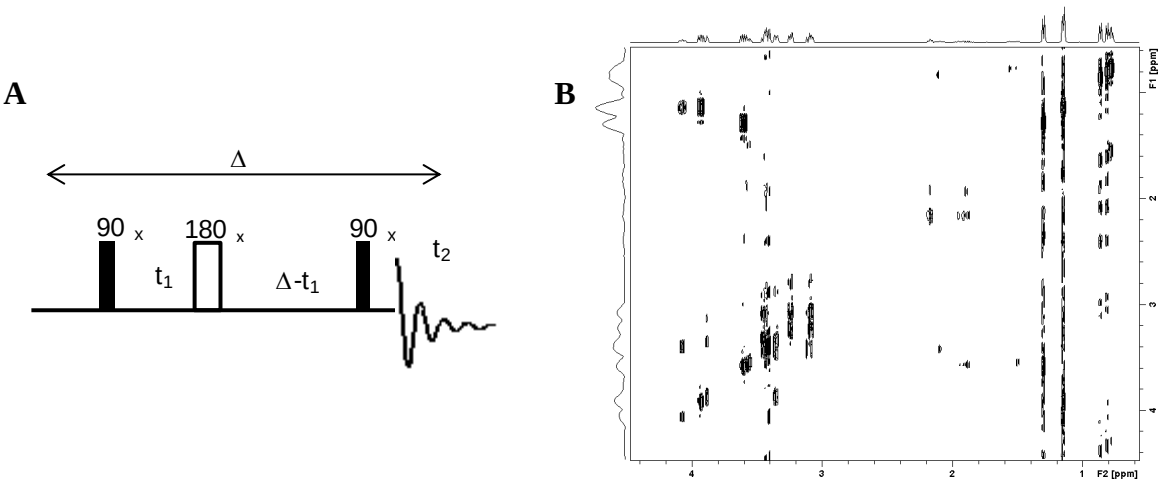

Figure 7: Pulse sequences of CT-COSY (A). CT-COSY spectrum (B) of a 100 mM model metabolic mixture, acquired in 34 minutes on a 400 MHz spectrometer. Proton chemical shifts are expressed in both dimensions.

Nevertheless these experiments still suffer from deficiencies. Particularly in crowded regions it is often difficult to obtain the correct connectivities due to overlapping of multiplets. Constant time COSY (CT-COSY) can be used to avoid overlapping cross-peak multiplets [75]

(Figure 7A). Choosing a constant delay Δ produces decoupling in F_1, and if Δ= 1/2*J*, it increases the intensity of the cross-correlation signals (Figure 7B).

1.6.3 Total COrrelation SpectroscopY (TOCSY & z-TOCSY)

TOCSY is also called HOHAHA (Homo-nuclear Hartmann-HAhn) [76]. It produces the same type of plot as COSY. However, it gives additional correlations between all the protons in a given spin system. The basic pulse sequence is given in Figure 8A. It is identical to the COSY; the difference is that the second 90° pulse is replaced by a spin-lock period [77, 78]. During this period, exchange of polarization takes place between all the coupled spins in a system [79]. In its simplest form, the spin-lock uses a continuous irradiation along a given axis. One of the most popular mixing schemes in TOCSY is the MLEV-17 [80]. The TOCSY sequence has the advantage that it leads to pure absorption spectra, which is an undeniable advantage for quantitative analysis. In addition, the TOCSY spectrum has more spots than the DQF-COSY spectrum of the same compound, which increases the chances of getting uncovered spots used for quantification. But it also increases the risk of overlapping. However, TOCSY spectra can be sometimes hampered by undesirable artifacts arising from zero-quantum coherences (ZQC) generated prior to and / or during the mixing scheme. This zero-quantum coherences leads to line shape distortions in TOCSY peaks which affects the quantification studies.

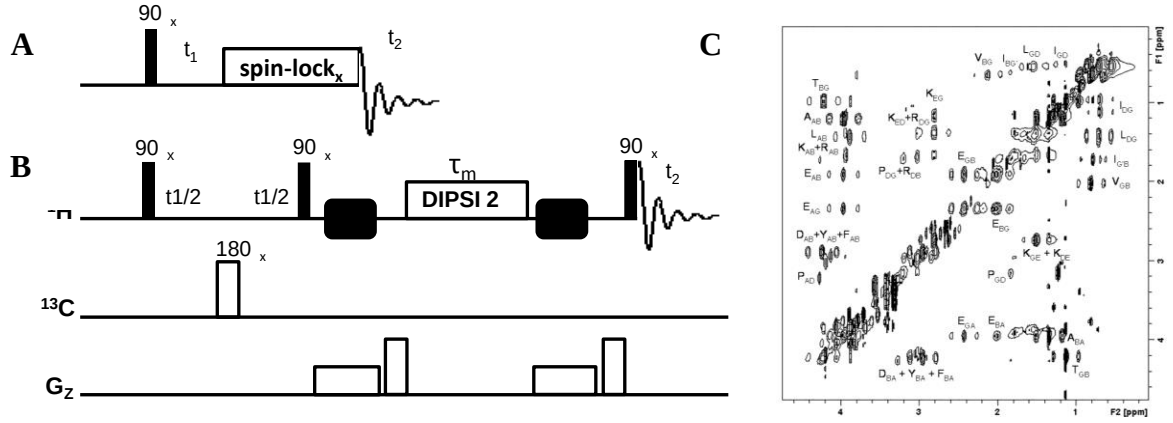

Figure 8: Pulse sequences of TOCSY (A) and z-TOCSY (B). z-TOCSY spectrum (C) of a biomass hydrolysate from *E. coli* cells grown on 50% of [U-^{13}C]-glucose and 50% of natural abundance glucose acquired in 10 h on a 500 MHz spectrometer with a cryoprobe [19]. Proton chemical shifts are expressed in both dimensions and $J_{C\text{-}H}$ are expressed in the horizontal dimension.

Z-filters based on chirp pulses have been proved very efficient in removing the zero-quantum coherences [81]. The zero quantum dephasing scheme was employed in TOCSY (Figure 8B) in order to study the site specific ^{13}C- measurements in fluxomics [82]. In the case of ^{13}C-enriched molecules, an additional 180° pulse on the ^{13}C channel in the middle of the evolution period is applied to perform ^{13}C decoupling in the indirect dimension. The determination of specific ^{13}C-isotopic enrichments in complex mixtures of ^{13}C-labeled metabolites is a powerful tool for studying metabolic fluxes in living systems. Proton spectra of unenriched biological extracts can contain thousands of ^{1}H resonances. Spectra of ^{13}C-enriched extracts are further complicated by $J_{C\text{-}H}$ - couplings. In isotope-based metabolomics studies, which involve complex mixtures of both ^{13}C-labeled and unlabeled metabolites, NMR spectra are too heavily overlapped to support comprehensive quantitative analyses. This pulse sequence allows metabolomics studies to capitalize on isotope-based methods without increasing the complexity of spectra. z-TOCSY was employed to record the spectrum of biomass hydrolysate from *E.coli* cells grown on 50% [U-^{13}C]-glucose and 50% of natural abundance glucose (Figure 8C) [19]. Proton chemical shifts are expressed in orthogonal dimensions whereas $J_{C\text{-}H}$ couplings are expressed in horizontal dimension only (see also Part D).

1.6.4 Hetero-nuclear Single Quantum Correlation (HSQC)

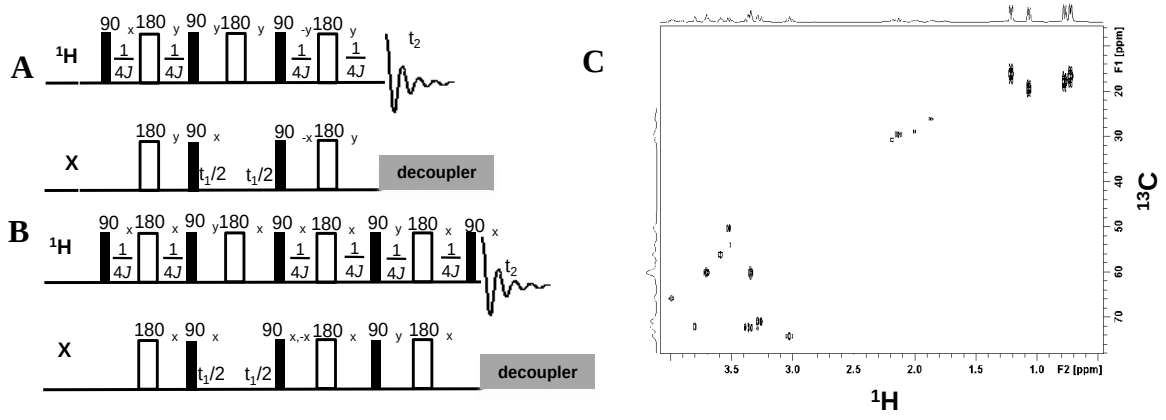

Figure 9: Pulse sequences of HSQC (A) and sensitivity enhanced HSQC (B). HSQC spectrum (C) of a 100mM model metabolic mixture, acquired in 48 minutes on a 400 MHz spectrometer. In the spectrum ^{1}H-chemical shifts are expressed in horizontal dimension whereas^{13}C -chemical shifts are expressed in the vertical dimension.

The simplest HSQC [83] experiment follows the scheme of Figure 9A. This experiment is built on two INEPT sequences [84]. It correlates protons (H) with their directly attached hetero-nuclei (X). Figure 9C shows the HSQC spectrum of a model metabolic mixture in which proton chemical shifts are expressed in the horizontal axis (F_2), whereas ^{13}C- chemical shifts are expressed in the vertical axis (F_1). Richardson et al. [85] quantified with this method the metabolites after extraction, to understand the cellular metabolism in breast cancer. Hu et al. used ^{1}H-^{13}C HSQC for studies of milk quality control, after optimization on a model mixture of metabolites to verify the proportionality between the measured signal and the concentration. After optimization on a model mixture of metabolites, successful results [56] have been accomplished with regards to applications on milk components. Xi et al. developed a program for peak assignment and calculation of the intensity [86]. This scheme was successfully applied to several biological matrices (such as abalone muscles, fish eggs and trout liver). Another approach was also used by Gronwald et al. [55] who built calibration curves and established the limits of detection and quantification of different metabolites, to quantify the metabolites in urine.

Another form of HSQC experiment was proposed by Palmer and his co-workers to improve sensitivity [87]. In the HSQC experiment, hetero-nuclear single-quantum magnetization that exists at the end of the t_1 period may be decomposed into two orthogonal components that lie along the x and y axes. The subsequent 90° pulses on H and X are able to transfer only one of these back into single-quantum proton magnetization, while the other gives rise to ^{1}H–X multiple-quantum coherences that remain unobservable, meaning only one-half of the initial proton magnetization contributes to the observed signal. In contrast, the sensitivity-enhanced version of these experiments (Figure 9B) enhances the S/N ratio by $\sqrt{2}$ for heteronuclei with a single attached proton. A modification of the INEPT transfer step back to ^{1}H, allows the conversion of multiple-qunatum into detectable coherently with its orthogonal partner. Rai et al. [42] successfully applied this scheme for the quantification of human urine samples.

Other research groups made a note of the parameters that may influence the quantification. Heikkinen et al. for example, with removal of the *J*-dependence of polarisation transfer, quantified a mixture of wood lignin using the Q-HSQC sequence [16]. Recently, by introducing an array of optimized rf pulses, Koskela et al. [88] reported an advanced version of this sequence (Q-OCCAHSQC), which is less sensitive to off-resonance effects. In this paper, a human blood

plasma sample of a healthy volunteer was used to compare this method with ^{1}H NMR and 1D CPMG spectra (Figure 10). Different peaks of α-glucose, β-glucose, alanine, lactate, and valine were integrated, and the integral of the anomeric proton H_1 of α-glucose was set as the reference (Figure 10). The QOCCAHSQC integration results were in good agreement with the 1D CPMG results but were slightly higher. However, this small difference can be explained by signal attenuation occurring during the T_2-filtering period of the 1D CPMG sequence.

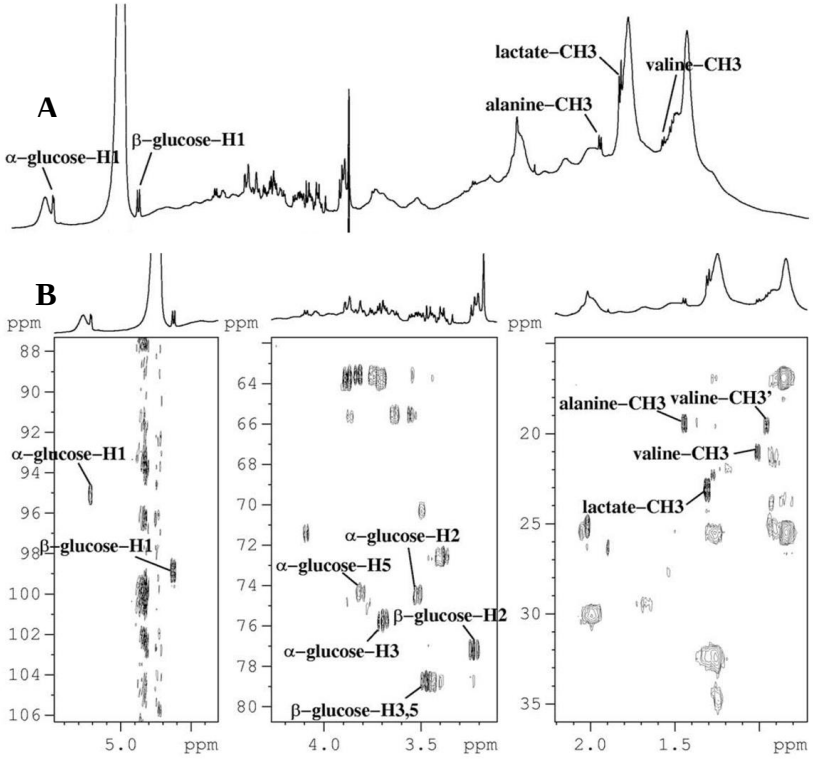

Figure 10: NMR spectra from a human blood plasma sample: (A) ^{1}H NMR spectrum, (B) expansions of Q-OCCAHSQC spectrum. The ^{1}H NMR spectrum was measured at 300 K with water signal presaturation, using 90° excitation pulse, and the repetition time was set to five times the longest T_{1H} of the sample (7.2 s). The Q-OCCAHSQC spectrum was measured with water signal presaturation and using 32 scans per increment. The spectral widths in the proton and carbon dimensions were 10 ppm and 200 ppm, respectively. The repetition time was set to 7.2 sec. Total measurement time was 26 h 41 min. *Adapted from* [88].

1.7 Experimental time

In spite of its high potentialities, the use of 2D NMR for quantitative studies is still limited by a long experimental time due to the numerous N_1 increments to get the indirect dimension with a good resolution. In the case of metabolic mixtures which are characterized by low

concentrations, it is needed to accumulate several transients for each N_1 increment to get good sensitivity. These long experimental durations have several consequences, the first being the overload of spectrometer schedules, which translates into non-negligible costs. A more fundamental consequence is the impossibility of studying samples in which composition evolves within the timescale of the nD experiment. This is not only the case for samples undergoing chemical reactions or dynamic processes, but also for biological samples with limited lifetimes. In addition long experiments are more likely to be affected by spectrometer instabilities over time [89, 90]. This includes electronic variations (variations in pulse angle, phase, receiver gain, etc.), lock instabilities, as well as magnetic field variations inside or outside the magnet. They generate additional noise in the indirect dimension, due to the long time interval (several seconds) between the acquisitions of two successive points of the pseudo-FID. As a consequence of this "t_1 noise", the signal-to-noise ratio (SNR) is always lower in the indirect F_1 dimension, leading to noise ridges parallel to the F_1 axis, as illustrated in Figure 11.

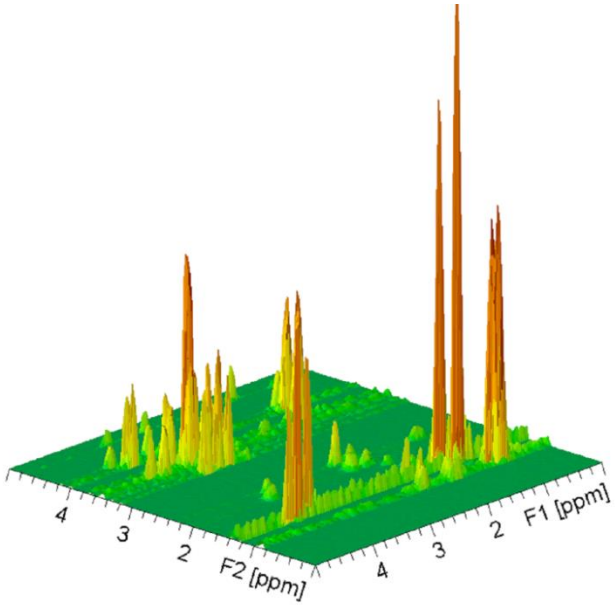

Figure 11: Stacked plot representation of a 2D COSY spectrum recorded on a model mixture of metabolites, on a 500 MHz spectrometer with a cryoprobe. t_1 noise ridges parallel to the indirect F_1 dimension are clearly visible, whereas the signal-to-noise ratio is much greater in the direct F_2 dimension.

While t_1 noise can be removed by subtraction or symmetrisation operations in routine experiments [91] the application of such mathematical treatments in quantitative experiments may affect the quantification [92]. Therefore, t_1 noise, which highly depends on the spectrometer and hardware configuration, potentially affects the precision of quantitative 2D experiments and also decreases the limit of concentration that can be measured precisely. These arguments tend to suggest a close relationship between the experimental duration and the quantitative nature of multi-dimensional experiments. The optimization of the experimental time is therefore a key feature for generalizing the use of 2D NMR for quantitative analysis.

Since 2007, a few studies have introduced strategies to preserve the quantitative characteristics of 2D NMR while reducing the experiment time. In 2007, our group demonstrated that *J*-resolved spectroscopy and DQF-COSY are efficient techniques for precise and accurate quantitative analysis of complex mixtures in a short time [43]. In this study, *J*-resolved and DQF-COSY quantitative spectra were obtained on an equimolar mixture of tropine and nortropine in 2.7 minutes and 12 minutes respectively. Our group also introduced the ^{1}H-INADEQUATE [57] sequence (Figure 12A) for quantitative applications in a recent paper.

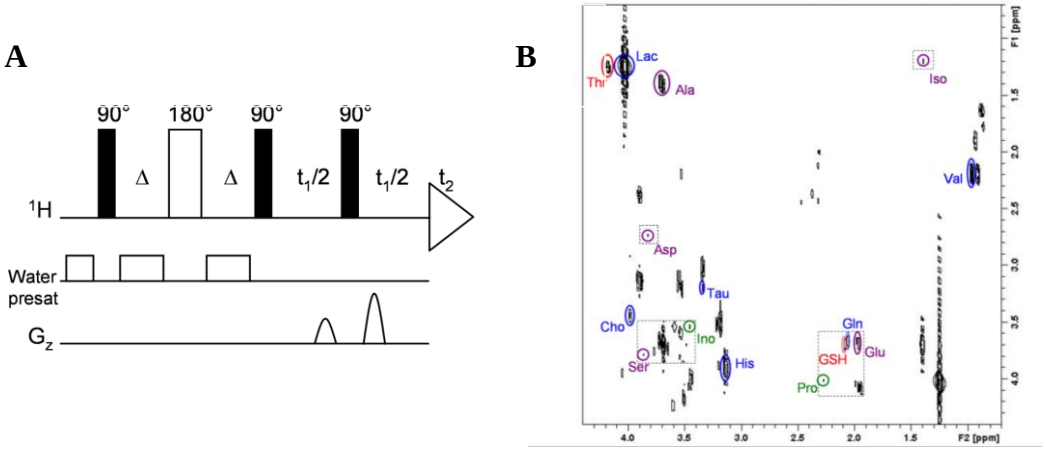

Figure 12: Pulse sequence for the acquisition of quantitative 2D 1H INADEQUATE spectra (A) and 2D spectrum obtained on a cellular extract of MCF-7 breast cancer cells (B). The 2D spectrum was acquired in 13 min (1 transient, 128 t_1 increments), at 298 K, with water signal presaturation, on a 500 MHz spectrometer with a cryogenic probe. The peaks chosen for integration are indicated for each metabolite. Ala : alanine; Lac : lactate; Thr: threonine; GSH : glutathione; Ino : myoinositol; Tau : taurine; Gln : glutamine; Val : valine; Iso : isoleucine; Pro : proline; Asp : aspartate; His : histidine; Ser : serine; Glu : glutamate; Cho : choline [12].

Quantitative ^{1}H-INADEQUATE 2D spectra of metabolite mixtures were obtained in 13 min with repeatability better than 2% for metabolite concentrations as low as 100 mM, and with an

excellent linearity. Compared to more prevalent experiments such as COSY or TOCSY, a higher analytical performance was demonstrated for the homonuclear INADEQUATE pulse sequence. The high degree of precision reached by this technique was credited to the much cleaner diagonal in the case of INADEQUATE (Figure 12B). This fast protocol was then applied to compare and contrast the metabolite content in three different breast cancer cell lines expressing different hormonal and tyrosine kinase receptors (SKBR3, MCF-7 and MDA-MB-468) [12].

Gowda et al. increased the sensitivity and resolution of TOCSY and HSQC experiments (^{1}H-^{15}N and ^{1}H-^{13}C) [93] by using enriched compounds by marking plasma ^{15}N-ethanolamine and ^{13}C-formic acid. Lewis et al. [15] introduced a fast protocol to measure the metabolite concentrations in complex solutions using 2D ^{1}H-^{13}C NMR, FMQ (for Fast Metabolite Quantification) which uses the HSQC pulse sequence. It has been validated for a model mixture of 26 metabolites and a spectrum was obtained in 12 minutes. Very recently our group proposed a fast quantitative HSQC approach to reach high precision for isotopic studies [94]. In spite of their high analytical quality, these experiments are still limited in terms of experimental time due to the nature of 2D NMR experiments themselves.

1.8 Methods for Fast 2D data acquisition

As previously mentioned conventional 2D NMR experiments are often affected by long experiment durations. Therefore, to overcome this problem, the NMR research community has been focusing on the design of fast methods to obtain 2D spectra in a reduced time period.

1.8.1 Fast pulsing Methods

These strategies are mainly based on reducing the relaxation delays in the experiments. The relaxation delay is required in NMR experiments to restore the spin system to its equilibrium state prior to repeating the experiments. This relaxation delay is generally 10 -20 fold longer than the sum of pulse sequence and acquisition time in the direct dimension (typically 5 times the highest longitudinal relaxation time T_1). Therefore, reducing this relaxation delay would reduce the experimental time. Moreover simple shortening this delay is not a solution since it leads to sensitivity problems due to the improper recovery of magnetization to the equilibrium. Two different approaches have been proposed to record the experiment faster.

1.8.1.1 SO-FAST-HMQC & BEST-NMR

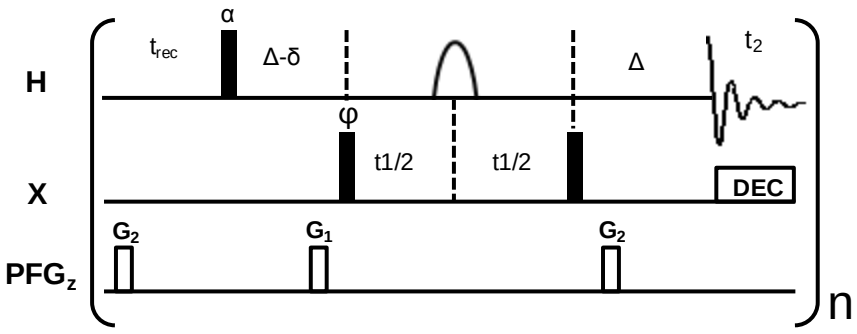

Figure 13: Pulse sequence to record SOFAST-HMQC ^{1}H-X correlation spectrum. *Adapted from* [95].

The Band-**S**elective **O**ptimized-**F**lip-**A**ngle **S**hort-**T**ransient (SOFAST)-HMQC experiment was developed by Brutscher [95] based on the scheme proposed by A. Ross et al. [96]. The experiment, which was developed in the context of protein NMR, is shown in Figure 13. It offers high sensitivity to perform fast 2D NMR. The pulse sequence has been optimized for very short inter scan delays (t_{rec}) for fast data acquisition. Moreover, the Ernst angle excitation [62] is used to get optimum sensitivity. The use of band selective ^{1}H pulses reduces the effective spin lattice relaxation (T_1) of the ^{1}H spins of interest which further improves the sensitivity [97]. Moreover HMQC experiments require only few rf pulses which limits the signal loss due to the rf field inhomgeneities and pulse imperfection compared to other hetero-nuclear experiments.

E. Lescop et al. [98] proposed a variant of SOFAST called BEST –NMR based on Band-selective Excitation Short-Transient pulses.

1.8.1.2 SMART NMR

In the case of small molecule NMR, spin lattice relaxation (T_1) plays a key role. For example in a simple COSY 2D NMR we always set $t_{rec} = \propto T_1$, where $\propto$ varies from 5 to 10. Although at $\propto$=1 we get acceptable signal to noise ratio, a large number of artifacts affect the spectrum quality. These artifacts are due to the interference of transverse and longitudinal magnetization components that diffuse from one scan to another. In order to overcome this problem Pelupessy and his co-workers proposed SMART NMR [99]. The SMART (SMALL Recovery

Time) NMR experiments are based on the work of Freeman [100], who in order to eliminate artifacts in 1D FT NMR varied the recovery delay from scan to scan. To quench these artifacts due to the single and multiple quantum coherences from previous scans, a gradient (G_Q) is applied. Figure 14 represents a simple SMART COSY experiment and its spectrum of a metabolic mixture. G_E & G_D gradients are applied to select the desired coherence pathways in addition to the quenching gradient (G_Q). In order to maintain the same experimental conditions, the gradients are applied in different directions from scan to scan.

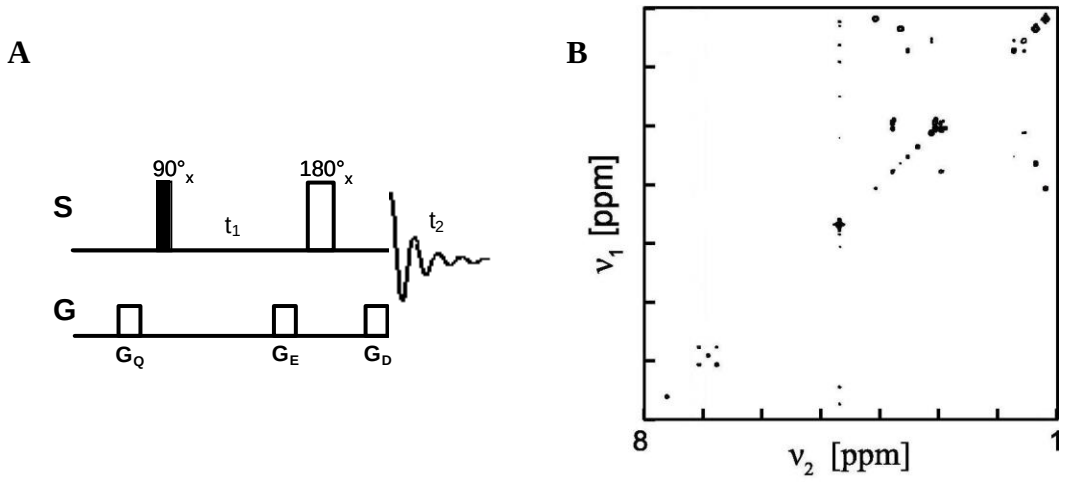

Figure 14: In the SMART-COSY experiment (A), simple 90° pulses (indicated by filled rectangles) are used for preparation and mixing. The quenching gradient G_Q is chosen to be different in orientation from the coherence pathway selection gradients $G_E = G_D$. SMART COSY spectrum (B) of a mixture of ~15 mM Alanine, ~7 mM Arginine, ~7 mM Histidine, ~10 mM Threonine and ~2 mM Tyrosine in D2O with TR = 10 ms, requiring about 70 s *Adapted from* [99].

1.8.2 Processing strategies

In conventional 2D NMR, the number of points of the pseudo-FID in the F_1 dimension (t_1) is of the utmost importance for the total duration of the experiment: it should be as short as possible, since it has a proportional influence on the experimental time. However the resolution of the spectrum is limited by these relatively short acquisition times in the indirectly detected dimension. A variety of approaches have been proposed based on signal processing to improve the resolution and sensitivity at small experimental times.

1.8.2.1 Linear prediction (LP)

By applying linear prediction, the missing part of a FID can be reconstructed [101]. This is a much better way of processing half good data than simply zero filling the missing portion. Linear prediction is extremely useful in 2D NMR as a way of reducing the experimental time and/or improving the quality of already existing data sets [102]. In the F_2 dimension it is fairly easy to acquire enough data points without adding much time to the experiment. However the addition of each increment in the F_1 dimension adds a large amount of time to the experiment. LP helps to gain a much better F_1 resolution from a limited number of N_1, especially in inverse experiments, e.g. HMQC, HSQC, HMBC, where the F_1 dimension is ^{13}C [103].

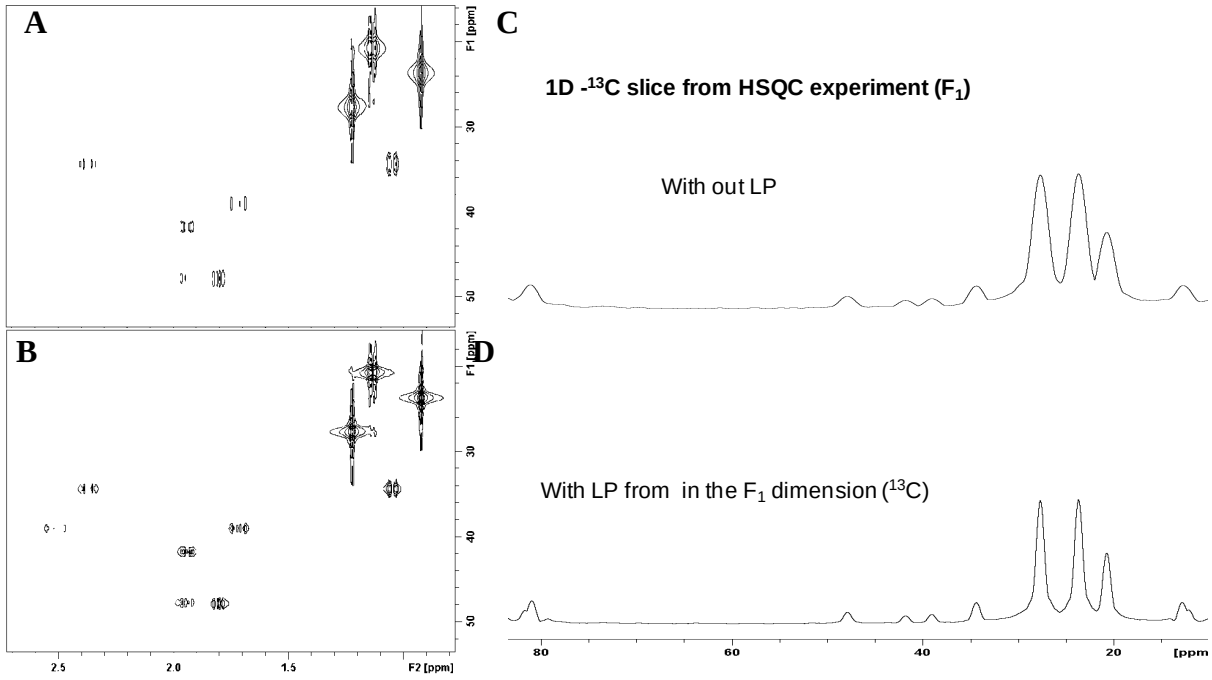

Figure 15: Contour plot of expanded HSQC spectra; without linear prediction (A), with forward linear prediction on real data (B), F_1 Cross- sectional ^{13}C spectra without linear prediction (C), with linear prediction from (D).

As shown in Figure 15(A&B), the HSQC spectra of a metabolic mixture have been compared, each of which was different from one another only in processing techniques, i.e. with and without forward F_1 Linear Prediction. One can easily realize the better sensitivity and resolution

on the ^{13}C projection of the spectrum with linear prediction (Figure 15D), compared to the spectrum without linear prediction (Figure 15C).

1.8.2.2 Covariance NMR Spectroscopy

While playing with the number of points in the F_1 dimension for short experimental time, the resolution is penalized. In order to improve the resolution in the indirect dimension (F_1) without increasing N_1, Brüschweiler et al. [104] proposed a new processing programme for 2D NMR called Covariance NMR [105]. In this method a covariance matrix is constructed from a set of 1D spectra recorded with different evolution periods (t_1). Application of the matrix square-root operation to the covariance matrix yields a spectrum that has an increased resolution along F_1 and otherwise is very similar to the 2D FT spectrum. However the peak volumes of the covariance spectrum vary from its FT NMR counterpart. In order to apply it to quantitative studies, the Covariance technique is modified by using regularization methods [106] which produce a modified covariance spectrum with cross peak volumes closely matching their FT analogues.

1.8.3 Spectral Aliasing

Using spectral aliasing in the F_1 dimension was proposed by Jeannerat [107] to reduce the experimental time by folding /aliasing in F_1 dimension. If the spectral width is smaller than the range of the chemical shift dispersion along the indirect dimension, peaks outside of the spectral width are either folded or aliased depending on the experiment's method of frequency discrimination (TPPI vs. STATES respectively). This small spectral width in the F_1 dimension leads to small N_1. It is clearly explained in Figure 16. The aliased spectrum was recorded with a small spectral width (10 ppm) in the F_1 dimension. Non-aliased peaks are highlighted in a rectangular box.

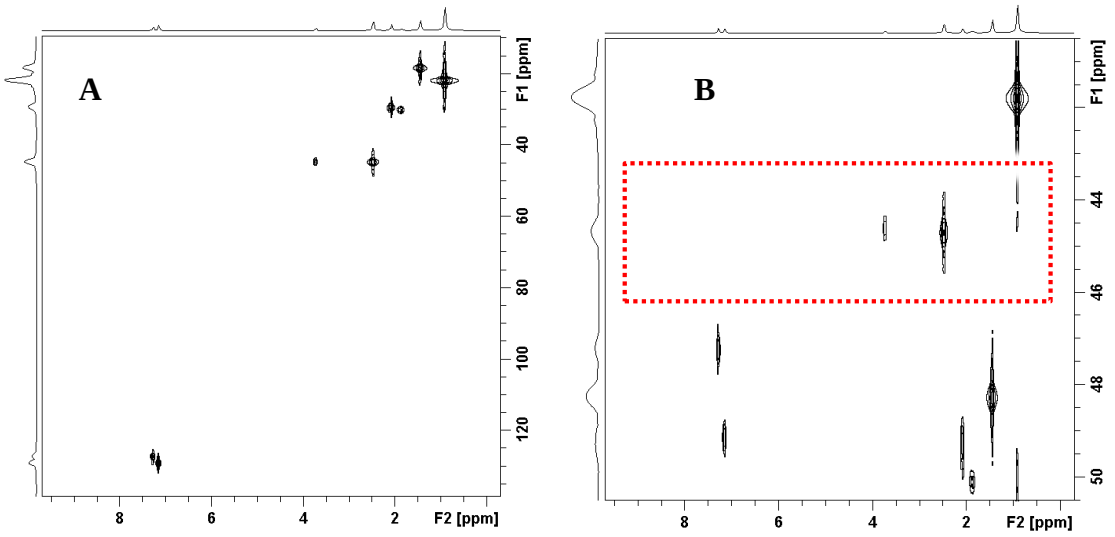

Figure 16: Non Aliased (A) and Aliased (B) HSQC spectra of ibuprofen in acetone-$d_6$recorded in 46 mn with 128 td_1 and 25 mn with 64 td_1 respectively on a 500 MHz Bruker spectrometer equipped with a cryoprobe. Aliased spectrum recorded with a 10 ppm spectral width; non-aliased peaks are highlighted with a red colour rectangular box.

1.8.4 Accordion and Reduced Dimensionality

For the first time in 1981 Bodenhausen and Ernst recorded the reduced dimensionality experiment which is known as the Accordion experiment [108]. The basic idea is to reduce the 3D experiment to a 2D experiment, in which the chemical shift evolution period and the mixing period are incremented simultaneously from one FID to the next one [109]. In early days these experiments were actually designed to measure the chemical exchange. It is a foundation stone for any Reduced Dimensionality experiments [110, 111]. However the acquisition of two coupled frequency dimensions leads to difficulties. The main problem is that the two dimensions being co-evolved are mixed and must be deconvoluted before any useful information can be extracted. Since the evolution linearly combines the two dimensions, their frequencies are "mixed" in the spectrum in a linear manner as well. The number of resonances observed in the lower dimensional spectrum depends on the number of linked dimensions. Thus, if two dimensions are linked, the RD spectrum will contain two peaks per resonance of the higher dimensional spectrum, whereas if three dimensions are coupled, each of the above two peaks will be split by the second frequency resulting in four resonances and so on. The position of the peaks in the spectrum can be used to extract the true

frequency of the resonances in the spectrum. The problem obviously becomes more complicated as the number of resonances is increased. However, if overlap can be avoided, it is possible to reduce experimental time drastically [112].

1.8.5 GFT NMR

To reduce overlap, GFT NMR, an extended version of RD was proposed by Kim and Szyperski [113]. They developed "G-matrix" to combine appropriately the hyper complex data of arbitrary dimensionality to produce "basic spectra". These spectra are much less complicated than the RD projections.

1.8.6 Non Uniform Sampling

One more interesting approach to reduce the experimental time is to reduce the number of sampled time domain data points by non-uniform sampling (NUS) [114]. It consists in acquiring only a reduced number of points in the (t_1, t_2) grid. There are mainly two methods in NUS/Sparse sampling, based on the way of distribution of reduced data points in the grid. They are radial sampling and random sampling which are shown in Figure 17.

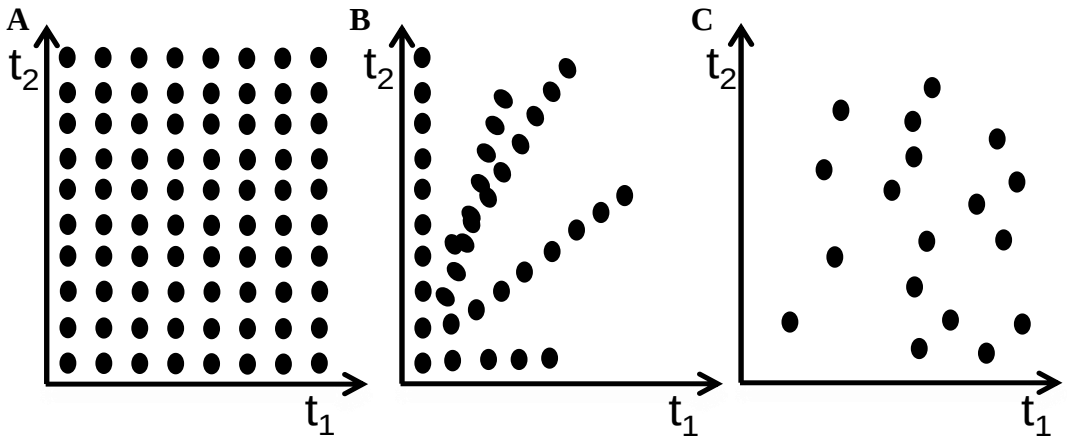

Figure 17: Schematic illustration of a conventional linear sampling grid (A) Radial sampling (B) and Irregular sampling (C). Each point on the grid corresponds to one repetition of a basic pulse sequence.

1.8.6.1 Radial Sampling

Radial sampling was the first non-uniform sampling approach introduced in NMR [115]. In this approach the data points are arranged in a set of lines in time domain. It means radial

spokes (Figure 17B). A projection reconstruction technique was then proposed to reconstruct the 2D spectrum.

Kupce and Freeman, in 2003, for the first time proposed the idea of acquiring projections of NMR spectrum and consequently input these projections to reconstruct the full spectrum [116]. Kupce and Freeman offered an intuitive proposal for a reconstruction method based on the unique nature of NMR spectra. With potential peaks located at the intersections of vectors extended from the projected peak positions, a set of orthogonal projections with either t_1 or t_2 set to zero can be used to establish a "peak lattice". Consequently, the degenerate peaks are resolved by examining the tilted projections, and data is acquired about the correspondence between each potential peak and each observed peak in the projection. For each projection, a space corresponding to the full spectrum is created, and the values observed on the projection are extended back along the lines of integration to fill the spectrum (this procedure is also known as back projection). These spaces are then compared on a point-by-point basis, and for each point, the lowest value from different spaces is considered. Initially Kupce and Freeman demonstrated the projection-reconstruction by reconstructing the 3-D HNCO spectrum of ubiquitin from two orthogonal projections taken along the axes and from one tilted projection at an angle of 30° [116, 117].

1.8.6.2 Random Sampling

Another mode of non-uniform sampling scheme is Random data sampling, in which reduced data points are distributed randomly in the sampling grid (Figure 17C). Such random sampled data sets cannot be transformed using the conventional fast Fourier transformation algorithm. Therefore, other processing methods are required to reconstruct the multidimensional NMR spectrum. Several methods have been proposed till date for the spectral reconstruction of such randomly sampled data sets.

1.8.6.2.1 Maximum Entropy Reconstruction

Maximum entropy reconstruction of NMR spectra is based on the maximum entropy principle, which states: maximizing the entropy of a probability distribution yields the most uniform distribution, given a set of constraints reflecting our knowledge about the probabilities. The aim

of Maximum Entropy Reconstruction (MER) is to calculate the frequency domain spectrum that fits best to the time domain signal [118].

In other words, the signal itself acts as a kind of constraint that averts this kind of process from culminating with a uniform spectrum, but instead, it looks for the NMR peaks. Mathematically, this can be achieved by maximizing the entropy and establishing consistency with experimental data, which corresponds to maximizing the target function, TF [119]:

$$\mathrm{TF}(f) = \mathrm{S}(f) - \lambda \mathrm{C}(f)$$

Where *f* represents the data points of the reconstructed spectrum, S(*f*) is a measure for its entropy, C(*f*) reflects the consistency of the reconstructed spectrum with the experimental data and λ is a Lagrange multiplier. An advantage of MER is the fact that it can handle non-linear sampling of the time domain FID [117, 120, 121].

1.8.6.2.2 Multi-Dimensional Decomposition

Like MER, it is another approach for processing Random data. It is based on a mathematical concept referred to as three-way decomposition [122]. The aim is to find a set of one–dimensional vectors that best describes the experimental data. The multidimensional signal can be described as the vector product of independent one dimensional vectors. An NMR spectrum is decomposed into a sum of components, with each component corresponding to one or a group of peaks. Each component is defined as the direct product of three one-dimensional shapes. The consequence is a reduction in dimensionality of the spectral data used in further analysis. The decomposition may be applied to frequency-domain or time-domain data, or to a mixture of these [117].

1.8.7 Hadamard NMR Spectroscopy

In a spectrum if the resonances are sparsely distributed and can be excited with selective rf pulses, then the acquisition of a multidimensional NMR spectrum can be accelerated [123]. On the basis of this idea, a new scheme called Hadamard NMR was recently proposed, in which there is a selective excitation of NMR resonances and their encoding in the form of a 'Hadamard matrix' [117, 124].

According to N different chemical sites in the indirect domain, the experiment is repeated N times and each of these peaks is encoded according to the different rows of the Hadamard matrix. The phases of these individual selective pulses are then varied in a series of scans. In a sample, for all chemical shifts, each scan will produce a positive or a negative peak. These peaks are further combined linearly from all N scans to produce a conventional spectrum.

Each of the previously described methods can reduce the time needed for performing the multidimensional NMR experiment. Most of them are still based on the time-incrementation scheme initially proposed by Jeener. Nonetheless, all of these methods require either prior knowledge of the chemical sites of interest or rely on processing methods rather than on true experimental NMR data. Furthermore the SOFAST and BEST techniques, which were initially designed for macromolecules, are not suitable for small molecule studies.. Finally, the analytical performance of these techniques was never evaluated for quantitative analysis. To the best of our knowledge, the only exception is a recent study from our group. Very recently E.Martineau et al. [94] studied and compared the analytical performance of several of these methods (LP, NUS and spectral aliasing) in the context of ^{13}C isotopic analysis on HSQC spectra.

In 2002, a completely new strategy, called ultrafast NMR (uf) was proposed inspired from imaging techniques. Among the different fast multidimensional NMR techniques, uf NMR [125, 126] is the only method that enables the acquisition of multidimensional NMR spectra within a single scan, and unlike other methods, it does it without the need for a prior knowledge of the targeted sample in order to accomplish its aim.

2. Ultrafast 2D NMR

2.1 Principle of ultrafast 2D NMR

The ultrafast methodology initially proposed by Frydman is based on spatial encoding [125, 126]. Its main idea is that, instead of repeating N successive experiments on a sample, the sample is divided into N virtual slices where the spins undergo different evolution periods, but simultaneously for all slices. The basic scheme of ultrafast experiments is presented in Figure 18.

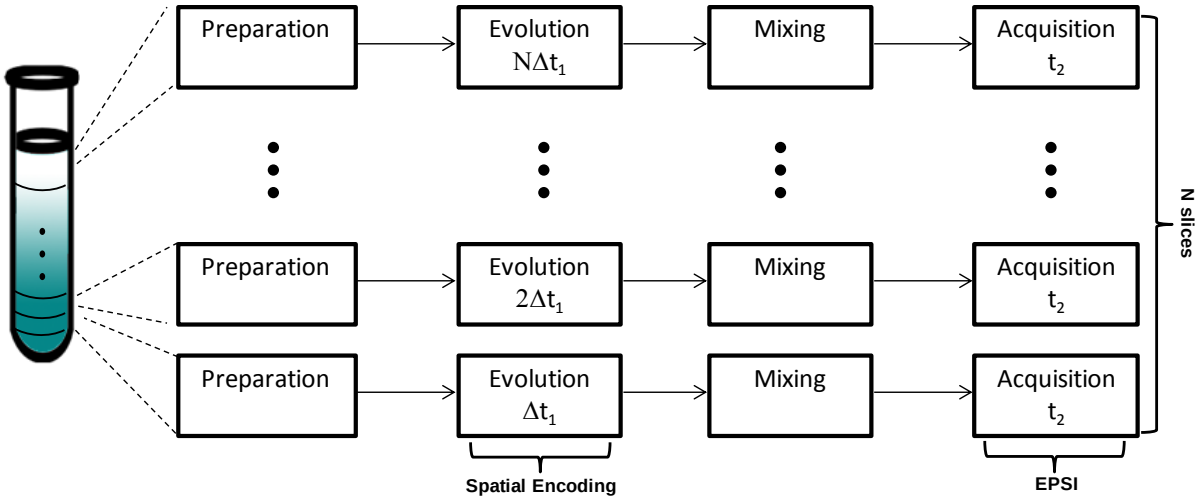

Figure 18: General principle of ultrafast 2D NMR experiments. Instead of repeating N transients on the same sample (as in conventional 2D NMR), the sample is virtually divided into N infinitesimal slices, which undergo different evolution periods within the same experiment by means of spatial encoding followed by an echo planar imaging-based detection.

2.1.1 Spatial encoding and excitation

The ultrafast NMR approach imposes different evolution times on different parts of the sample. This was originally performed by applying a series of frequency-selective pulses together with pairs of bipolar gradients (G_e) along the z-axis. In this approach, applying a strong magnetic field gradient (typically along the sample axis) creates an inhomogeneous spatial distribution within the sample (Figure 19). The resonance frequency is then space-dependent and the sample can be viewed as composed of independent subsamples, which can be manipulated independently by frequency-selective rf pulses. In this encoding module

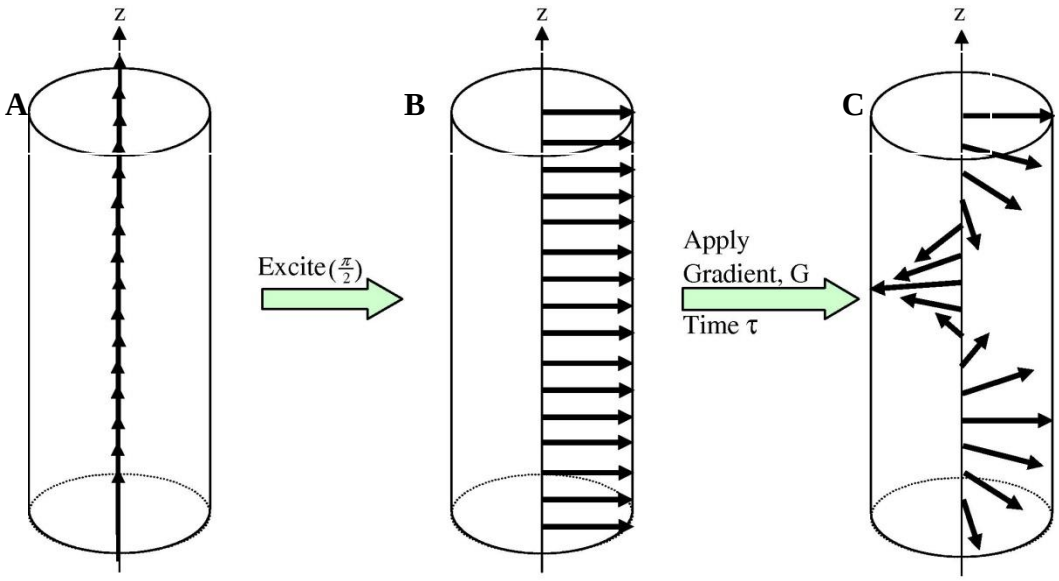

Figure 19: The effect of a z-gradient, G=Gz. The spins are initially in thermal equilibrium condition in the direction of the field (A). They are then excited onto the plane using a hard -pulse (B). The application of a gradient G for a time τ will cause spins at different positions to precess at different rates, effectively winding them in the transverse plane (C) [127].

a discrete train of N_1 RF pulses are applied at a constant frequency increment $\Delta O = |O_{j+1}\text{-}O_j|$ where j=1,2,….N_1 and spaced by a constant delay Δt_1 (figure 20A). Each excitation pulse is applied in combination with a pair of bipolar z-gradients (G_e and G_{-e}). The module effectively partitions the sample into N_1 independent slices positioned at specific z_j coordinates, whose evolution phase encoded along z-orientation is written as [126]:

$$\phi(z) = C\cdot\Omega_1\cdot (z_j - z_{N1}) \tag{1}$$

Where Ω_1 is the internal frequency shift of spins during spatial encoding and C is the spatial encoding constant which is defined as [126]:

$$C = \frac{\Delta t_1}{\Delta z} = \frac{\Delta t_1 \gamma_e G_e}{\Delta O} \tag{2}$$

2.1.2 Decoding the information

After this spatial encoding, a spatially homogeneous mixing sequence is applied as in standard experiments. In order to monitor the signals from these slices an echo-planar spectroscopic

imaging (EPSI) technique is applied [128]. In this detection block, the evolution time at different coordinates are decoded with the help of a pair of bipolar *z*-gradients (G_a and $-G_a$).

2.1.2.1 Spatially encoded Dimension

To detect the signal, an acquisition gradient G_a is applied after the mixing period, leading to a series of echoes at positions proportional to the resonance frequencies (Figure 20). The position of the echoes represented a wavenumber (*k*) which is dependent on the acquisition gradient (G_a) [125]:

$$k = -C\Omega_1 = \gamma_a \int_0^t \mathrm{G_a}\,(\mathrm{t}^1)\mathrm{dt}^1 \qquad (3)$$

The position of such echoes will thus reveal the nature of the internal spin evolution frequencies, making the *k* wave number equivalent to an indirect–domain frequency axis. There is no need of Fourier transformation. This axis is referred as ultrafast dimension.

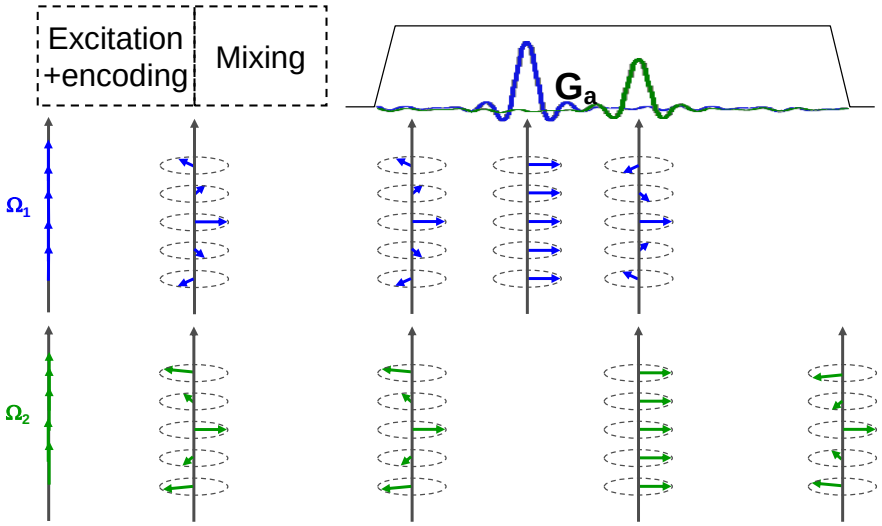

Figure 20: Signal detection in ultrafast 2D NMR. Acquisition of the ultrafast dimension for a sample containing two resonance frequencies Ω_1 and Ω_2. A magnetic field gradient G_a is applied while the receiver is open, which refocuses the dephasing induced in the course of spatial encoding. It leads to the formation of echo peaks whose positions are proportional to resonance frequencies.

2.1.2.2 Conventional Dimension

In order to obtain the second dimension of the 2D spectrum, a technique similar to echo-planar-imaging (EPI) [128] is used while detecting the signal. The alternated gradients provoke a series of refocusings and defocusings, leading to the formation of mirror-image echoes (Figure 21).

Thus, the detected signal depends on both the position of spins and their internal evolution frequency, which can be summarized by a phase of evolution $\phi = k.z + t_2.\nu_2$. The evolution in the presence of an oscillating $\pm G_a$ can be represented by a zig-zagging trajectory through the space (k,t_2). Therefore, an appropriate data rearrangement followed by a conventional Fourier transform is required to separate the different resonance frequencies, resulting in the second dimension of the 2D NMR spectrum. It is generally referred to as "conventional dimension".

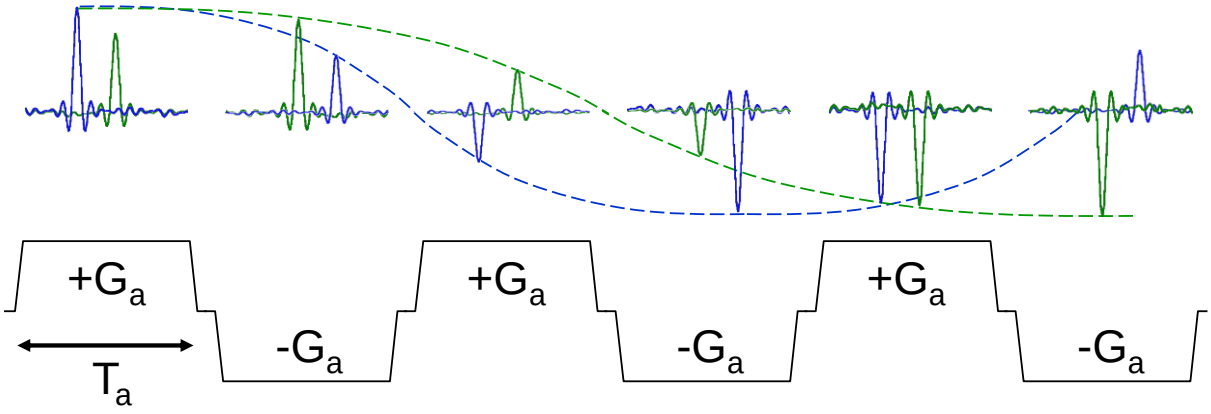

Figure 21: Acquisition of the conventional dimension. A series of sub-spectra are detected during a train of bipolar gradient pulses, while the system evolves under the influence of conventional parameters (relaxation, resonance frequency, couplings, etc.). Data rearrangement and Fourier Transform along the conventional dimensions are necessary to obtain the final 2D Spectrum.

A specific processing is necessary to obtain the resulting 2D spectrum [129]. This procedure is exemplified in Figure 22. The signals detected during the gradients $+G_a$ and $-G_a$ are reversed to each other (Figure 22A). The signals of positive and negative gradients are collected separately as two different data sets (Figure 22B). A Fourier transformation is performed along the second dimension of the two sets of spectra. This results in two mirror-image 2D spectra (Figure 26C) that can be added after inverting one of them.

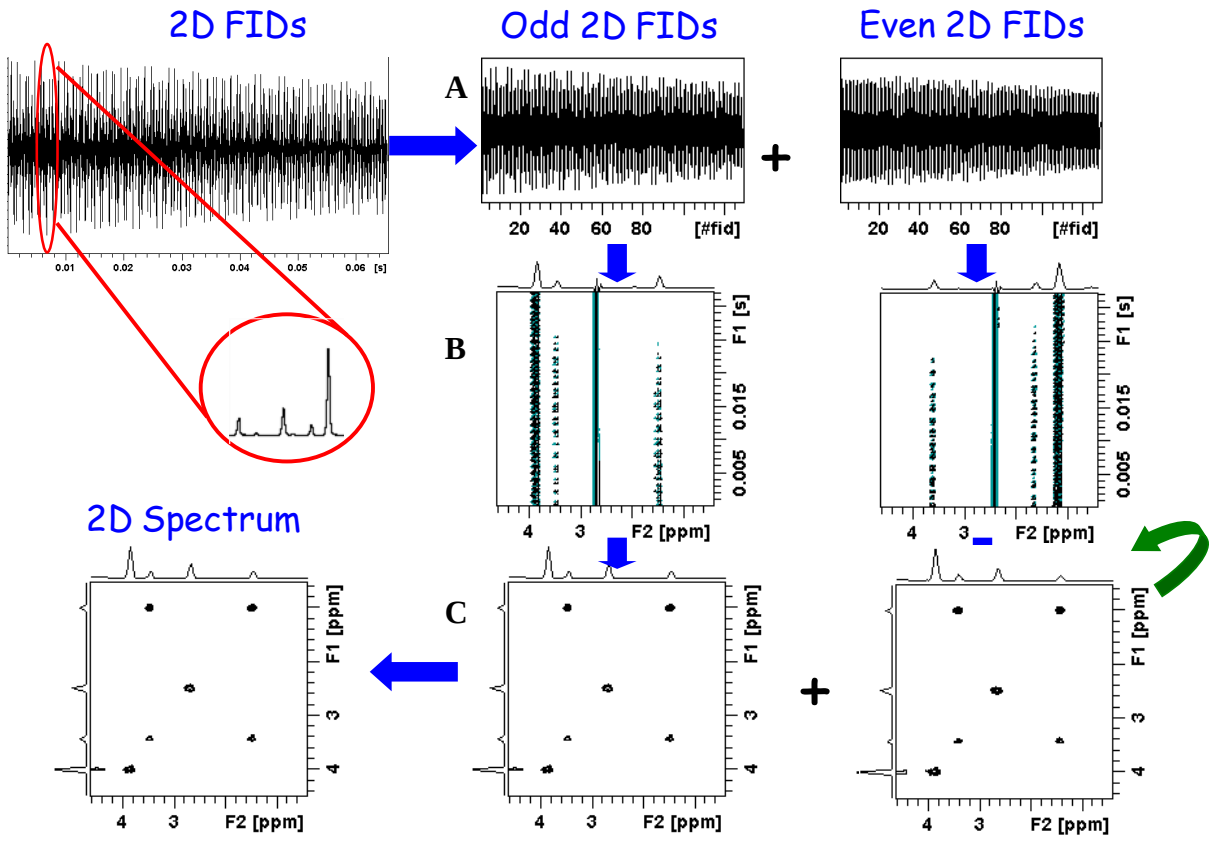

Figure 22: Summary of the processing treatment of ultrafast 2D NMR data. Example of a COSY spectrum of ethanol. Succession of FIDs obtained when applying gradients oscillating ± Ga (A). Rearrangement of the data in space (k, t_2) and separating the data corresponding to the gradients of opposite sign (B). Mirror-image spectra obtained after Fourier transformation (C).

2.2 Spatial encoding schemes

The initially proposed discrete encoding scheme (Figure 23A) is limited by a number of drawbacks such as fast switching gradients along with rf pulses at the same time and ghost peaks [130]. To deal with these limitations a number of continuous spatial encoding strategies have been proposed (Figure 23).

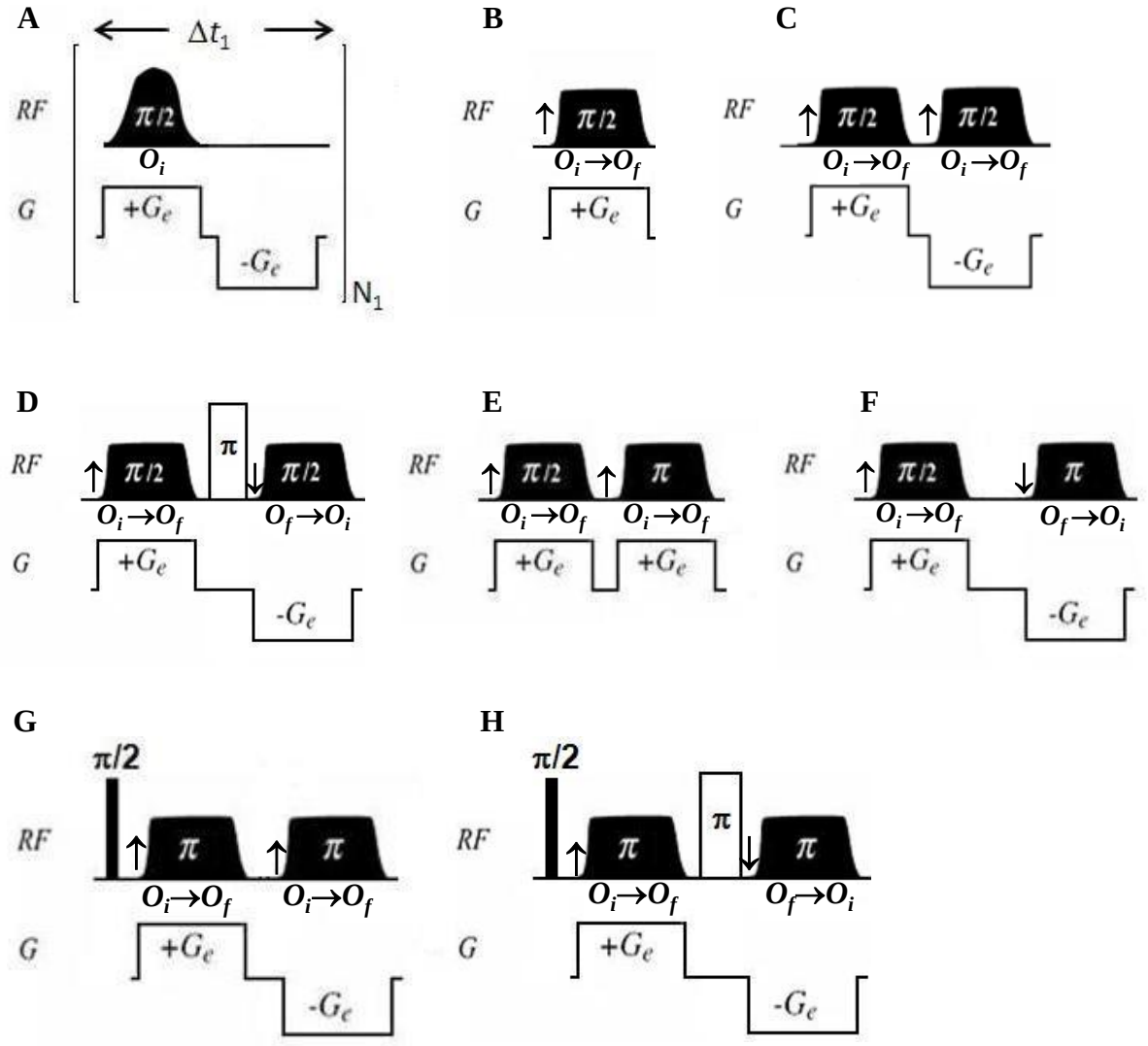

Figure 23: Different versions of continuous spatial encoding strategies: Initially proposed discrete encoding (A) by Frydman [129]. Single sweep encoding (B) proposed by Y. Shrot [131]. Amplitude-modulated encoding [132] (C) and it's variant (D) proposed by Y. Shrot [131]. Phase-modulation encoding strategies proposed by A. Tal [133] (E) and Andersen [134] (F) respectively. Constant time encoding proposed by P. Pelupessy [135] (G) and modified version of it proposed by T. Roussel [136] (H).

2.2.1 Encoding with amplitude modulation

In this scheme, the original train of discrete frequency-shifted rf excitation pulses (Figure 23A) is replaced by a single sweep encoding, in which the π/2 pulse with gradient ($+G_e$) excites the spins at a *z* position and shifts them into the transverse plane. (Figure 23B) [131]. The chirp pulse has

a frequency that varies as a function of time. The total phase obtained by the spins at *z* is given by [131]:

$$\Phi(\mathrm{z}) = -\frac{\left(\gamma_e \mathrm{G_e}^{\pi/2}\right)^2}{2R} z^2 + \gamma_e \mathrm{G_e}^{\pi/2}\left(\delta^{\pi/2} + \frac{O_i^{\pi/2} - \Omega_1}{R}\right) z + \left(-\frac{\left(O_i^{\pi/2} - \Omega_1\right)^2}{R} + \Omega_1 \delta^{\pi/2} - \frac{\pi}{2}\right) \quad (4)$$

The quadratic term (z^2) creates undesired effects in the spectrum which can be removed by post–acquisition manipulation or by applying the second sweep pulse with with a negative gradient (-G_e) of same amplitude (Figure 23C). The overall phase obtained by spins after the second sweep pulse is expressed as [132]:

$$\Phi(\mathrm{z}) = \Omega_1\left(\frac{O_f^{\pi/2} - O_i^{\pi/2}}{R}\right) - 2\frac{\gamma_e \mathrm{G_e}^{\pi/2}}{R}\left[\Omega_1 - \left(\frac{O_i^{\pi/2} + O_f^{\pi/2}}{2}\right)\right] z \quad (5)$$

Where $O_i^{\pi/2}$ and $O_f{}^{\pi/2}$ are the initial and final sweep frequencies of the π/2 chirp pulse respectively. *R* is the rate of the chirp pulse which can be defined as: $R = \frac{\Delta O}{\delta^{\pi/2}} == \frac{\gamma_e \mathrm{G_e}^{\pi/2} L}{\delta^{\pi/2}}$. $\delta^{\pi/2}$ is the chirp pulse duration and Δ*O* is the chirp's bandwidth: $\Delta O = O_i^{\pi/2} - O_f{}^{\pi/2}$. *L* is the effective length of rf excitation. In eq (5) the term $(O_i^{\pi/2} + O_f{}^{\pi/2})/2$ plays a prominent role on the offset value, and impact the peak position in the spatially encoded dimension. Another important term in eq (5) is $-2\frac{\gamma_e \mathrm{G_e}^{\pi/2}}{R} = -2\frac{\gamma_e \mathrm{G_e}^{\pi/2}\delta^{\pi/2}}{\Delta O} = -2\frac{\delta^{\pi/2}}{L}$ which recalls the coefficient took in the discrete excitation case eq (2). Eq (5) can be written as:

$$\Phi(\mathrm{z}) = \Omega_1 \delta^{\pi/2} - C\left[\Omega_1 - \left(\frac{O_i^{\pi/2} + O_f^{\pi/2}}{2}\right)\right] z \quad (6)$$

In the above equation, the first order term leads to phase distortion that affects the peak shapes. However, in terms of gradient demand this scheme turns out to be much less taxing than its discrete counterpart. In order to overcome this phase distortion problems Y. Shrot et al. (Figure 23D) proposed a variant of amplitude-modulated encoding [131]. The general scheme is

modified by introducing an additional a π-pulse between the excitation and storage pulses (Figure 23D) which makes the T_2 effects constant throughout the sample [131].

2.2.2 Encoding with phase modulation

An alternate method to the schemes presented above uses a 'π/2-π' chirp pulse scheme replacing the amplitude –modulation encoding by a phase-modulated scheme [133] (Figure 23E). The π/2 chirp pulse sweeps from an initial frequency $O_i^{\pi/2}$ offset to final offset $O_f^{\pi/2}$ with a positive gradient $G_e^{\pi/2}$ and the π pulse sweeps from O_i^{π} to O_f^{π} with a positive gradient G_e^{π}. $\delta^{\pi/2}$ and δ^{π} are the durations of chirp pulses π/2 and π respectively. At the end of the π/2 pulse the spins are excited onto the transverse plane and will have occurred the phase given by eq (4). In order to cancel the quadratic z^2-term, a π-pulse is applied with a condition $2G_e^{\pi}\delta^{\pi} = G_e^{\pi/2}\delta^{\pi/2}$ [133]. Then the overall phase of the spins is

$$\Phi(z) = \frac{\delta^{\pi/2}}{2}\left(\Omega_1 + \frac{\gamma_e G_e^{\pi/2} L}{2}\right) + \gamma_e\left[\frac{\delta^{\pi/2} G_e^{\pi/2}}{2} + \frac{\delta^{\pi/2}}{L}\left(1 - \frac{G_e^{\pi/2}}{G_e^{\pi}}\right)\Omega_1\right] z \qquad (7)$$

The phase distortions caused by the first order term (z) can be avoided by using a gradient spoiler before the acquisition. In addition when the conditions $G_e^{\pi/2} = G_e^{\pi}$ and $\delta^{\pi/2} = 2\delta^{\pi}$ are fulfilled, the chemical shift evolution is refocused, and *J*-couplings only are expressed in the ultrafast dimension

S. Andersen et al. [134] suggested a variant of this method, based on the use of gradients of opposite sign. The excitation pattern is identical to A except that the gradients are of opposite sign (Figure 23F). According to these authors, the two pulses used in this case must have opposite directions of scan to make the spatial encoding possible.

2.2.3 Constant time encoding

In addition to the above scheme, Pelupessy [135] proposed a constant-time, phase-modulated encoding described in Figure 23G. It begins with a π/2 hard pulse, followed by two π-chirp pulses of duration δ^{π} with identical sweeps but reversed gradients $+G_e^{\pi}$ and $-G_e^{\pi}$. The phase imparted by the first π-swept pulse is given by [137]:

$$\Phi(\mathrm{z}) = -\frac{\delta^{\pi}\Omega_1^2}{\gamma_e \mathrm{G}_\mathrm{e}^{\pi} L} - \frac{\delta^{\pi}\gamma_e \mathrm{G}_\mathrm{e}^{\pi} L}{4} - \frac{2\delta^{\pi}\Omega_1 z}{L} - \frac{\delta^{\pi}\gamma_e \mathrm{G}_\mathrm{e}^{\pi} z^2}{L} \tag{8}$$

In order to remove the quadratic term (z^2) a second π-chip pulse is applied, the overall phase after the spatial encoding is given by

$$\Phi(\mathrm{z}) = \frac{4\delta^{\pi}}{L}\Omega_1 z \tag{9}$$

T. Roussel et al. proposed a variant of Pelupessy's scheme [136] for the implementation of uf 2D NMR in localized spectroscopy,in which the two π-chirp pulses are separated by a π-hard pulse (Figure 23F).

2.2.4 Advantages and Disadvantages of each method

Table 1: Summary of spatial encoding for different excitation used in ultrafast 2D NMR patterns.

Type of excitation	$\mathbf{T_e}$	$\boldsymbol{C}$
Discrete encoding	$N_1\Delta t_1$	$\frac{\Delta t_1 \gamma_e G_e}{\Delta O}$
Shrot (90° - 90°)	$2\delta^{\pi/2}$	$\frac{T_e}{L}$
Shrot (90° - 180°-90°)	$2\delta^{\pi/2}$	$\frac{T_e}{L}$
Shrot (90°)	$\delta^{\pi/2}$	$\frac{T_e}{L}$
Tal (90° - 180°)	$\frac{\delta^{\pi/2}}{2} + \delta^{\pi}$	$\frac{2T_e}{L} \cdot \frac{1 - G_e^{\pi/2}/G_e^{\pi}}{1 + G_e^{\pi/2}/G_e^{\pi}}$
Andersen (90° - 180°)	$\frac{\delta^{\pi/2}}{2} + \delta^{\pi}$	$\frac{2T_e}{L}$
Pelupessy (180° - 180°)	$2\delta^{\pi}$	$\frac{2T_e}{L}$
Roussel (180° - 180° - 180°)	$2\delta^{\pi}$	$\frac{2T_e}{L}$

The basis of all spatial encoding schemes is to get an effective evolution t_1 with respect to position. The time of spatial encoding varies from scheme to scheme. In order to compare these schemes, the spatial encoding terms (*C*) and the spatial encoding durations (T_e) are summarized in Table 1.

In the amplitude–modulation scheme, the signal is decreased to half due to the storage of spins along the z-axis [132] when compared to the other schemes. In addition π/2 chirp pulses are more sensitive to field inhomogeneities when compared to the π-chirp pulses, and their precise calibration is more difficult from the experimental point of view. Whereas constant-time spatial encoding controls the relaxation problem by exciting all the spins at the same time, the other schemes are affected by *z*-dependant T_2 effects. In addition P. Giraudeau et al. [137] proved that Pelupessy's scheme is superior to other spatial encoding schemes in terms of sensitivity and resolution. For all these reasons, Pelupessy's scheme will be chosen for the present study.

2.3 Alternatives for decoding

P. Giraudeau et al. [138] proposed a new acquisition scheme by substituting detection gradient echoes by spin echoes, to obtain ultrafast *J*-resolved spectra where the coupling constants are encoded along the direct F_1 domain. The acquisition gradients (G_a) are separated by non-selective π pulses that refocus the effect of internal chemical shifts while the homo-nuclear *J*-evolution remains unaffected (Figure 24B). The π pulses also refocus the effect of acquisition gradients; there is no need for gradient inversion, contrary to the initial EPI pattern. This scheme, repeated $2 \cdot N_2$ times, results in a $2 \cdot T_a \cdot N_2$ total digitization time. Two interleaved mirror-image datasets are obtained and can be separated in the same manner as the ones obtained by the usual EPI block, to lead to the 2D spectrum after FT in the F_1 dimension.

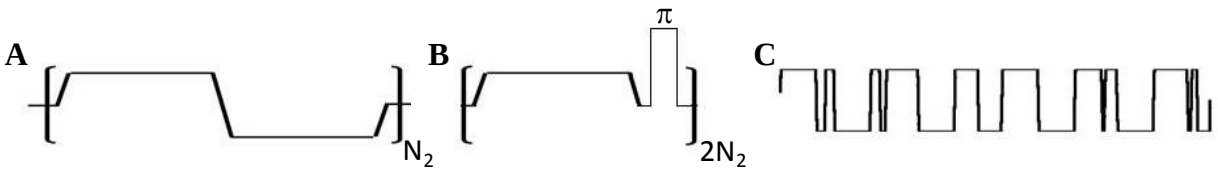

Figure 24: Strategies explored for ultrafast 2D NMR acquisitions. Initial scheme based on a constant square-wave modulation of the acquisition gradient G_a (A). New detection scheme for *J*-resolved (B). Pseudo-random approach assayed for the sake of an iterative v_2 reconstruction (C).

In addition to the above schemes Y. Shrot [139] proposed a non-uniform sampling scheme for the ultrafast dimension. In order to get non-uniform sampling data, the regular square wave gradient scheme (Figure 24A) is replaced by Pseudo-random gradients (Figure 24C). Then reconstruction techniques are applied to get the full 2D spectrum.

2.4 Mathematical description of ultrafast 2D NMR

2.4.1 Spectral widths

An ultrafast acquisition consists of a number N_2 of gradients pairs ($+G_a$ and $-G_a$), each having a duration of T_a. The total acquisition time depends on $N_2.T_a$. The spectral width in the conventional dimension (SW_1) is given as in any FT-NMR experiment by the inverse of the dwell time (Δt) = $2T_a$ [129]:

$$SW_1 = \frac{1}{2\mathrm{T_a}} \tag{10}$$

The spectral width in the spatial encoding (ultrafast) dimension (SW_2) is given by [129]:

$$SW_2 = \frac{K_{max}}{C} \tag{11}$$

Where $K_{max} = \gamma_a G_a T_a$ is the maximum wavenumber and C is the spatial encoding constant. Therefore:

$$SW_2 = \frac{\gamma_a \mathrm{G_a T}_a}{C} \tag{12}$$

In addition, SW_1, SW_2, and the resolution along the ultrafast dimension (SW_2) are linked by the relation [140]:

$$\gamma_a \mathrm{G_a} L = \frac{2SW_2 SW_1}{\delta \nu^{1/2}} \tag{13}$$

Where $\delta\nu^{1/2}$ is the resolution in the ultrafast dimension. This relation shows that increasing the spectral width in any of the two dimensions without altering the resolution is limited by the maximum gradient amplitude available (ca. 60 G/cm on most spectrometers). Moreover, even if

higher G_a values can be reached, the subsequent larger frequency dispersion induced by the acquisition gradients would make it necessary to increase the receiver bandwidth (*fb*), thus resulting in sensitivity losses [127], as shown by the following relation:

$$fb = \frac{\mathrm{G_a} l \gamma_a}{2\pi} \tag{14}$$

2.4.2 Resolution and Sensitivity

In ultrafast 2D NMR, the spectral resolution $(\Delta\nu_1)$ in the conventional dimension (SW_1) is governed by the acquisition time. That is the total duration for a pair of acquisition gradients multiplied by the number of acquisition loops.

$$\Delta\nu_1 = \frac{1}{2\mathrm{T}_a N_2} = \frac{SW_1}{N_2} \tag{15}$$

The resolution in the ultrafast dimension (SW_2) is defined by [137]:

$$\delta\nu^{1/2} \approx \frac{1.21}{LC} \tag{16}$$

$\delta\nu^{1/2}$ is the half–height width of the echo peaks. i.e resolution depends on the spatial encoding time. The resolution should be easily increased by applying a greater spatial encoding duration. However, this leads to large sensitivity losses, mainly due to the effects of molecular diffusion in the presence of gradients [137, 141]. This loss of sensitivity leads to the modification of the line shapes [142, 143]. Subsequently, a compromise has to be made between resolution and sensitivity. P. Giraudeau et al. made a study on resolution with respect to sensitivity (Figure 25) [137]. Based on this a spatial encoding duration of 30 ms is generally chosen, as it offers a reasonably good resolution while limiting sensitivity losses. Moreover, increasing T_e further increases the demand on acquisition gradients to refocus the dephasing induced by the spatial encoding and therefore limits the accessible spectral widths.

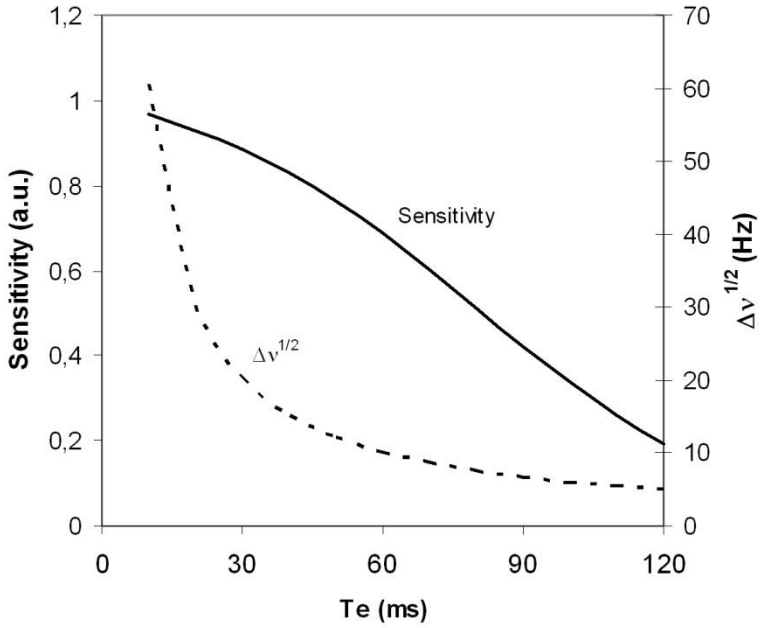

Figure 25: Simulated sensitivity and resolution of homo-nuclear ultrafast 2D experiments based on Pelupessy's spatial encoding scheme as a function of the spatial encoding duration T_e. The graph shows the necessary compromise between the sensitivity and the peak width $\Delta\nu^{1/2}$ in the spatially-encoded dimension [92].

2.4.3 Line shapes

All peaks are characterized by a sinc shape along the ultrafast dimension, due to the excitation stage of the pulse sequence, has been fully described by Shapira et al. [144]. However, all these sinc shapes are distorted due to the asymmetry, which affect the spectral quality. In conventional dimension the line shapes are lorentz shape like conventional 2D NMR due to fourier transformation.

2.5 Progress to by-pass the limitations

2.5.1 Spectral widths

In conventional NMR, peaks lying outside of the observed spectral width are easily detected by means of spectral aliasing or folding which automatically occurs given the violation of the Nyquist condition. Should this aliasing procedure be optimized, the whole spectral range can be observed within a limited width, a strategy proposed by Jeannerat [107] which applies equally in the conventional dimension of ultrafast experiments.

In the ultrafast dimension, the problem is much more complex, as regular aliasing is intrinsically impossible due to the non-FT character of this dimension. To overcome this limitation a number of strategies have been proposed.

2.5.1.1 Serial spectral/Spatial encoding

In this method a series of spectrally selective pulses followed by gradients imparting site-specific spatial windings replace the π/2 excitation [140, 145] (Figure 26A). If suitably chosen, these gradients will shift the ultrafast-domain resonances into arbitrary positions within the ultrafast 2D spectrum; these spatial/spectral manipulations are done to place all peaks in a reduced final window, compatible with the minimal G_a acquisition gradients desired.

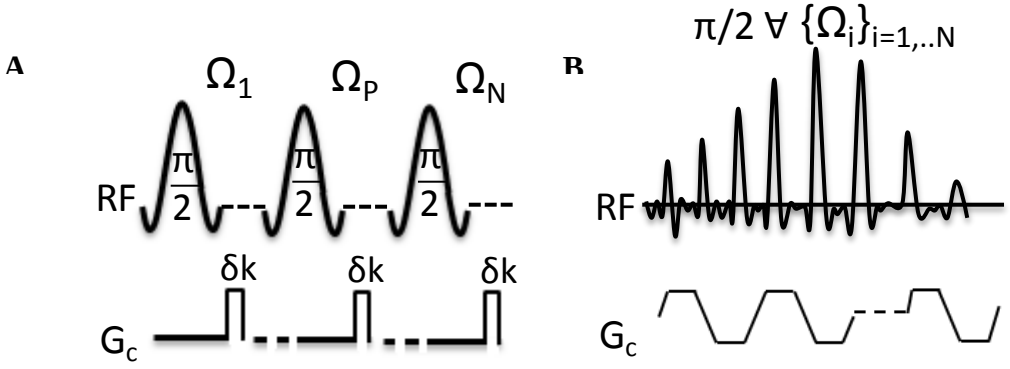

Figure 26: Serial Spatial/Spectral Encoding (SSE) (A): Employs a train of selective pulses to sequentially excite each of the sites of interest, and interleave the rf manipulations with a train of identical gradient pulses characterized by the minimal wave number separation δk. Parallel Spatial/Spectral Encoding (PSE) (B): All the chemical sites Ω_i are endowed with their specific dephasing factors simultaneously [145].

In addition to the above method there is one more method introduced by Y. Shrot [145], known as parallel selective encoding. In this method all the chemical sites are excited and dephased simultaneously by using selectively wavelet rf pulses with gradients (Figure 26B). However, these approaches require *a priori* knowledge of the precise position of the resonances to be encoded, a prerequisite which is not compatible with unknown, and *a fortiori* complex, samples.

2.5.1.2 Pelupessy's approach

Pelupessy proposed a new approach to fold the ultrafast dimension [146]. He introduced a band-selective refocusing pulse (BSRP) to recover the missing part of the spectrum. This π-pulse is

flanked by a bipolar gradient pair before the mixing period as shown in the dashed box in Figure 27. The missing part of the spectrum can be shifted in the region of interest by fine-tuning the parameters of the gradients.

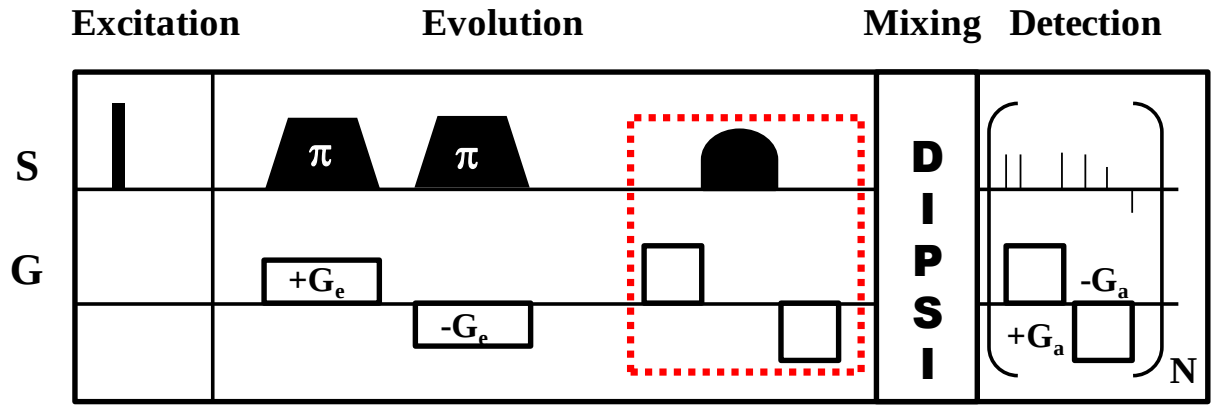

Figure 27: Folding scheme proposed by Pelupessy for single-scan 2D experiments. The element in the red dashed box, comprising a bipolar pulse pair with a frequency-band-selective refocusing pulse (BPP-BSRP) has the effect of shifting the signals in the circled part of the spectrum into the observable range. *Adapted from* [146].

2.5.1.3 Gradient folding

Giraudeau et al. proposed an efficient and simple approach known as gradient folding [147]. This relies on suitably chosen gradients placed on each side of the mixing period and can be applied to almost all ultrafast pulse sequences (Figure 28). Therefore, the missing part of the spectrum can be shifted into the region of interest by fine-tuning the parameters of the gradients.

The signal detected during the acquisition gradient (G_a) can be described as the sum of two symmetric signals with respect to $k = 0$. It creates two echo mirror images of (k). From eq (3):

$$k = -C\Omega_1 \text{and } k = C\Omega_1 \tag{16}$$

The addition of two gradients (G_1 & G_2) on both side of the mixing period symmetrically shifts the two mirror-images. Eq (16) can be re-written as:

$$k = -C\Omega_1 - \gamma_e \mathrm{G_e} \tau_1 - \gamma_a \mathrm{G_a} \tau_2 \text{and}$$
$$k = C\Omega_1 + \gamma_e \mathrm{G_e} \tau_1 - \gamma_a \mathrm{G_a} \tau_2 \tag{17}$$

Where τ_1 and τ_2 are the durations of the folding gradients G_1 and G_2 respectively. γ_e and γ_a are the gyromagnetic ratio of the spatially encoded and detected nucleus respectively. By changing the two gradient parameters (amplitude and/or duration), the two symmetric signals can be partially superimposed and all the relevant signals can be observed in a reduced spectral width.

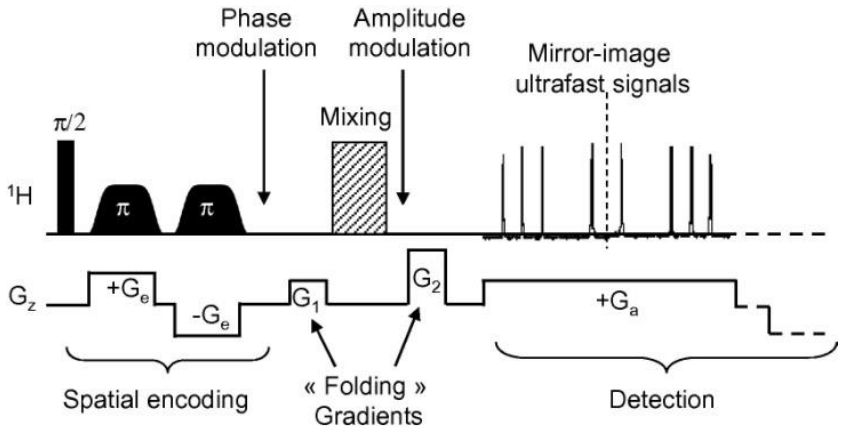

Figure 28: Generic ultrafast pulse sequence illustrating the principle of gradient-controlled folding. The relative position of the two mirror-image signals can be modified by adjusting G_1, G_2, τ_1 and τ_2.

2.5.2 Sensitivity and line shapes

The quality of ultrafast spectra can be improved by an appropriate processing protocol, such as that which was recently proposed by Giraudeau and Akoka for enhancing the line shape and sensitivity in the ultrafast dimension [148]. In the ultrafast dimensions, the peak shapes were characterized by asymmetric sinc wiggles due to phase distortions. The non-idealities of excitation or gradient coils on the edge of the sample cause this phase distortions. The method described in Figure 29 consists in Fourier transforming each line of the 2D spectrum, resulting in a smoothed square excitation profile modulated by phase dispersion due to the different resonance frequencies present in the sample. This profile is then multiplied by an optimized mathematical function designed to minimize the contribution from the edges of the sample. Finally, an inverse Fourier transform regenerates the original peak, but the asymmetry is completely removed. Not only does this procedure improve the line shape in the ultrafast dimension, but it also increases the sensitivity by a factor of 2 at no cost in terms of resolution. Routinely implemented, this greatly helps in improving the quality of ultrafast spectra.

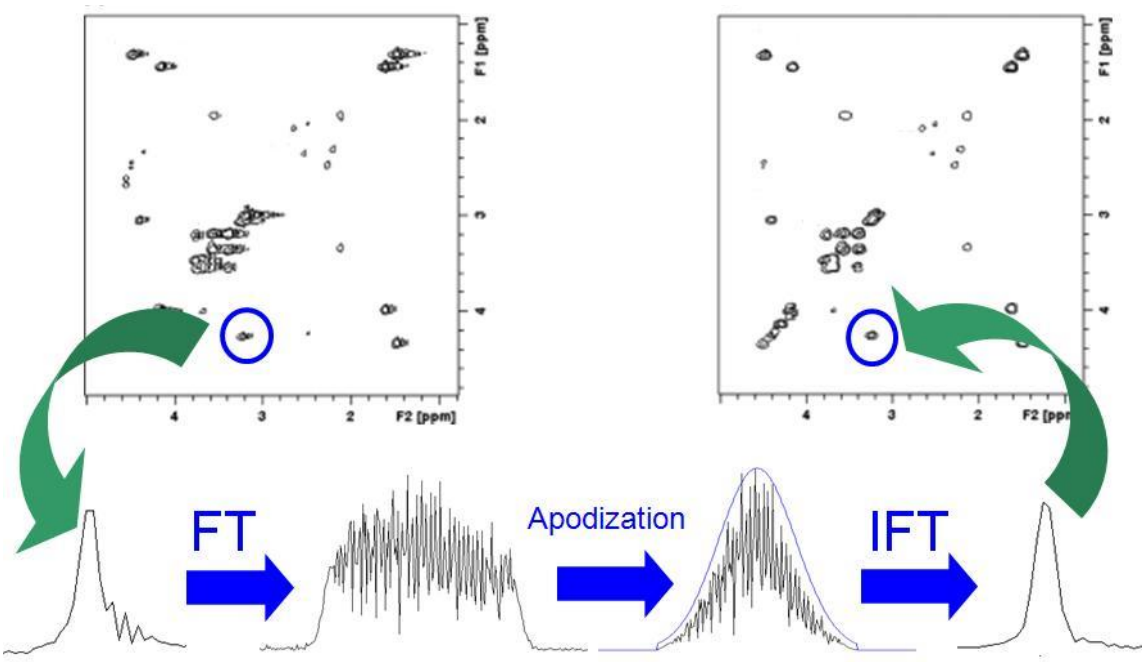

Figure 29: Apodisation procedure designed to improve lineshape in the spatially-encoded dimension of ultrafast spectra, illustrated on the ultrafast COSY spectrum of a 50 mM mixture of six metabolites in D2O. Each line of the 2D spectrum is Fourier transformed, multiplied by an optimized mathematical function minimizing the non-uniformities on the edge of the sample, and finally inverse-Fourier transformed, giving rise to lineshape almost exempt from asymmetric distortions. *Adapted from* [148].

2.5.3 Reduction of diffusion effects

Giraudeau et al. proposed a multi-echo excitation scheme to improve sensitivity by controlling the effect of transverse relaxation diffusion due to a long spatial encoding duration [137]. It consists in replacing the two π-chirp pulses by a succession of shorter π-pulse pairs applied during alternated gradients for the same of value of T_e (Figure 30). By using this scheme the sensitivity can be improved and line shape distortions can be reduced.

In addition to multi-echo scheme, L.Rouger et al. [149] proposed a new approach to control the diffusion effects based on the sample preparation. This new sample preparation protocol is based on the encapsulation of the analytes inside phospholidic vesicles to reduce the diffusion.

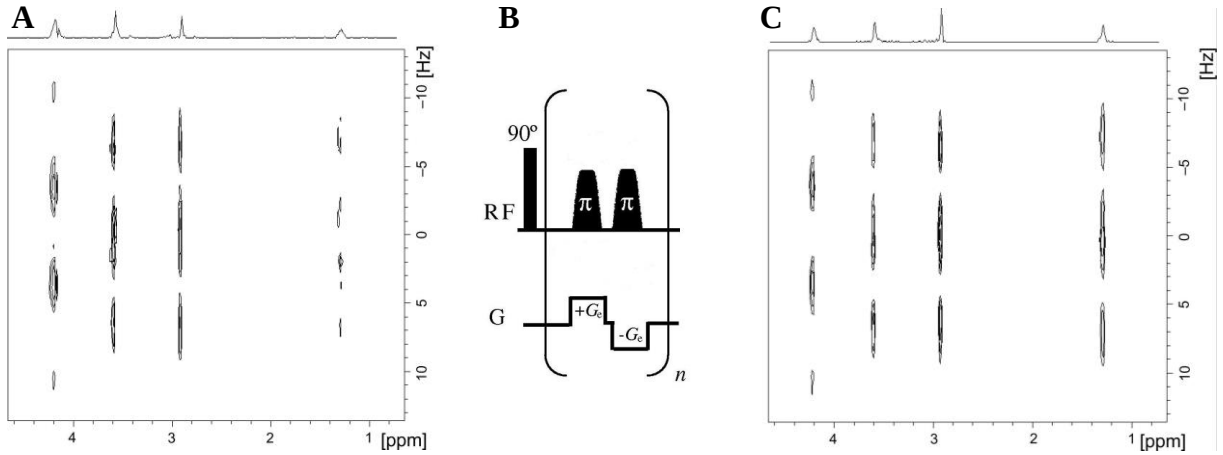

Figure 30: Spectrum of 3-ethyl bromopropionate obtained with Pelupessy's encoding scheme consisting of two 60 ms 180° pulses (A). Multi-echo phase-modulated excitation scheme proposed by Giraudeau et al. to minimize diffusion effects (B). Spectrum (C) obtained with multi-echo excitation scheme formed by six 20 ms 180° pulses [137].

2.6 Quantitative ultrafast 2D NMR

Ultrafast 2D NMR offers promising perspectives for quantitative analysis. It potentially allows a significant reduction in the experimental duration, which is substantial when considering the calibration procedure required for quantitative 2D NMR and also the frequent need to analyze a large number of samples. For the first time Giraudeau et al. [17] reported the analytical evaluation of ultrafast 2D NMR on model mixtures. Two homo-nuclear ultrafast techniques, namely *J*-resolved spectroscopy and TOCSY, were evaluated on model mixtures in terms of repeatability and linearity. The repeatability obtained was noted to be better than 1% for ultrafast *J*-resolved spectra and better than 7% for TOCSY spectra. Both methods were characterized by an excellent linearity. Moreover, ultrafast NMR is potentially less sensitive to the hardware instabilities.

In addition to this, Giraudeau et al. presented the first application of ultrafast 2D NMR to real metabolic samples, in the context of fluxomics [19]. Two homo-nuclear experiments, ufCOSY and ufTOCSY were designed to measure the site specific enrichments of ^{13}C in fluxomics. These results highlight the potential of ultrafast 2D NMR for quantitative analysis and provide promising perspectives related to this new quantitative methodology called ufo-qNMR (ultrafast optimized quantitative NMR).

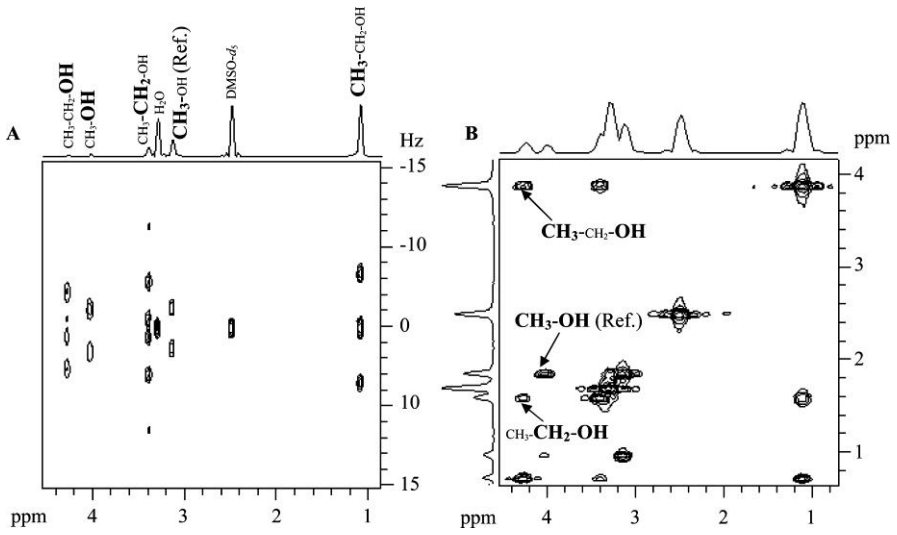

Figure 31: Ultrafast 500 MHz *J*-resolved (A) and TOCSY (B) spectra acquired in 800 ms (A) and 100 ms (B) on a methanol (100 mmol L−1) and ethanol (200 mmol L−1) mixture in DMSO-d6 at 298 K. *J*- resolved experiment give excellent repeatability (better than 1%) whereas TOCSY gives nearly 7% [17].

2.7 Other applications

Recent papers have highlighted the potentialities of ultrafast 2D NMR to follow kinetics of chemical reactions occurring on a short timescale. Total Correlation Spectroscopy (TOCSY) has been successfully applied to real-time monitoring of organic reactions [150]. Herrera et al. reported the application of ultrafast hetero-nuclear 2D NMR to follow the structural changes on a carbonyl carbon atom [151]. Our group has reported the ability of ultrafast 2D NMR to study dynamic processes by studying D-glucose mutarotation in water [18]. Recently Luiz H. K. Queiroz Jr et al. monitored the acetyl hydrolysis by using ufHSQC [152].

Hyphenated techniques are another domain where uf 2D NMR sounds particularly promising. As these techniques are irreversible, single-scan experiments are often the only way of acquiring NMR spectra in this case. The spatial encoding strategies coupled with hyperpolarisation [145, 153] opens promising perspectives for the real-time study of metabolic reactions which will dramatically enhance the sensitivity of NMR-based metabolic studies, thus providing great help for applications which are currently limited by their sensitivity, such as metabolomics of low-sensitive nuclei or in vivo metabolomics.

Shapira et al. demonstrated the potentialities of coupling ultrafast NMR with chromatography [154]. He used UF TOCSY to follow the real time elution of analytes. On the basis of this strategy Luiz H. K. Queiroz Jr et al. further coupled ufNMR with HPLC for separation of natural products [155].

Part B

Practical implementation of ultrafast 2D NMR

Chimie Et Interdisciplinarité
Synthèse, Analyse,
Modélisation
UMR CNRS 6230
UNIVERSITÉ DE NANTES

1. Quantum project

The QUANTUM project in which this work is included aims to develop a comprehensive methodology to set ultrafast 2D NMR as a standard tool for fast and precise quantitative analysis of complex metabolic structures. In order to make 2D NMR suitable for fast, precise and robust quantitative analysis of complex mixtures, this project takes the information from original NMR developments and programming aspects. An analytical validation of these optimized methods is performed in order to make them suitable for quantitative studies of real metabolic samples such as tumor cell lines differentiation. The project also includes the development of pre-acquisition and processing routines for quantitative ultrafast 2D experiments, which consequently will be easier to implement in routine.

2. Practical implementation of ultrafast 2D NMR

The implementation and use of ultrafast 2D NMR by non-specialists are far from being straightforward, due to the specific acquisition and processing procedures and parameters characterizing uf NMR. Moreover, a major limitation affecting these experiments is their incapacity to cover large spectral widths without losing resolution. To make this methodology implementable and applicable by non-specialists, we developed a simple routine capable of translating the conventional parameters (spectral widths, transmitter frequencies) into specific uf parameters (gradients and chirp pulse parameters).

By defining simple parameters - such as spectral widths in both dimensions - equivalents to those of conventional 2D NMR experiments, the user can obtain all uf-specific parameters without prior knowledge of this methodology. Moreover, our routine also takes into account the possibility of folding a user-defined region of the spectrum into the main observation window along the spatially-encoded dimension (see paragraph 2.5.1.3).

This routine was implemented in a webpage which is available for external users for free of cost. Its direct implementation in the commercial software is also being developed. The routine was

designed for two widely used 2D experiments: COSY and HSQC, but can be easily extended for any other pulse sequence.

To evaluate the performance of this routine, we applied it to record the COSY spectrum of Ibuprofen. The ^{1}H spectra of the Ibuprofen sample show resonances between 0 ppm and 8 ppm (Figure 32). Therefore, the gradient controlled folding method is necessary to obtain the corresponding ultrafast 2D spectrum in a single scan. Thanks to our routine, the user simply defines conventional input parameters such as spectral widths SW_2 (spatial encoded dimension) and SW_1 (conventional dimension). Then the routine automatically calculates the ultrafast specific parameters to be applied, such as T_a (duration of Acquisition gradients), G_a (acquisition gradient amplitude), and G_e (spatial encoding gradient amplitude). The spatial encoding duration T_e was also optimized to achieve a good resolution [137].

Furthermore, to record the folded spectra in the spatial encoding dimension, the user defines, as input parameters, the center of the main observation window (ν) as well as the center of the window to be folded (ν^1) on the 1D proton spectra (Figure 32). The routine automatically calculates, as output parameters, the gradient folding parameters G_1 and G_2 that should be applied. Natural folding also occurs in the conventional dimension.

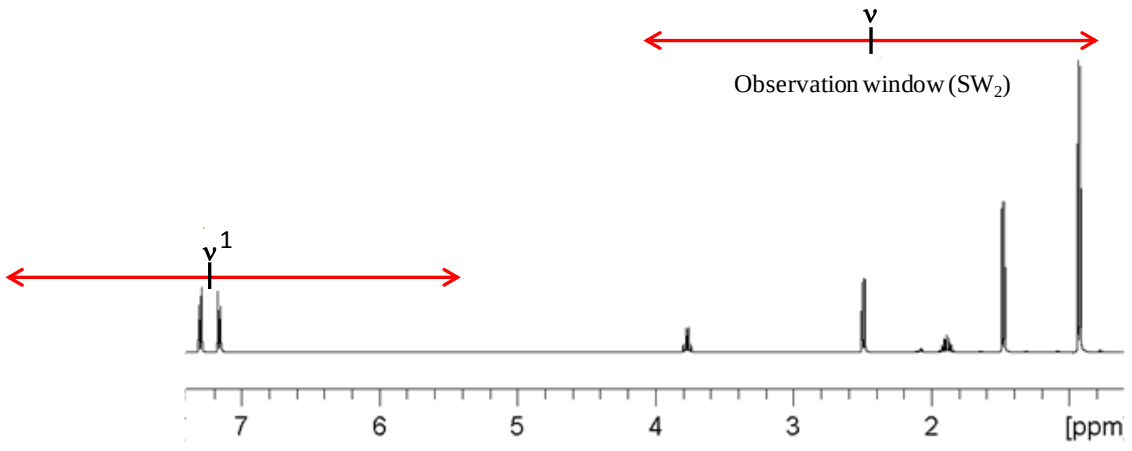

Figure 32: ^{1}H spectra of Ibuprofen. ν and ν^1 are center of unfolded and folded regions respectively.

The corresponding pulse scheme and resulting folded spectra are shown in Figure 33.

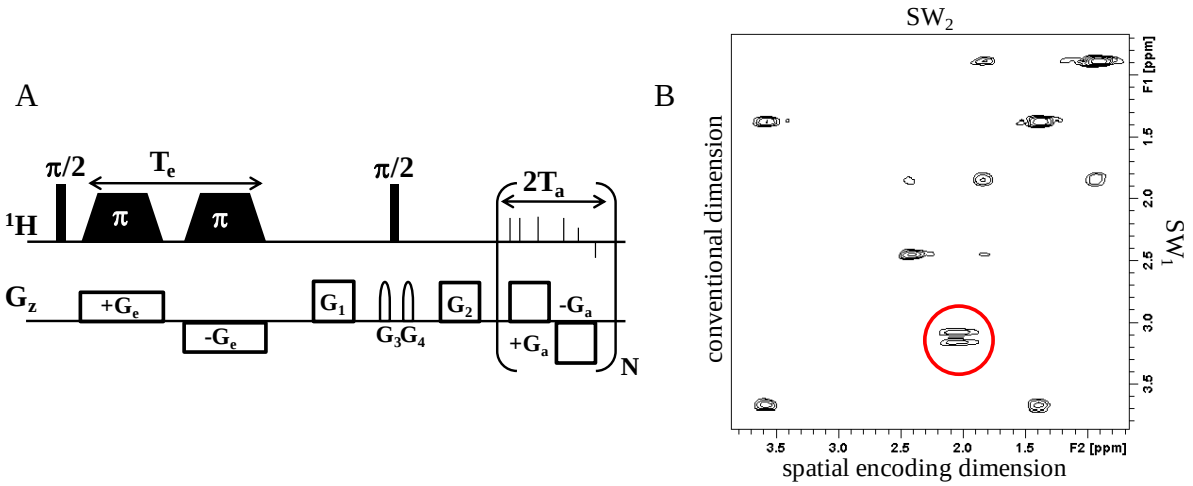

Figure 33. Pulse sequence of ufCOSY (A): G_1 and G_2 are folding gradients. G_3 and G_4 are coherence selection gradients. G_a and G_e are acquisition and spatial encoding gradients respectively. UfCOSY spectrum of Ibuprofen (B). The folded peak is circled with red color.

The results exemplify the efficiency of our webpage. A similar algorithm and webpage were designed for HSQC, and other pulse sequences will be implemented. The whole set up is shown in Figure 34. We hope that this tool will eliminate much of the mystery surrounding ultrafast 2D NMR and will make the technique acessible by a wider audience of organic and analytical chemists.

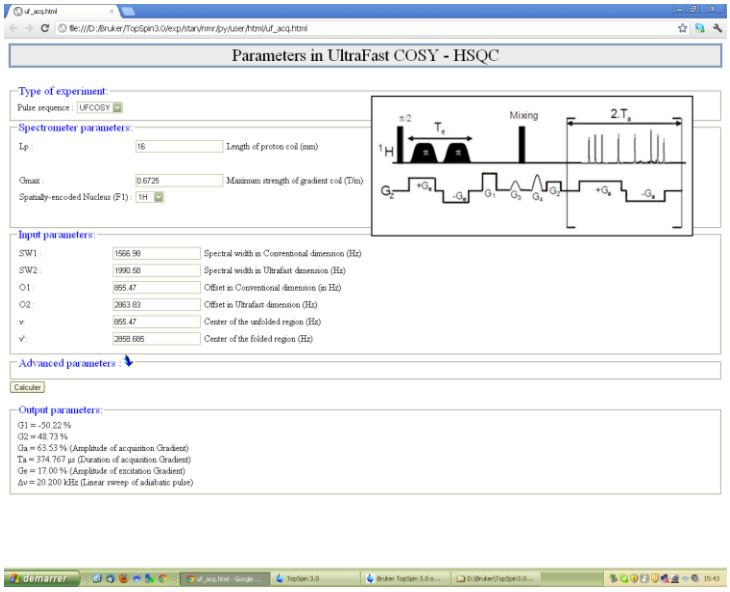

Figure 34. Screen shot of the webpage designed to facilitate the implementation of ultrafast 2D NMR experiments.

Research Article

Magnetic Resonance in Chemistry

Received: 26 October 2012 Revised: 21 December 2012 Accepted: 22 December 2012 Published online in Wiley Online Library: 24 January 2013

(wileyonlinelibrary.com) DOI 10.1002/mrc.3927

New practical tools for the implementation and use of ultrafast 2D NMR experiments

Meerakhan Pathan, Benoît Charrier, Illa Tea, Serge Akoka and Patrick Giraudeau*

Ultrafast (UF) 2D NMR is a very promising methodology enabling the acquisition of 2D spectra in a single scan. In the last few years, the analytical performance of UF 2D NMR has been highly increased, consequently maximizing its range of applications. However, its implementation and use by non-specialists are far from being straightforward, because of the specific acquisition and processing procedures and parameters characterizing UF NMR. To make this methodology implementable and applicable by non-specialists, we developed a simple routine capable of translating conventional parameters (spectral widths and transmitter frequencies) into specific UF parameters (gradient and chirp pulse parameters). This macro was subsequently implemented in a Web page, which is available for external users. Although the algorithm was designed for two widely used 2D experiments, COSY and HSQC, it can easily be extended to any other pulse sequence. The robustness of this routine was verified successfully on a variety of small molecules. We believe that this tool will eliminate much of the technical difficulties related to UF 2D NMR and will make the technique accessible to a wider audience of organic and analytical chemists.

Keywords: NMR; ^{1}H; ^{1,3}C; ultrafast 2D NMR; spatial encoding; spectral widths; COSY; HSQC; routine implementation

Introduction

Two-dimensional NMR spectroscopy (2D NMR) has revolutionized the utility of NMR as an analytical technique.[1,2] Apart from being a powerful structural elucidation tool, this technique has found applications in organic chemistry, pharmaceutical, biochemical or biomedical studies. Despite its utility, one of the major disadvantages of multidimensional NMR sequences is the time-consuming experiment duration due to the t_1 incremental procedure that is necessary to sample the indirect F_1 dimension. Several methodologies have been established to reduce the acquisition time of multidimensional NMR spectra,[3–6] amongst which stands out the so-called ultrafast (UF) 2D NMR approach proposed by Frydman and co-workers. This methodology is the one with the most drastic reduction in the experiment time, as the acquisition of 2D NMR data is carried out in a single scan.[6,10] The usual t_1 encoding is replaced by spatial encoding, followed by a conventional mixing period and by a detection block based on echo-planar imaging.[11] The principles and features of UF 2D NMR experiments have been described in details in recent literature.[12–14]

Despite its high potential, UF 2D NMR still presents limitations in terms of sensitivity, resolution and spectral width, which have been described in recent reports.[15–18] Fortunately, several improvements have contributed to significant advances in the performance of UF experiments, such as the replacement of the originally proposed discrete spatial-encoding scheme by a continuous encoding pattern,[19–22] the introduction of a multi-echo excitation scheme to deal with sensitivity losses caused by molecular diffusion[23,24] or the implementation of various strategies to overcome spectral width and line shape limitations.[16,18,25–27] Owing to these developments, it is now possible to apply this methodology to samples of increasing complexity and use it for a wide range of applications.[15,28–33]

Although UF 2D NMR presents a high potential, only a few research groups have implemented and applied this methodology.[14,15,34–40] The main reason is probably that its implementation and use by non-specialists are far from being straightforward, because of the specific acquisition and processing procedures and parameters characterizing UF NMR. Although setting a conventional 2D NMR experiment is a routine even for non-specialists, it is not so simple in the case of UF 2D NMR. In addition to the conventional parameters, the user needs to set up a number of specific parameters associated with the UF pulse sequences, such as gradient amplitudes and durations, or chirp pulse parameters. These are quite difficult to choose without a sound knowledge of this methodology.

To make this methodology implementable and applicable by non-specialists, we have developed a simple routine to make the implementation and use of UF NMR experiments accessible to non-specialists. This routine is capable of translating the conventional parameters (spectral widths and transmitter frequencies) into specific UF parameters (gradients and chirp pulse parameters). Here, we describe the principles of this simple algorithm, and we demonstrate its efficiency on a variety of small molecule samples for two of the most widely used 2D NMR experiments: COSY and HSQC.

* *Correspondence to: Patrick Giraudeau, Chimie et Interdisciplinarité: Synthèse, Analyse, Modélisation (CEISAM), UMR 6230, Faculté des Sciences, Université de Nantes, BP 92208, 2 rue de la Houssinière, F-44322 Nantes Cedex 03, France. E-mail: patrick.giraudeau@univ-nantes.fr*

CNRS, Chimie et Interdisciplinarité: Synthèse, Analyse, Modélisation (CEISAM), UMR 6230, Faculté des Sciences, Université de Nantes, BP 92208, 2 rue de la Houssinière, F-44322 Nantes Cedex 03, France

Method

Recording a conventional 2D NMR spectrum is now a routine operation as it just requires setting the spectral widths and offsets in both dimensions. On the contrary, in UF NMR, the user needs to set specific parameters (gradient durations and amplitudes, and chirp pulse parameters), which can highly impact the spectral width and resolution of the resulting spectrum. These parameters are indicated in Fig. 1 for two widely used pulse sequences: UF COSY and UF HSQC. Both sequences include a continuous spatial-encoding scheme initially proposed by Pelupessy.[39] Two 180° chirp pulses are applied following a non-selective 90° excitation, thus resulting in a constant-time spatial encoding of duration T_e. This scheme leads to a linear dephasing proportional to the product of the position along the *z*-axis and the resonance frequency. After reaching this dephasing, a mixing period is generally applied, allowing a transfer of information between coupled spins, similar to conventional 2D NMR. It preserves the dephasing obtained after spatial encoding. To refocus this dephasing and obtain an observable signal, an acquisition gradient of duration T_a and amplitude G_a is applied while the receiver is open, leading to a series of echoes at positions that are proportional to the resonance frequencies. A signal equivalent to a 1D spectrum is observed during this gradient while no FT is needed. This forms the first dimension of the 2D spectrum and is generally called 'UF dimension' as it results from the spatial-encoding process characterizing this method.

To obtain the second dimension of the 2D spectrum, a technique similar to echo-planar imaging[41] is employed. It consists in applying a series of *N* bipolar gradient pairs while detecting the signal. The alternated gradients provoke a series of refocusing and defocusing, leading to the formation of mirror-image echoes, i.e. to a series of symmetric 1D spectra. This process is performed within the same scan, typically in 100 ms. Still during this gradient train, the system continues evolving under the influence of conventional parameters such as T_2 relaxation, resonance frequency and *J*-couplings. Therefore, an appropriate data rearrangement followed by a conventional FT is required to separate the different resonance frequencies, resulting in the second dimension of the 2D NMR spectrum.[10] As this dimension arises from the evolution under the effect of conventional interactions, it is generally referred to as 'conventional dimension'.

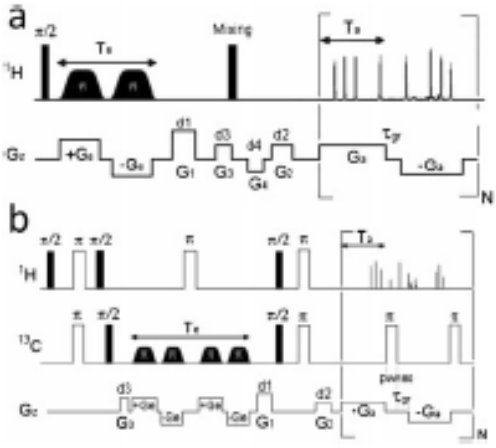

Figure 1. Pulse sequences for the acquisition of ultrafast 2D COSY (a) and HSQC (b) spectra, with phase-modulated encoding schemes proposed by Pelupessy followed by the usual echo-planar imaging detection block. G_1 and G_2 are additional gradients adjusted to fold a desired spectral region in the spatially encoded dimension.

The specific parameters of these experiments will of course impact the spectral widths and offsets of the final 2D spectrum. These parameters are specific to this kind of experiments, but relations exist that link UF parameters to the spectral ones of the final 2D spectrum. First, in the conventional FT dimension, spectral width considerations are exactly the same as in the F_1 dimension of conventional 2D NMR. The spectral window SW_1 is given by the inverse of the sampling rate $(\Delta t)^{-1}$. Therefore, SW_1 can be linked to the acquisition gradient duration T_a by the relation[14]

$$SW_1 = \frac{1}{2\left(T_a + \tau_{gr} + pw180\right)} \quad (1)$$

Here, T_a represents the duration of a single acquisition gradient, τ_{gr} stands for an intergradient delay allowing gradient recovery and *pw*180 stands for the length of the optional additional decoupling pulse in the case of heteronuclear experiments (Fig. 1). Setting the number of acquisition gradients (*N*) also defines the maximum spectral resolution in the conventional dimension. The maximum *N* value is given by the stability of the gradient system. In our experiments, we set 128 as default value: it is high enough to preserve a good resolution while avoiding the gradient instabilities that may affect the spectrum for higher values. The total number of complex points (*Td*) being collected along the spatial-encoding dimension is therefore given by $2 \cdot N \cdot T_a/dw$, where *dw* is the physical dwell time, i.e. the time between the acquisition of two successive data points. This dwell time should be chosen as short as permitted by the spectrometer to ensure a good digitization of the data in the UF dimension.

The spectral width needed in the UF dimension (SW_2) can be related to the amplitude of the spatial-encoding gradients (G_a) on the basis of the following condition[14]:

$$SW_2 \cdot f = \frac{G_a \cdot L \cdot \gamma_a}{2\pi} \quad (2)$$

where γ_a is the gyromagnetic ratio of the spatially encoded nucleus, *L* is the length of the coil of the encoded nucleus and *f* is a constant factor. To optimize the *f* value, we ran additional experiments (data not shown) where *f* ranged from 1 to 10. Beyond 10, sensitivity and resolution losses were observed because of the effect of molecular diffusion.[21,42] For *f* lower than 1, the spatial encoding is not performed homogeneously for all the chemical shifts, leading to spectral width and line shape deterioration. From these additional experiments, we chose 5 as the optimum value of *f* based on the resolution, sensitivity and spectral widths, whatever the pulse sequence used. SW_2 also fixes the frequency width of the spatial-encoding chirp pulse. The total sweep of the chirp pulse $\Delta\nu$ must be equal to the frequency dispersion induced by the spatial-encoding gradients:

$$\Delta\nu = f \cdot SW_2 \quad (3)$$

We generally set the duration of spatial encoding (T_e) as a default value of 30 ms on the basis of the optimum compromise between sensitivity and resolution,[24] which in turn sets the

Magnetic Resonance in Chemistry

duration of one chirp pulse to 15 ms. However, experimentally the spatial encoding does not have a 100% efficiency, because of numerous gradient and pulse non-idealities, particularly on the edge of the sample. Moreover, the effective T_a may be slightly dependent on chemical shift, depending on the choice of the *f* factor described earlier. To account for these non-idealities, we define an efficiency factor *e* for the spatial encoding, which leads to an effective spatial-encoding duration $T_{aff} = e \cdot T_a$. The exact value of *e* is hardware dependent and can only be determined *a posteriori* by measuring the effective characteristics of the spectrum obtained after a first implementation of the technique. However, several implementations on various NMR spectrometers show that $e = 75\%$ is generally a good approximation for using the protocol described in this report. Knowing the value of T_{aff}, we obtain the G_a value needed in order to accommodate the desired SW_i by

$$G_a = \frac{2 \cdot SW_i \cdot T_{aff} \cdot \gamma_e \cdot G_e}{T_a \cdot \gamma_a \cdot \Delta r} \quad (4)$$

where γ_a and γ_e are the gyromagnetic ratios of the detected and spatially encoded nuclei, respectively.

Once we know G_a, another parameter that needs to be determined is the filter bandwidth (*fb*), which is used to record the data points. *fb* must be set large enough to observe the frequency dispersion induced by G_a over the sample during the detection, whereas increasing it further would just add noise to the spectrum. Therefore, we have to set the *fb* with regard to the following equation[14]:

$$fb = \frac{G_a \cdot L \cdot \gamma_a}{2\pi} \quad (5)$$

Finally, the role of the additional gradient (G_z) placed just before the acquisition is to shift all the peaks of interest in the UF dimension in order to center the spectrum.[14] However, we recently showed that this gradient can also be used in combination with another gradient (G_1) placed just before the mixing period in order to fold a desired spectral region in the UF dimension.[25] This 'gradient-folding' strategy makes it possible to deal with one of the main limitations of UF NMR, i.e. the maximum accessible spectral width due to the maximum gradient amplitude available on the spectrometer.[18] The additional gradients make it possible to play with the position of the peaks in the *k*-space, thus creating some kind of folding in the spatially encoded dimension. As described in Ref. [25], this folding departs from the conventional Nyquist-based folding, as no FT is applied in this dimension. Actually, the effect of these two gradients is to shift symmetrically the two mirror-image signals that are actually detected during the first acquisition gradient, leading to the appearance of echo peaks for[25]

$$k = -C\,\Omega_1 - \gamma_a \cdot G_1 \cdot \tau_1 - \gamma_a \cdot G_2 \cdot \tau_2 \text{ and}$$
$$k' = +C\,\Omega_2 + \gamma_a \cdot G_1 \cdot \tau_1 - \gamma_a \cdot G_2 \cdot \tau_2 \quad (6)$$

where $k = G_a \cdot t_a \cdot \gamma_a$,[10] $C = 2 \cdot T_a / L$,[24] and τ_1 and τ_2 are the durations of the folding gradients G_1 and G_2, respectively. t_a represents the time when the echo is detected for a resonance frequency Ω_1. Let us assume that Ω_1 is the center of the main spectral region to be detected and that Ω_2 is the center of the spectral region that we need to fold. The pre-mixing and post-mixing gradient parameters can be chosen so that the center of these two regions appear at the center of the UF dimension, i.e. $k = k' = G_a \cdot T_a \cdot \gamma_a / 2$.

On the basis of the aforementioned relations, we developed a simple pre-acquisition routine (Fig. 2), which is capable of translating the conventional parameters such as spectral widths and offsets into UF specific parameters. It also includes the possibility of folding a desired region in the UF dimension. For that, the user just needs to define a limited number of conventional

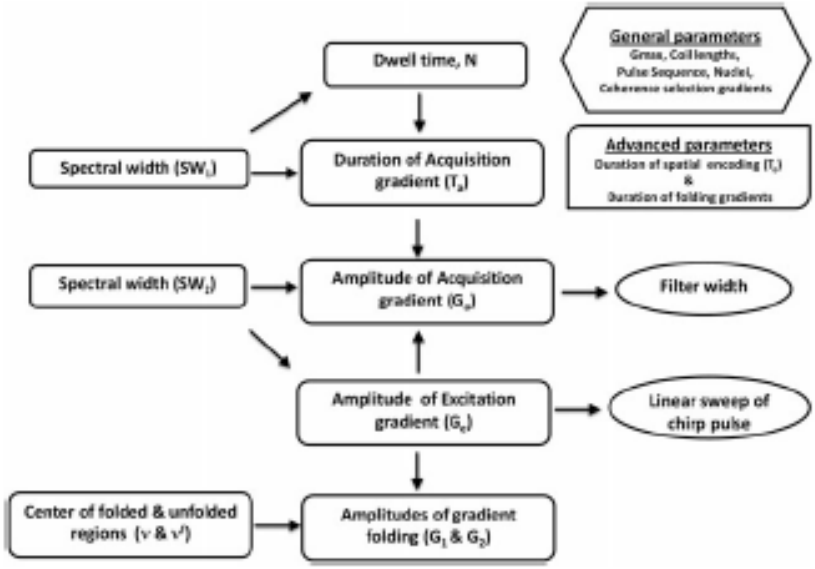

Figure 2. Basic scheme of our pre-acquisition routine. By defining the spectral widths and offsets in both dimensions, we can automatically calculate the ultrafast specific parameters. The macro also offers the possibility to fold a desired region in the spatially encoded dimension.

parameters, provided that the experiments have been implemented on the spectrometer once. The user first sets the desired spectral widths and offsets in the two dimensions, exactly as he or she would do for a conventional acquisition. Then he or she has the option to choose the offset of the region that he or she may want to fold in the UF dimension. If the option is not chosen, the algorithm will ensure that a region devoid of peaks (0 to −5 ppm for ^{1}H NMR, for example) is folded. From these initial input parameters, our algorithm automatically calculates the UF specific parameters, and the user just needs to set them on the spectrometer. To use this pre-acquisition macro, a number of general parameters also need to be defined, such as the length of the coil (available from the manufacturer), the maximum gradient strength (which can be obtained either from the manufacturer's specifications or by using simple calibration protocols[46]), the gyromagnetic ratios of the nuclei or the conventional coherence selection gradients.

The full routine has been implemented onto a Web page (http://www.sciences.univ-nantes.fr/CEISAM/ebci/ultrafast/uf_acq.html), so far, for COSY and HSQC. Other pulse sequences can be implemented on demand. The Web page can also be downloaded for local use. Together with this routine, the files necessary for acquiring and processing the data are available, as well as a protocol describing how to implement these experiments on a Bruker spectrometer (Bruker Biospin, Rheinstetten, Germany).

Applications and Discussion

As described earlier, this routine was developed and tested for the UF COSY and UF HSQC pulse sequences (Fig. 1). It was first tested to record the COSY spectrum of a metabolic mixture, which exhibits resonances between 0.78 and 4.5 ppm; on the basis of which, spectral widths $SW_1 = SW_2 = 1700$ Hz and offsets $O_1 = O_2 = 1005$ Hz were chosen and were set as input parameters onto the Web page. It provided us a set of UF specific parameters whose values are given in Table 1. We further prepared a translation between these values into Bruker pulse sequence parameters (also given on the Web page), set them directly on the spectrometer and recorded the UF COSY spectrum of metabolic mixtures (Fig. 3) with no other setting or adjustment than classical NMR experiment settings (i.e. shimming, matching and tuning, and calibration of the hard pulses). After processing the spectrum with our homemade routine working in Topspin, the spectral widths on both dimensions and the offsets were measured. As can be seen in Fig. 3, the spectral widths and offsets are in good agreement with the input values. However, there is a slight deviation between the input and observed values, which cannot be avoided because of the numerous non-idealities of the pulses and gradients. To obtain a reliable chemical shift scale, this deviation needs to be corrected, and this can be easily carried out with a graphical calibration tool that is also available for download and fully integrated to the commercial software.

To illustrate the efficiency of our algorithm in the case of heteronuclear 2D NMR, we applied it to record the ^{1}H–^{13}C HSQC spectrum of a D-glucose sample. We first recorded the ^{1}H and ^{13}C 1D spectra, as one would do before recording a conventional HSQC spectrum. The ^{13}C NMR spectrum shows that the corresponding resonances cover a 60-ppm range, which is too big to obtain a UF spectrum in a single scan without losing resolution. Therefore, we chose to use the folding option in our Web page. In the proton dimension, we defined $SW_1 = 1300$ Hz and

Table 1. Input parameters used for the determination of ultrafast specific parameters with our routine and output parameters obtained for different samples and pulse sequences

Sample	Input parameters					Output parameters							
	SW_1 (Hz)	SW_2 (Hz)	O_1 (Hz)	O_2 (Hz)	γ' (Hz)	T_e (µs)	G_e (T/m)	G_e (T/m)	$\Delta\nu$ (Hz)	dw (µs)	fb (kHz)	G_1 (T/m)	G_2 (T/m)
UF COSY													
Metabolic mixture	1700	1700	1005	1005	—	274	0.41	0.0125	8500	0.574	279	−0.1107	0.0995
Ibuprofen	1500	1500	855.5	855.5	2893.4	300	0.34	0.0114	7750	0.63	230	−0.1441	0.1338
Ethylacetonate	1500	1500	1028.7	1028.7	2573.5	300	0.34	0.0114	7750	0.63	230	−0.1408	0.1306
UF HSQC													
D-glucose	1300	3000	1653	6884	9446.3	341	0.362	0.0135	15000	0.75	383	−0.41	−0.01
Ibuprofen	1238	3330	855.5	3199.8	13460.5	367	0.381	0.0114	16650	0.79	399	−0.36	0.22

SW_1 and SW_2 spectral widths in the conventional and ultrafast dimensions, respectively; O_1, offset in the conventional F_1 dimension; O_2, offset in the ultrafast F_2 dimension; γ', center of the folded region in the ultrafast dimension; T_e, duration of the acquisition gradients; G_e, amplitude of the acquisition gradients; G_e, amplitude of the spatial-encoding gradients; $\Delta\nu$, sweep width of chirp pulses; dw, dwell time; fb, filter width of the spectrometer; G_1 and G_2 amplitude of folding gradients.

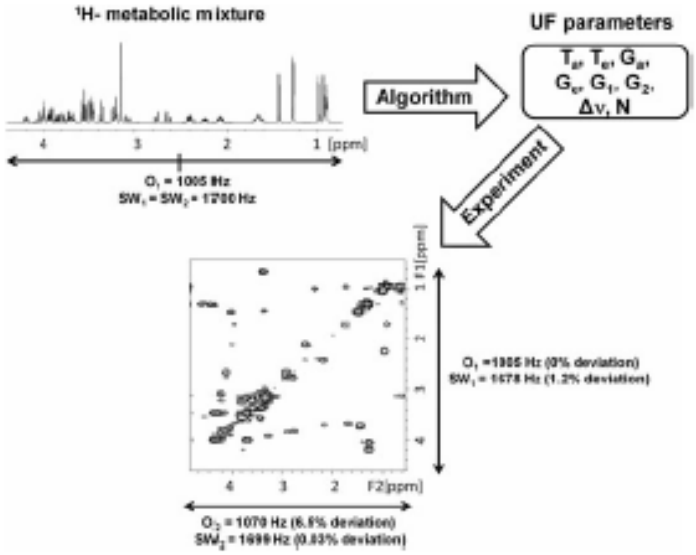

Figure 3. Illustration of the setting of an ultrafast (UF) COSY experiment with our pre-acquisition routine. The ^{1}H spectrum of the sample (here, a metabolic mixture) is first recorded to define the target spectral width and offset. From these parameters, the macro calculates the UF specific parameters, which are then set on the spectrometer to record the 2D UF COSY spectrum. After processing and calibration, the spectral characteristics of the final spectrum are compared with the initial input values. The spectra were recorded at 298 K and 400.13 MHz on a Bruker AVANCE I spectrometer.

O_1 = 1653 Hz. In the carbon dimension, we set SW_2 = 3000 Hz as observable window, O_2 (center of the main, unfolded region) = 6884 Hz and $\sqrt{}$ (center of folded region) = 9446 Hz. By setting these parameters as input in our Web page, we calculated the UF specific parameters shown in Table 1. Then we set them directly on the spectrometer and recorded the UF HSQC spectrum of theo-glucose sample (Fig. 4). The folded peaks are highlighted with a circle in the spectrum. We measured the deviation between the input and observed values of spectral widths and offsets. As for the precedent example, the spectral characteristics of the final spectrum are in good agreement with the input values. Still, there is a slight deviation between the input and observed values that needs to be corrected with our graphical calibration tool.

To determine the overall robustness of our algorithm, UF COSY and UF HSQC spectra were recorded for a variety of samples by using our Web page. The input and output parameters are given in Table 1 for each molecule. We measured the deviations between the input and observed values of spectral widths and offsets. This deviation is less than 10% for all the samples (Table 2) and can be perfectly corrected with the calibration tool described earlier. The results highlight the efficiency of our algorithm.

Troubleshooting

Despite all the care taken to design a robust user interface, it may happen that the user meets additional difficulties in setting the UF experiments described in this paper. These problems are generally the result of the user's specific hardware limitations or sometimes of a misunderstanding of the non-conventional behavior of UF techniques. To help the user in dealing with such problems, we provide, in addition to the implementation protocol mentioned previously, a troubleshooting table (Table 3) describing the most common errors that can be met in the setting of UF experiments, as well as a description of their causes and remedies. This table also includes, when available, a reference to a more detailed description of the problem. Of course, Table 3 is not exhaustive, and the authors would appreciate receiving comments and questions about problems that are not listed here.

The stability of the gradient amplifier is of particular importance to the success of UF experiments. As described in Table 3, a small gradient offset is very common on modern spectrometers and leads to a linear deviation of the position of echoes in the course of acquisition, resulting in twisted 2D peak shapes. Fortunately, such a deviation is automatically compensated by a shearing transformation included in the processing routine provided online or, if necessary, by slightly adjusting the amplitude of the negative acquisition gradient. In some very rare cases, a nonlinear deviation of the peak position was observed, which is characteristic of a more serious instability of the gradient amplifier. Such non-idealities, which increase for high gradient amplitudes, result in poor quality 2D spectra and can only be solved by updating the hardware.

Experimental

To obtain the metabolite solution, a phosphate buffer solution (pH 7.4, 0.1 M) in D_2O was prepared. A reference sample containing eight metabolites (alanine, glutamic acid, lactic acid, myo-inositol, taurine, threonine, leucine and valine) was dissolved in 1 ml of this buffer solution to obtain a sample at a

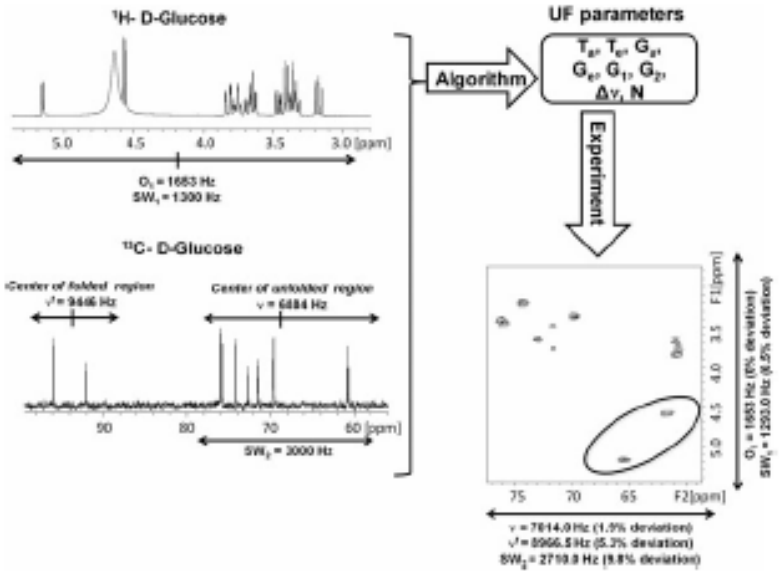

Figure 4. Illustration of the setting of an ultrafast (UF) HSQC experiment with our pre-acquisition routine. The ^{1}H and ^{13}C spectra of the α-glucose sample are first recorded to define the target spectral widths and offsets in the two dimensions. On the ^{13}C spectrum, the center $\sqrt{\nu}$ of the spectral region to be folded in the ultrafast dimension is also defined. From these parameters, the macro calculates the UF specific parameters, which are then set on the spectrometer to record the 2D UF COSY spectrum. After processing and calibration, the spectral characteristics of the final spectrum are compared with the initial input values. The spectra were recorded at 298 K and 400.13 MHz on a Bruker AVANCE I spectrometer.

Table 2. Deviation between the spectral characteristics of the ultrafast spectra obtained from the parameters set with our pre-acquisition routine and the input parameters used to calculate the acquisition parameters

	Input parameters				Deviation (experimental)			
Sample	SW_1 (Hz)	SW_2 (Hz)	O_2 (Hz)	$\sqrt{\nu}$ (Hz)	SW_1 (%)	SW_2 (%)	O_2 (%)	$\sqrt{\nu}$ (%)
UF COSY								
Metabolic mixture	1700	1700	1005	—	1.2	−0.03	6.5	—
Ibuprofen	1550	1550	855	2893	−0.9	−1.05	2.5	−1.07
Ethyl crotonate	1550	1550	1028	2573	−0.6	−8.6	2.7	−7.4
UF HSQC								
α-glucose	1300	3000	6884	9466	0.5	−9.6	1.9	−5.3
Ibuprofen	1228	3330	3199	13460	0.2	−3.0	−3.3	−0.4

SW_1 and SW_2, spectral widths in the conventional and ultrafast dimensions, respectively; O_1, offset in the conventional F_1 dimension; O_2, offset in the ultrafast F_2 dimension; $\sqrt{\nu}$, center of the folded region in the ultrafast dimension.

10-mM concentration of each metabolite. The ibuprofen sample was prepared at a 100-mM concentration as described in Ref. [29]. The α-glucose solution was prepared by dissolving 270 mg of α-glucose in 750 µl of D_2O. The sample was transferred to the NMR tube after several hours for analysis, to make sure that the mutarotation equilibrium was reached. The ethyl-crotonate was prepared in deuterated dimethyl sulfoxide at a 100-mM concentration. All the samples were analyzed in 5-mm NMR tubes.

The NMR spectra were recorded at 298 K on a Bruker AVANCE I 400 spectrometer, at a ^{1}H frequency of 400.13 MHz with a 5-mm dual probe equipped with z-axis gradients. The conventional 1D experiments were recorded with routine pulse sequences available within the commercial software Bruker Topspin 2.1. For all the UF experiments, the spatial encoding was performed using a constant-time spatial-encoding scheme with two successive 15-ms smoothed chirp encoding pulses. The UF specific parameters were set from the user-defined spectral widths and offsets, according to our routine, as described in Table 1. To set the gradient amplitudes in percentage, we calculated the maximum gradient amplitude (G_{max} = 0.816 T/m) available on the spectrometer in accordance with the protocol described in Refs [42,46]. L values are 0.016 and 0.0165 m for the proton and carbon coils, respectively, for the probe used in this study. It was not always possible to set exactly the filter bandwidth (fb) values calculated by our routine on our spectrometer. This was

Table 3. Frequently encountered difficulties in setting the ultrafast experiments with the protocol described in this paper

Problems	Possible causes	Solutions	Ref.
The peaks appear twisted	Gradient linear offset leading to data shearing in the course of the acquisition	(1) The processing macro (ufproc) provided should correct it (2) If it does not, try to slightly modify the ratio between acquisition gradients (for example, by setting $+G_z = 80\%$ and $-G_z = -80.01\%$)	[44]
The peaks are not well defined and spread over a wide range	Gradient amplitude instabilities in the train of acquisition gradients	(1) Reduce the acquisition gradient amplitude (2) If the problem persists, this may come from the instability of your gradient amplifier. Contact your manufacturer	
The peaks show asymmetric sinc wings	Gradient non-uniformity on the edge of the sample	Apply a Gaussian spatial apodization in F_2 (included in the processing routine)	[27]
The resolution in F_2 is disappointing	(1) The chirp pulses are overcalibrated	(1) Decrease the power of the spatial-encoding pulses and see if resolution is improved (may decrease the spectral width in F_2)	
	(2) The spatial apodization is too strong	(2) Decrease the line broadening of the spatial apodization	
All the peaks are split in two along F_2	The processing program does not manage to adjust the offset between datasets corresponding to + and − acquisition gradients	Run the processing with the positive gradients only (ufproc +)	
The spectrum is shifted in F_2	The pre-acquisition gradient is not adjusted	Adjust the pre-acquisition gradient (G_z or d_2) to move the spectrum in the center of the window	[28]
The peaks are folded in F_1	(1) The spectral width you are trying to observe is too high	(1) Decrease the F_1 spectral width (SW_1) in the pre-acquisition Web page	
	(2) The F_1 offset is not correctly defined	(2) Adjust the offset in the conventional dimension (F_1)	
The folding procedure in F_2 is not working	Gradient calibration error	(1) Check that your gradients are correctly calibrated (see protocol provided with the Web page) (2) Run the pre-acquisition macro again and perform a new acquisition (3) If the problem persists, slightly change the amplitude of the pre-acquisition gradient G_1	[28]
The observed spectral width in F_2 does not correspond to my input *SW*	(1) The chirp pulses are overcalibrated or	(1) Decrease the power of the spatial-encoding pulses	
	(2) The efficiency of spatial encoding (see advanced parameters) is not correct	(2) Try different values for the efficiency parameter and run successive acquisitions until the observed *SW* matches the expected one. Once calibrated, the efficiency parameter is valid for other experiments	
Numerous artifacts are present on the spectrum	(1) The coherence selection is not working properly	(1) Check that all the coherence selection gradients are correctly set	
	(2) The hard pulses are not well calibrated	(2) Check that the probe is correctly tuned and matched and that the hard pulse calibration is correct	
	(3) The chirp pulses are undercalibrated	(3) Increase the power of the spatial-encoding pulses	
I do not see any signal	(1) There is an error in parameter setting	(1) Check that all the acquisition parameters conform to those given by the pre-acquisition routine and implementation protocol	[30]
	(2) The sensitivity is not sufficient	(2) Check that the sample is concentrated enough and/or increase the number of scans	

due to the limited available *fb* values; therefore, we selected the nearest higher *fb* available. All the spectra were acquired and analyzed using the Bruker program Topspin 2.1. The specific processing and calibrating for the UF spectra was performed using our home-written routine in Topspin, including apodization and zero filling as described in Ref. [29]

The routine for setting the UF specific NMR parameters was written in the Javascript programming language. The processing and graphical calibration tools working under the Bruker Topspin commercial software were written using the Jython language (Jython is Python using Java classes).

Conclusion

The results highlight the potentialities of our routine for setting up UF 2D NMR experiments. It unlocks a new door towards the implementation of UF 2D NMR as a routine methodology. Our Web page is available for free download at http://www.sciences.univ-nantes.fr/CEISAM/ebsi/ultrafast/uf_acq.html. In addition to the Web page, we have provided a detailed protocol for the initial implementation of experiments, as well as processing programs, calibration tool and pulse programs of UF COSY and UF HSQC.

Acknowledgements

The authors acknowledge Michel Giraudeau for the linguistic assistance. This research was supported by funding from the 'Agence Nationale de la Recherche' for young researchers (ANR grant 2010 JCJC 080401).

References

[1] J. Jeener, *Lecture Presented at Ampere International Summer School II*, Basko Polje, Yugoslavia, **1971**.
[2] W. P. Aue, E. Bartholdi, R. R. Ernst. *J. Chem. Phys.* **1976**, *64*, 2229–2246.
[3] V. A. Mandelshtam, H. S. Taylor, A. J. Shaka. *J. Magn. Reson.* **1998**, *133*, 304–312.
[4] R. Brüschweiler, F. Zhang. *J. Chem. Phys.* **2004**, *120*, 5253–5260.
[5] E. Kupce, R. Freeman. *J. Magn. Reson.* **2003**, *162*, 300–310.
[6] E. Kupce, R. Freeman. *J. Am. Chem. Soc.* **2004**, *126*, 6429–6440.
[7] P. Schanda, B. Brutscher. *J. Am. Chem. Soc.* **2005**, *127*, 8014–8015.
[8] B. Vitorge, G. Bodenhausen, P. Pelupessy. *J. Magn. Reson.* **2010**, *207*, 149–152.
[9] L. Frydman, T. Scherf, A. Lupulescu. *Proc. Natl. Acad. Sci. USA* **2002**, *99*, 15858–15862.
[10] L. Frydman, A. Lupulescu, T. Scherf. *J. Am. Chem. Soc.* **2003**, *125*, 9204–9217.
[11] P. Mansfield. *Magn. Reson. Med.* **1984**, *1*, 370–386.
[12] M. Gal, L. Frydman, in *Encyclopedia of NMR*, vol. 10 (Eds.: D. M. Grant, R. K. Harris), Wiley, New-York, **2009**.
[13] M. Mishkovsky, L. Frydman. *Annu. Rev. Phys. Chem.* **2009**, *60*, 429–448.
[14] A. Tal, L. Frydman. *Prog. Nucl. Magn. Reson. Spectrosc.* **2010**, *57*, 241–292.
[15] P. Giraudeau, G. S. Remaud, S. Akoka. *Anal. Chem.* **2009**, *81*, 479–484.
[16] P. Pelupessy, L. Duma, G. Bodenhausen. *J. Magn. Reson.* **2008**, *194*, 169–174.
[17] Y. Shrot, L. Frydman. *J. Am. Chem. Soc.* **2008**, *128*, 16451-3.
[18] Y. Shrot, L. Frydman. *J. Chem. Phys.* **2009**, *131*, 224516.
[19] P. Pelupessy. *J. Am. Chem. Soc.* **2003**, *125*, 12345–12350.
[20] B. Shapira, Y. Shrot, L. Frydman. *J. Magn. Reson.* **2006**, *178*, 33–41.
[21] Y. Shrot, B. Shapira, L. Frydman. *J. Magn. Reson.* **2004**, *171*, 163–170.
[22] Y. Shrot, L. Frydman. *J. Chem. Phys.* **2008**, *128*, 052209.
[23] P. Giraudeau, S. Akoka. *J. Magn. Reson.* **2008**, *195*, 9–16.
[24] P. Giraudeau, S. Akoka. *J. Magn. Reson.* **2008**, *190*, 339–345.
[25] P. Giraudeau, S. Akoka. *J. Magn. Reson.* **2010**, *205*, 171–176.
[26] P. Giraudeau, Y. Shrot, L. Frydman. *J. Am. Chem. Soc.* **2009**, *131*, 13902–13903.
[27] P. Giraudeau, S. Akoka. *Magn. Reson. Chem.* **2011**, *49*, 307–313.
[28] A. Herrera, E. Fernandez-Valle, E. M. Gutiérrez, R. Martínez-Alvarez, D. Molero, Z. D. Pardo, E. Saez. *Org. Lett.* **2010**, *12*, 144–147.
[29] P. Giraudeau, S. Massou, Y. Robin, E. Cahoreau, J.-C. Portais, S. Akoka. *Anal. Chem.* **2011**, *83*, 3112–3119.
[30] M. Pathan, S. Akoka, I. Tea, B. Charrier, P. Giraudeau. *Analyst* **2011**, *136*, 3157–3163.
[31] M. Pathan, S. Akoka, P. Giraudeau, *J. Magn. Reson.* **2012**, *214*, 335–339.
[32] T. Roussel, P. Giraudeau, H. Rattney, S. Akoka, S. Caravella. *J. Magn. Reson.* **2012**, *215*, 50–55.
[33] P. Giraudeau, T. Montag, B. Charrier, C. M. Thiele, *Magn. Reson. Chem.* **2012**, *50*, 553–557.
[34] M. Gal, T. Kern, P. Schanda, L. Frydman, B. Brutscher. *J. Biomol. NMR* **2009**, *43*, 1–10.
[35] P. Giraudeau, P. Lemeunier, M. Coutand, J.-M. Doux, A. Gilbert, G. S. Remaud, S. Akoka. *J. Spectrosc. Dyn.* **2011**, *1*, 2.
[36] N. S. Andersen, W. Kiddenberger. *Magn. Reson. Chem.* **2005**, *43*, 791–794.
[37] Z. D. Pardo, G. L. Olsen, M. E. Fernández-Valle, L. Frydman, R. Martínez-Álvarez, A. Herrera. *J. Am. Chem. Soc.* **2012**, *134*, 2706–2715.
[38] A. Herrera, E. Fernández-Valle, R. Martínez-Álvarez, D. Molero, Z. D. Pardo, E. Sáez, M. Gal. *Angew. Chem. Int. Ed.* **2009**, *48*, 6274–6277.
[39] C. Wu, M. Zhao, S. Cai, Y. Lin, Z. Chen. *J. Magn. Reson.* **2010**, *204*, 82–90.
[40] L. H. K. Queiroz Junior, D. P. K. Queiroz, L. Dhooghe, A. G. Ferreira, P. Giraudeau. *Analyst* **2012**, *137*, 2357–2361.
[41] P. Mansfield, P. G. Morris, *NMR Imaging in Biomedicine*, Academic Press, New-York, **1982**.
[42] Y. Shrot, L. Frydman. *J. Chem. Phys.* **2008**, *128*, 164513.
[43] L. H. K. Queiroz Junior, A. G. Ferreira, P. Giraudeau, *Química Nova* **2012**, *in press*.
[44] M. Gal, L. Frydman, in *Encyclopedia of Magnetic Resonance* (Eds.: G. A. Morris, J. W. Emsley), Wiley, Chichester, **2010**, pp. 43–60.

Part C

Multi-Scan-Single-Shot (M3S) ultrafast 2D NMR

Chimie Et Interdisciplinarité
Synthèse, Analyse, Modélisation
CEISAM
UMR CNRS 6230
UNIVERSITÉ DE NANTES

The analytical performances of uf 2D NMR have been highly increased in the last few years. Our group has sucessufully evaluated the analytical performance of ultrafast homo-nuclear experiments in terms of repetability and reproducibility [17]. However little is known about the sensitivity of ultrafast experiments versus conventional 2D NMR. A fair and relevant comparison has to consider the SNR ratio per unit of time, in order to answer the following question: for a given experiment time (*e.g.* 1 h), should we run a conventional 2D experiment or is it preferable to accumulate ultrafast acquisitions.

To answer this question, we introduced a "Multi-Scan-Single Shot" (M3S) strategy in ultrafast experiments and performed a systematic comparison between accumulated-ultrafast experiments and conventional acquisitions, for different experiment times and pulse sequences. SNRs were measured along both dimensions for accumulated ultrafast and conventional experiments with identical experiment durations on the same sample. Assuming that the sensitivity of 2D experiments is limited by the dimension where the SNR has the lowest value, it was found that the sensitivity per unit of time is much higher in ultrafast NMR (*e.g.* by a factor of 5 for COSY). This result is mainly attributed to the absence of t_1 noise in ultrafast experiments and highlights the interest of accumulating ultrafast signals instead of conventional ones to improve sensitivity. Moreover, these "M3S" experiments offer a high flexibility, due the possibility to interleave acquisitions to access larger spectral widths.

We applied this "multi-scan single shot" (M3S) COSY strategy, for measuring absolute metabolite concentrations in complex mixtures with a high precision in a reasonable time. The analytical performance of this methodology was compared to the one of conventional 2D-NMR. Later the M3S COSY approach was then applied to measure the absolute metabolite concentration in breast cancer cell line extracts, relying on a standard addition protocol.

In the last section, we introduce the M3S strategy in hetero-nuclear experiments, particulary in ufHSQC (unpublished results). We evaluated the analytical performance of this technique by applying on a model metabolic mixture with respect to conventional 2D HSQC. We introduced a CPMG block in ufHSQC to study the influence of the *J*-modulation effects on the relative standard deviation of the peak volumes. At the end we introduced the adiabatic and Fantastic pulses to improve the analytical performance of the M3S HSQC experiments.

1. Interest of the M3S approach

Analyst

Dynamic Article Links

Cite this: *Analyst*, 2011, **136**, 3157

www.rsc.org/analyst

PAPER

"Multi-scan single shot" quantitative 2D NMR: a valuable alternative to fast conventional quantitative 2D NMR

Meerakhan Pathan, Serge Akoka, Illa Tea, Benoît Charrier and Patrick Giraudeau*

Received 4th April 2011, Accepted 20th May 2011
DOI: 10.1039/c1an15278e

Quantitative Ultrafast (UF) 2D NMR is a very promising methodology enabling the acquisition of 2D spectra in a single scan. The analytical performances of UF 2D NMR have been highly increased in the last few years, however little is known about the sensitivity of ultrafast experiments *versus* conventional 2D NMR. A fair and relevant comparison has to consider the Signal-to-Noise Ratio (SNR) per unit of time, in order to answer the following question: for a given experiment time, should we run a conventional 2D experiment or is it preferable to accumulate ultrafast acquisitions? To answer this question, we perform here a systematic comparison between accumulated ultrafast experiments and conventional ones, for different experiment durations. Sensitivity issues and other analytical aspects are discussed for the COSY experiment in the context of quantitative analysis. The comparison is first carried out on a model sample, and then extended to model metabolic mixtures. The results highlight the high analytical performance of the "multi-scan single shot" approach *versus* conventional 2D NMR acquisitions. This result is attributed to the absence of t_1 noise in spatially encoded experiments. The multi-scan single shot approach is particularly interesting for quantitative applications of 2D NMR, whose occurrence in the literature has been greatly increasing in the last few years.

1. Introduction

Two-dimensional Nuclear Magnetic Resonance (2D NMR)[1,2] is a widely used methodology in analytical chemistry, whose applications have been mainly directed towards structural analysis of molecular species. More recently, a number of studies have highlighted the high potential of 2D NMR for quantitative analysis of complex mixtures presenting a high level of spectral overlap on 1D NMR spectra.[3–8] However, the routine use of 2D NMR for quantitative analysis is not straightforward, first because quantitative analysis by 2D NMR generally requires a calibration procedure due to the multi-pulse nature of 2D NMR experiments, and above all because of the long experiment duration that is necessary to obtain such a calibration curve. This duration is due to the necessity of collecting an array of transients to sample the indirect dimension. It makes 2D NMR experiments particularly sensitive to spectrometer instabilities, leading to the formation of t_1 noise in the indirect dimension.[9,10] From the quantitative point of view, it was shown that long experiments were more sensitive to these instabilities, leading to a degradation of precision.[6] Consequently, beyond the timetable constraints caused by the experiment duration, short experiments are less sensitive to such instabilities and show a better repeatability, as long as the sensitivity and the resolution are sufficient to quantify relevant peaks with the target precision. Therefore, recent studies have highlighted the need to decrease as much as possible the duration of quantitative 2D NMR experiments by optimizing acquisition and processing parameters.[3,6,11] A variety of homonuclear and heteronuclear methods have been optimized, and quantitative 2D NMR measurements can now be obtained in a short time (typically 5 to 20 minutes) with a good precision and linearity.

On the other hand, NMR spectroscopists have recently developed a number of approaches departing from the classical parametric incrementation scheme in order to drastically reduce the duration of 2D NMR experiments,[12–18] but most of them have never been evaluated for quantitative analysis. The most impressive one is probably ultrafast 2D NMR,[13,19,20] capable of providing a complete 2D correlation in a single scan, *i.e.* in a fraction of a second. It relies on a spatial-encoding procedure over the sample length which has been described in detail in recent papers.[21–23] This methodology initially suffered from important limitations in terms of resolution and sensitivity,[24–26] but over the last few years, several significant improvements have increased its analytical performance,[27–29] making it suitable for quantitative analysis of complex mixtures.[30] Thanks to these high potentialities, we recently applied ultrafast 2D NMR to quantitative kinetic studies,[31] and to the measurement of specific isotopic enrichments in complex biological mixtures.[32]

The ultrafast quantitative approach is potentially much faster than its conventional counterpart provided that the sensitivity is

Université de Nantes, CNRS, Chimie et Interdisciplinarité : Synthèse, Analyse, Modélisation (CEISAM), UMR 6230, Faculté des Sciences, BP 92208, 2 rue de la Houssinière, F-44322 Nantes Cedex 03, France. E-mail: patrick.giraudeau@univ-nantes.fr; Fax: +33 (0)2 51 12 57 12; Tel: +33 (0)2 51 12 57 09

sufficient. However, the question of the relative sensitivity per unit of time of ultrafast 2D NMR *versus* its conventional counterpart has never been addressed so far. It is a central question for quantitative analysis of mixtures, as sensitivity determines the quantification and detection limit of an analytical method. It is fairly intuitive that a one-scan ultrafast experiment is less sensitive than a conventional experiment where signal is accumulated during several minutes or hours. But a fair and relevant comparison has to consider the Signal-to-Noise Ratio (SNR) per unit of time, in order to answer the following question: for a given experiment time (*e.g.* 30 min), should we run a conventional 2D experiment or is it preferable to accumulate ultrafast acquisitions for 30 min? The latter strategy, which could be named "multi-scan single shot" 2D NMR, has never been evaluated and compared to conventional 2D NMR.

To answer this question, we perform here a systematic comparison between accumulated ultrafast experiments and conventional ones, for different experiment durations. Sensitivity issues and other analytical aspects are discussed for the COSY experiment in the context of quantitative analysis. The comparison is first carried out on a model sample, and then extended to model metabolic mixtures. The advantages and drawbacks of the two approaches are discussed.

2. Results and discussion

2.1 Analytical performance on a model sample

The COSY experiment was chosen as a model to compare the relative sensitivity of ultrafast *versus* conventional 2D experiments, due to its widespread use in analytical chemistry and to its simplicity in terms of pulse sequences. The two strategies to obtain quantitative 2D NMR spectra are described in Fig. 1. The Ultrafast COSY pulse sequence (Fig. 1a) is a constant-time experiment,[26] therefore it is compared to its conventional counterpart, constant-time (CT) COSY (Fig. 1b), which offers a higher sensitivity than conventional COSY in the indirect domain.[33]

In Ultrafast 2D NMR (Fig. 1a), the whole 2D FID is recorded in a single scan, but several FIDs can be accumulated for the sake of sensitivity. Therefore the total experiment duration T_a is given by NS × TR, where NS is the number of accumulations and TR is the duration of the pulse sequence, mainly dictated by the recovery delay. In conventional 2D NMR (Fig. 2b), the experiment duration is N_1 × NS × TR, where N_1 is the number of increments in the indirect dimension.

In order to compare the sensitivity of both experiments per unit of time, a series of COSY spectra was recorded on a model ethanol sample characterized by a unique pair of correlation signals on the COSY spectrum. The spectra were recorded under quantitative conditions (TR = $5T_1^{max}$, where T_1^{max} was found equal to 5.5 s for both CH_2 and CH_3) with experiment durations ranging from *ca.* 30 s to 1 h for ultrafast COSY. For conventional 2D NMR, only two T_a values (30 min (NS = 1) and 1 h (NS = 2)) were employed with N_1 = 64, as shorter durations led to a considerable decrease in resolution due to lower N_1 values. As detailed in the Experimental section, all the acquisition and processing parameters were optimized to ensure the highest sensitivity for each method. All the spectra were recorded five times successively to obtain average SNR values associated with standard deviations.

The SNR values were measured for all the spectra in the two dimensions of the 2D correlation for the CH_3–CH_2 correlation peak. SNR was plotted as a function of $T_a^{1/2}$, as SNR = $f(T_a^{1/2})$ is expected to give a linear relationship.[34] The corresponding results are plotted in Fig. 2. In this figure, the vertical dimension corresponds to the indirect t_1 dimension for the conventional experiments and to the so-called "conventional" dimension of ultrafast experiments (*i.e.* the dimension where data acquired during successive acquisition gradients are Fourier-Transformed). The

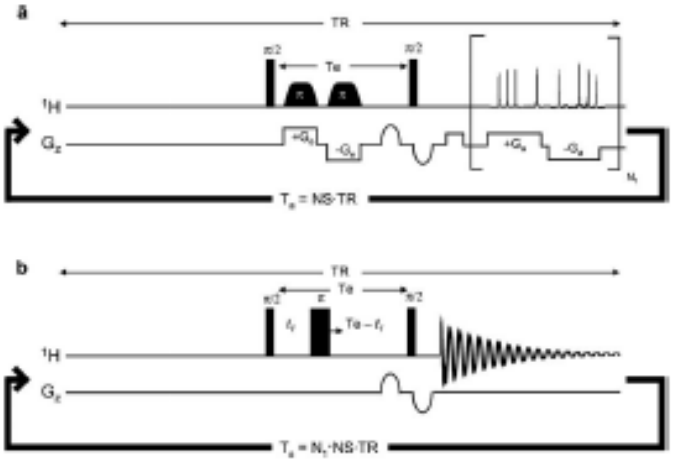

Fig. 1 Strategies for recording quantitative 2D NMR constant-time COSY spectra, (a) by accumulating NS ultrafast experiments or (b) by accumulating NS scans for each N_1 increment of a conventional 2D pulse sequence.

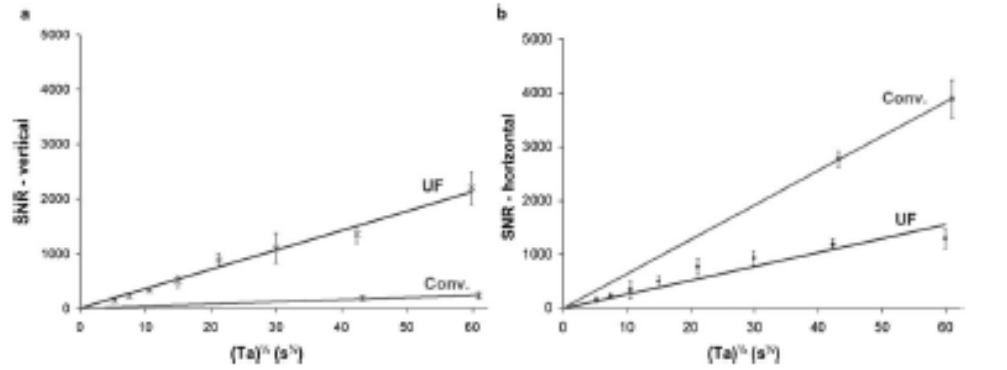

Fig. 2 Signal-to-noise ratio (SNR) as a function of the square root of the acquisition time, in the vertical (a) and horizontal (b) dimensions of ultrafast and conventional constant-time COSY spectra. The spectra were acquired on a 100 mM model ethanol sample on a 400 MHz spectrometer, with experimental parameters as indicated in the manuscript. Each data point in the graph is the average of 5 successive experiments.

horizontal dimension stands for the direct dimension of conventional experiments and corresponds to the spatially encoded dimension of ultrafast spectra. It clearly appears in Fig. 2 that the SNR in each dimension highly depends on the acquisition method. In the vertical dimension (Fig. 2a), the sensitivity is much higher for ultrafast experiments (*e.g.* by a factor of 9 for 1 h experiments). This result is attributed to the presence of t_1 noise in the indirect dimension of conventional experiments, whereas t_1 noise is intrinsically absent from ultrafast 2D correlations. On the other hand, the sensitivity in the horizontal dimension is better for conventional experiments than for their ultrafast counterpart. This is mainly due to much larger receiver bandwidths in ultrafast acquisitions.[11,20] Moreover, ultrafast experiments are sensitive to diffusion losses in the spatially encoded dimension.[20,38]

In view of these apparently ambivalent results, it is necessary to define a precise criterion to compare the sensitivity of the two approaches. From the quantitative point of view, the detection and quantification limits are determined by the "limiting SNR", *i.e.* the SNR in the dimension where it reaches its lowest value. It is relatively straightforward to conceive that a spectrum with a SNR of 2800 in one dimension but with a SNR of 180 in the other one would be far less precise than an experiment with a SNR of 1200 in both dimensions (approximate values obtained in Fig. 2 for $T_a = 30$ min). From the results plotted in Fig. 2, it appears that this limiting SNR stands in the vertical dimension for conventional experiments and in the horizontal dimension for ultrafast ones. But whereas SNR values in the two dimensions are not very different on ultrafast spectra, there is more than one order of magnitude between SNR values in the two dimensions of conventional spectra. As a consequence, the limiting SNR is much lower for conventional spectra. Based on the limiting SNR values, ultrafast 2D NMR appears far more efficient for quantitative purposes than conventional 2D, *e.g.* by a factor of 5 for one-hour experiments.

In addition to these considerations, ultrafast 2D NMR offers a higher flexibility, as it is possible to decrease the experiment duration without affecting the resolution provided that the concentration is sufficient, an option that is not conceivable in conventional 2D NMR where a minimum number of t_1 increments have to be recorded to preserve a minimum resolution.

2.2 Potentialities for quantitative analysis of complex mixtures

In order to discuss further this unexpected analytical performance, and to evaluate the sensitivity and resolution issues of multi-scan single shot experiments on realistic samples presenting a real analytical interest, we applied a similar strategy to a 5 mM model mixture of 8 metabolites as described in the Experimental part. A 5 mM concentration is consistent with the average metabolite concentrations in biological extracts analyzed by 2D NMR in previous studies.[5,36] For this model mixture, an experiment duration of 34 minutes was chosen for comparison between the two approaches. It corresponds to conditions where conventional spectra are acquired under quantitative conditions ($TR = 5T_1^{max}$, where T_1^{max} was found equal to 6.4 s) with a sufficient resolution ($N_1 = 64$) corresponding to quantitative conditions previously reported.[5,6] The ultrafast spectra were therefore recorded with the same TR and 64 scans.

The corresponding spectra are plotted in Fig. 3, together with examples of cross-sections for the lactate peak. Both spectra are characterized by the same expected COSY pattern, however the conventional spectrum (Fig. 3b) shows additional t_1 noise ridges parallel to the indirect dimension and clearly visible on the projection (Fig. 3c). In order to compare the relative sensitivity of the two approaches, limiting SNR values were measured for 8 peaks corresponding to the 8 relevant metabolites. The results plotted in Table 1 highlight the highest performance of ultrafast COSY. For the latter, all limiting SNR values are above 30, whereas more than half of them are below this threshold in the case of conventional COSY. The relative performance of ultrafast *versus* conventional 2D NMR can be evaluated by calculating the ratio between limiting SNR values (Table 1). For 7 of the 8 metabolites, this ratio is higher for ultrafast COSY and reaches values higher than 4. For one metabolite, conventional COSY has a slightly better sensitivity, but the SNR value

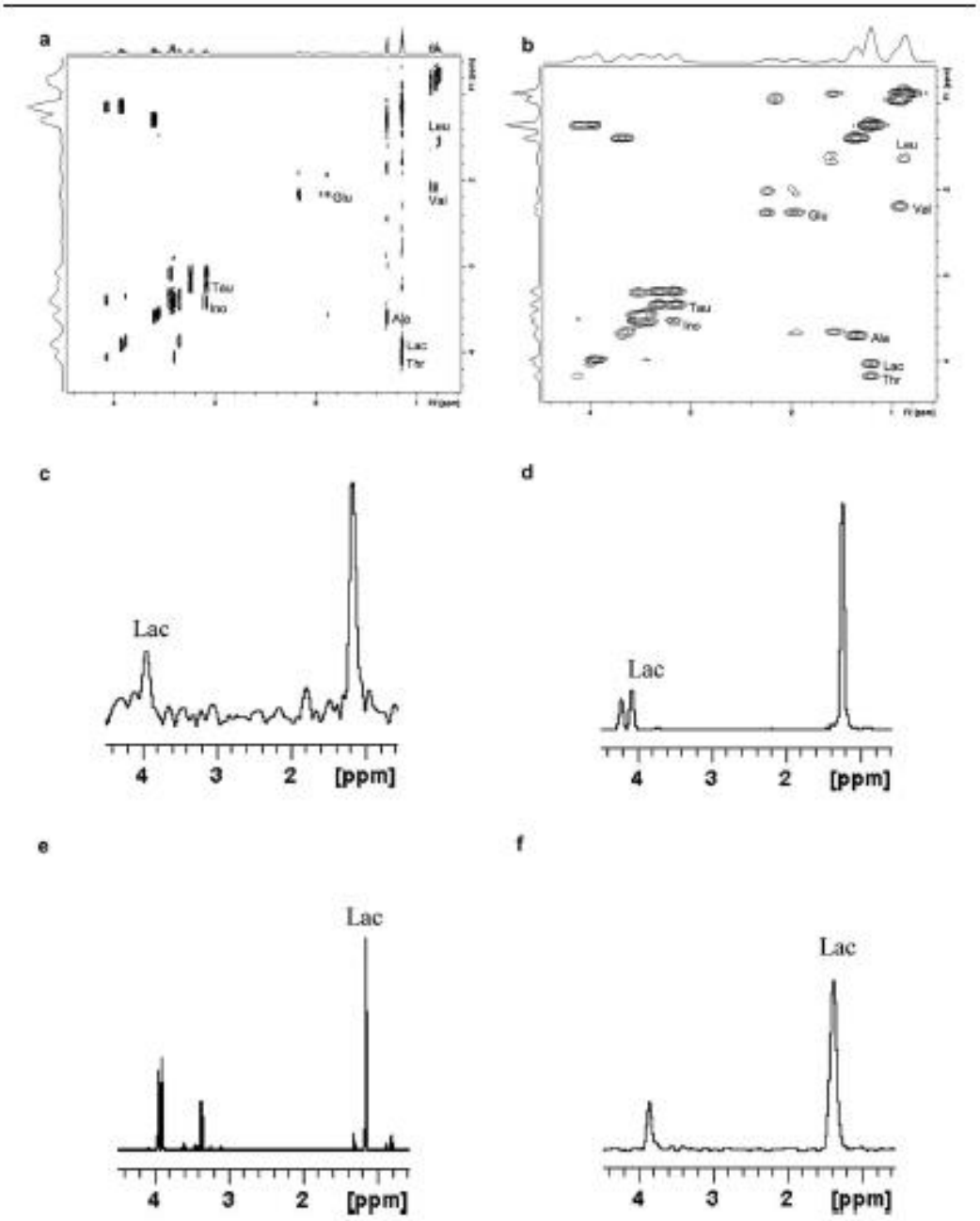

Fig. 3 Conventional (a) and ultrafast (b) constant-time COSY spectra of a 5 m*M* metabolic mixture, acquired in 34 minutes on a 500 MHz spectrometer with a cryoprobe. Vertical (c and d) and horizontal (e and f) cross-sections are shown for the lactate peak, for the conventional (c and e) and ultrafast (d and f) spectra. The spectra were acquired with the pulse sequences described in Fig. 1. Other relevant parameters are indicated in the Experimental section. The metabolite peaks used for quantification are indicated using the standard international three-letter code.

Table 1 Limiting signal-to-noise ratio (SNR) for the ultrafast and conventional COSY spectra of a 5 mM model metabolic mixture, acquired in 34 min on a 500 MHz spectrometer. The ratio between ultrafast and conventional SNR values is also indicated

	Limiting SNR[a]		
Metabolite	Ultrafast	Conventional	SNR^{UF}/SNR^{Conv}
Alanine	**71**	16	4.4
Glutamic acid	**53**	31	1.7
Lactic acid	**72**	16	4.5
Leucine	**31**	12	2.6
Myo-inositol	36	**47**	0.8
Taurine	**107**	42	2.6
Threonine	**54**	13	4.2
Valine	**50**	7	7.1

[a] The limiting SNR is defined by the SNR in the dimension where it reaches its lowest value. Bold characters indicate the highest value between ultrafast and conventional experiments.

obtained with ultrafast NMR is still reasonable in the perspective of quantitative measurements.

Sensitivity is an important feature of analytical methods, however other relevant aspects should be considered. In particular, the repeatability on the NMR response should be evaluated. For that, we calculated the standard deviations (SD) on relative peak volumes for five successive experiments, by dividing each metabolite peak volume by the sum of the 8 volumes. Even though this procedure does not give a direct quantitative measurement, it leads to accurate concentration values provided that a calibration procedure is carried out.[5,6] The repeatability calculations led to SD values between 0.5% and 3% depending on the metabolite. The average repeatability is below 2% for both approaches, therefore it can be concluded that ultrafast and conventional approaches are characterized by similar precision values, but with a smaller limit of quantification for ultrafast 2D NMR.

Another analytical aspect to be evaluated is resolution, as the overlap between peaks can be a limiting hurdle even on 2D NMR spectra, for complex mixtures with a high number of resonances. Similarly to the limiting SNR, we define the limiting half-height width ($\Delta\nu^{1/2}$) as the $\Delta\nu^{1/2}$ value in the dimension where it reaches its highest value. For conventional 2D COSY (Fig. 3a), the resolution is clearly limited by the vertical (indirect) dimension, where it is directly linked to the experiment duration T_A. For ultrafast COSY (Fig. 3b), the resolution in the vertical dimension is only limited by the number of alternated gradient pairs that can be applied during the ultrafast acquisition process. On the contrary, the limiting resolution appears in the spatially encoded horizontal dimension. This is an intrinsic limitation of ultrafast experiments which has been widely described.[27,28] It can be improved by increasing the spatial-encoding duration T_e, however it leads to sensitivity losses due to molecular diffusion.[24,28] Here we chose experimental conditions corresponding to the best compromise between resolution and sensitivity. Under these conditions, the limiting $\Delta\nu^{1/2}$ for ultrafast 2D COSY, observed in the horizontal dimension, is 54 Hz (average between the limiting $\Delta\nu^{1/2}$ for the 8 relevant peaks), whereas it is 63 Hz (observed in the vertical dimension) for conventional 2D COSY. Therefore, under the conditions described here, the limiting resolution is slightly better for ultrafast COSY. Still, an argument playing in favor of conventional 2D NMR is that its resolution can be increased at will by increasing N_1, however this procedure is associated with a proportional increase in the experiment duration which affects the precision of quantitative measurements.[3,4]

2.3 Flexibility and limitations of the multi-scan single shot approach

Beyond the sensitivity and resolution aspects discussed above, it is interesting to consider the flexibility of the two approaches presented in Fig. 1. The experimental conditions applied to obtain the conventional quantitative spectrum in Fig. 3a (1 scan, $N_1 = 64$) can be considered as the most drastic parameters that can be chosen, as NS already has a minimum value, and because decreasing N_1 further would lead to resolution losses preventing precise quantitative analysis. It means that even if the available concentration is high enough to allow for a reduction of the experimental time, it is simply not possible to decrease T_A any further for the conventional approach. On the contrary, ultrafast experiments offer a much higher flexibility, as T_A can be decreased *ad libitum* by decreasing NS without affecting the resolution. To illustrate this flexibility, we recorded UF COSY spectra on identical metabolic mixtures, but with higher concentrations. The experiment duration was decreased to obtain approximately the same limiting SNR values, as illustrated in Table 2. When the concentration is high enough, the experiment duration can be highly decreased with identical analytical performance, which was simply not possible with conventional 2D NMR.

The adaptability of ultrafast experiments also offers interesting opportunities, such as the possibility to apply phase-cycling schemes whose number of steps is only limited by the number of scans. Another potentially powerful approach is to take advantage of the repeated experiments to perform interleaved acquisitions as suggested by Frydman *et al.*,[29] by regularly shifting the starting time of the acquisition gradients to perform a more efficient sampling of the (k, t_2) space. This interleaved approach decreases the effective dwell time in the conventional dimension, thus giving access to higher spectral widths at no cost. This approach was not necessary here due to the 4 ppm spectral range observed, but can be easily implemented for larger spectral widths and/or to reduce the demand on gradient amplitudes.

Potential users of the multi-scan single shot methodology should also keep in mind its intrinsic limitations, which mainly

Table 2 Limiting signal-to-noise ratio (SNR) for the ultrafast COSY spectra of 5 mM, 10 mM and 25 mM model metabolic mixtures, acquired in 34 min, 8.5 min and 1 min, respectively

Metabolite	5 mM, 64 scans	10 mM, 16 scans	25 mM, 2 scans
Alanine	71	82	72
Glutamic acid	53	45	41
Lactic acid	72	83	63
Leucine	31	31	25
Myo-inositol	36	38	35
Taurine	107	113	105
Threonine	54	60	52
Valine	50	45	45

include sensitivity losses due to molecular diffusion, as described above.[24,25] However, we recently proposed a multi-echo spatial-encoding scheme that should help to limit these effects for samples with high diffusion coefficients.[27] Another practical limitation is that the ultrafast methodology is not implemented by manufacturers on commercial spectrometers. However, ultrafast 2D NMR does not require any specific hardware, apart from a *z*-gradient probe. Therefore, it can be easily implemented within a few hours, thanks to our specific acquisition and post-processing routines available on demand.

A last point worth discussing is the generality of the results presented in this study. The superiority of the spatially encoded approach lies in the absence of t_1 noise, which is a characteristic feature of conventional 2D experiments. However, t_1 noise is spectrometer- and experiment-dependent, and consequently quite unpredictable. Therefore, it would be interesting to generalize the comparison between the two strategies to a variety of experimental settings. Moreover, t_1 noise, contrary to thermal noise, is theoretically proportional to concentration. This means that for conventional experiments, one may decrease the concentration without affecting the signal-to-noise ratio in the indirect dimension. As a consequence, for concentrations lower than those employed in this study, one may find a value of the concentration below which it is preferable to perform a conventional 2D experiment. Of course, this critical concentration depends on the cross-peak, on the experiment and on the spectrometer; therefore it is impossible to give a general equation to determine this critical concentration. However, for the COSY experiment presented in this study, assuming that the limiting SNR of ultrafast experiments varies linearly with concentration (and does not for conventional experiments), this critical concentration would be approximately 1 mM (depending on the cross-peak considered).

3. Conclusion

The results presented above highlight the high analytical performance of the multi-scan single shot approach *versus* conventional 2D NMR acquisitions. The highest sensitivity per unit of time of the spatially encoded approach is attributed to the absence of t_1 noise in this kind of experiments. This is particularly interesting in quantitative conditions, where the long recycling delays generate high t_1 noise ridges in the indirect dimension of conventional experiments. Therefore, the superiority of the ultrafast approach would probably be less significant when working under fast, non-quantitative conditions where the short recycling delays of conventional 2D NMR will tend to reduce t_1 noise. Consequently, the spatially encoded methodology is particularly interesting for quantitative applications of 2D NMR, whose occurrence in literature has been highly increasing in the last few years.

The experimental data acquired in this study were recorded for COSY experiments, but the general trends observed above are not specific to this 2D correlation, as the preparation and mixing periods which differentiate the different types of 2D NMR correlations are identical for conventional and ultrafast methodologies. In particular, we expect to report on multi-scan single shot experiments for heteronuclear correlations in future studies.

The good analytical capabilities of spatially encoded experiments, together with their ease of implementation on routine spectrometers, should contribute to increase their application to quantitative analysis, in particular in the growing field of metabolomics where quantitative 2D NMR experiments have been reported.

4. Experimental

4.1 Sample preparation

The model ethanol sample was prepared by diluting ethanol in a D_2O/DMSO-d_6 1 : 4 mixture so as to obtain a 100 mM solution. For the model metabolite sample, a phosphate buffer solution (pH = 7.4, 0.1 M) in D_2O was prepared. A reference sample containing eight metabolites (alanine, glutamic acid, lactic acid, myo-inositol, taurine, threonine, leucine and valine) was dissolved in 1 mL of this buffer solution to obtain samples with identical metabolite concentrations. Three samples were prepared with this procedure, leading to metabolite concentrations of 25 mM, 10 mM and 5 mM. All samples were filtered and analyzed in 5 mm tubes.

4.2 NMR acquisition and processing

NMR spectra of the model ethanol sample were recorded at 298 K on a Bruker Avance I 400 spectrometer, at a frequency of 400.13 MHz with a dual+ probe including *z*-axis gradients and $PW_{90} = 9.9$ μs. NMR spectra of the metabolic mixtures were recorded at 298 K on a Bruker Avance III 500 spectrometer, at a frequency of 500.13 MHz with a cryogenically cooled probe including *z*-axis gradients and $PW_{90} = 6.9$ μs.

Ultrafast COSY experiments were performed by using the pulse sequence represented in Fig. 1a. Spatial encoding was performed using a constant-time spatial encoding scheme[28] with 15 ms smoothed chirp[17] encoding pulses. The sweep range for the encoding pulses (60 kHz) was set to be significantly larger than the chemical shift range. The amplitude of encoding gradients was set to $G_e = 7.0$ G cm^{-1} and 5.3 G cm^{-1} for the experiments on the 400 MHz and 500 MHz spectrometers respectively. The mixing period included opposite coherence-selection gradients (sin shape; 91.6 G cm^{-1}, 1 ms (400 MHz); 58.5 G cm^{-1}, 0.8 ms (500 MHz)). For the acquisition, 128 acquisition gradient pairs were applied, with the following amplitude and duration: 57.8 G cm^{-1} and 281.6 μs (400 MHz) or 58.5 G cm^{-1} and 256 μs (500 MHz). The amplitude and duration of the pre-acquisition gradient were adapted to adjust the peak position in the ultrafast dimension.

Conventional CT COSY 2D spectra[33] were recorded with a 5 ppm spectral width. Free induction decays (FIDs) were recorded with 10774 points and an acquisition time of 2.7 s (400 MHz) or 10012 points and an acquisition time of 2.0 s (500 MHz). 64 t_1 increments were recorded with 1 or 2 scans, depending on the experiment duration.

For metabolic mixtures, conventional and ultrafast experiments included water signal presaturation during the recovery delay. For all experiments, the recovery delay was adjusted to set $TR = 5T_1^{max}$ as indicated in the text. Longitudinal relaxation times were measured with a conventional inversion-recovery pulse sequence.

Before Fourier Transformation, 2D FIDs were weighed with apodization functions leading to the optimum sensitivity for the relevant peaks. For conventional spectra, a sinebell function and a π/8 shifted sinebell function were applied in the direct and indirect dimensions, respectively. For ultrafast spectra, a π/8 shifted sinebell function was applied in the conventional dimension. In the ultrafast dimension, an apodization was performed in the spatial dimension with optimized cosine apodization functions designed according to the procedure that we recently described.[39] Conventional spectra were zero-filled in both dimensions and ultrafast spectra were zero-filled in the conventional dimension. The optimum processing parameters, particularly the apodization functions, are of course dependent on the experimental conditions (digital resolution, natural linewidth) and should be optimized again for different experiments in order to obtain optimum sensitivity and resolution.

All the spectra were processed in the magnitude mode, which is known to have an influence on the quantification of 2D peaks. As recently described,[32] the integral of a Lorentzian peak diverges in magnitude mode. Still, accurate quantitative results can be obtained by carefully defining constant integration limits to obtain the same level of truncation for all peaks.

All the spectra were acquired and analysed using the Bruker program Topspin 2.1. The specific processing for the ultrafast spectra (as described in ref. 19) was performed using our home-written routine in Topspin. All the pulse sequences, apodization functions and processing programs described in this paper are available on demand.

Signal-to-noise (SNR) ratios were measured with the SNR measurement tool included in Topspin, on lines and columns extracted from 2D spectra and corresponding to the maximum intensity of the 2D peaks. Peak volumes were measured using the 2D integration tool in Topspin. All the sensitivity and resolution values given in the manuscript are average values calculated from the five successive experiments that were systematically recorded.

Acknowledgements

The authors acknowledge Estelle Martineau for discussions, as well as Michel Giraudeau for linguistic assistance. This research was supported by funding from the "Agence Nationale de la Recherche" for young researchers (ANR grant 2010-JCJC-0804-01).

References

1 W. P. Aue, E. Bartholdi and R. R. Ernst, *J. Chem. Phys.*, 1976, **64**, 2229–2246.
2 J. Jeener, *Lecture Presented at Ampere International Summer School II*, Basko Polje, Yugoslavia, 1971.
3 P. Giraudeau, N. Guignard, H. Hillion, E. Bagnat and S. Akoka, *J. Pharm. Biomed. Anal.*, 2007, **43**, 1243–1248.
4 H. Koskela, *Annu. Rep. NMR Spectrosc.*, 2009, **66**, 1–31.
5 I. A. Lewis, S. C. Schommer, B. Hodis, K. A. Robb, M. Tonelli, W. Westler, M. Sussman and J. L. Markley, *Anal. Chem.*, 2007, **79**, 9385–9390.
6 E. Martineau, P. Giraudeau, I. Tea and S. Akoka, *J. Pharm. Biomed. Anal.*, 2011, **54**, 252–257.
7 S. Massou, C. Nicolas, F. Letisse and J.-C. Portais, *Metab. Eng.*, 2007, **9**, 252–257.
8 L. Zhang and G. Gellerstedt, *Magn. Reson. Chem.*, 2007, **45**, 37–45.
9 A. F. Mehlkopf, D. Korbee, T. A. Tiggelman and R. Freeman, *J. Magn. Reson.*, 1984, **58**, 315–323.
10 G. A. Morris, *J. Magn. Reson.*, 1992, **100**, 316–328.
11 I. A. Lewis, R. H. Karsten, M. E. Norton, M. Tonelli, W. Westler and J. L. Markley, *Anal. Chem.*, 2010, **82**, 4558–4563.
12 R. Brüschweiler and F. Zhang, *J. Chem. Phys.*, 2004, **120**, 5253–5260.
13 L. Frydman, T. Scherf and A. Lupulescu, *Proc. Natl. Acad. Sci. U. S. A.*, 2002, **99**, 15858–15862.
14 E. Kupce and R. Freeman, *J. Magn. Reson., Ser. A*, 2003, **162**, 300–310.
15 E. Kupce and R. Freeman, *J. Am. Chem. Soc.*, 2004, **126**, 6429–6440.
16 V. A. Mandelshtam, H. S. Taylor and A. J. Shaka, *J. Magn. Reson.*, 1998, **133**, 304–312.
17 P. Schanda and B. Brutscher, *J. Am. Chem. Soc.*, 2005, **127**, 8014–8015.
18 B. Vitorge, G. Bodenhausen and P. Pelupessy, *J. Magn. Reson.*, 2010, **207**, 149–152.
19 L. Frydman, A. Lupulescu and T. Scherf, *J. Am. Chem. Soc.*, 2003, **125**, 9204–9217.
20 P. Pelupessy, *J. Am. Chem. Soc.*, 2003, **125**, 12345–12350.
21 M. Gal and L. Frydman, in *Encyclopedia of NMR*, ed. D. M. Grant and R. K. Harris, Wiley, New York, 2009, vol. 10.
22 M. Mishkovsky and L. Frydman, *Annu. Rev. Phys. Chem.*, 2009, **60**, 429–448.
23 A. Tal and L. Frydman, *Prog. Nucl. Magn. Reson. Spectrosc.*, 2010, **57**, 241–292.
24 P. Giraudeau and S. Akoka, *J. Magn. Reson.*, 2008, **192**, 151–158.
25 P. Giraudeau and S. Akoka, *J. Magn. Reson.*, 2008, **195**, 9–16.
26 P. Pelupessy, L. Duma and G. Bodenhausen, *J. Magn. Reson.*, 2008, **194**, 169–174.
27 P. Giraudeau and S. Akoka, *J. Magn. Reson.*, 2008, **190**, 339–345.
28 P. Giraudeau and S. Akoka, *J. Magn. Reson.*, 2010, **205**, 171–176.
29 Y. Shrot and L. Frydman, *J. Chem. Phys.*, 2009, **131**, 224516.
30 P. Giraudeau, G. S. Remaud and S. Akoka, *Anal. Chem.*, 2009, **81**, 479–484.
31 P. Giraudeau, P. Lemaunier, M. Couturaud, J.-M. Doux, A. Gilbert, G. S. Remaud and S. Akoka, *Journal of Spectroscopy and Dynamics*, 2011, advanced online publication.
32 P. Giraudeau, S. Massou, Y. Robin, E. Cahoreau, J.-C. Portais and S. Akoka, *Anal. Chem.*, 2011, **83**, 3112–3119.
33 M. E. Girvin, *J. Magn. Reson., Ser. A*, 1994, **108**, 99–102.
34 R. R. Ernst, G. Bodenhausen and A. Wokaun, *Principles of Nuclear Magnetic Resonance in One and Two Dimensions*, Oxford Science Publications, Oxford, 1987.
35 Y. Shrot and L. Frydman, *J. Chem. Phys.*, 2008, **128**, 164513.
36 Y. Xi, J. S. de Ropp, M. R. Viant, D. Woodruff and P. Yu, *Anal. Chim. Acta*, 2008, **614**, 127–133.
37 J. M. Böhlen and G. Bodenhausen, *J. Magn. Reson.*, 1992, **102**, 293–301.
38 P. Giraudeau and S. Akoka, *Magn. Reson. Chem.*, 2011, **49**, 307–313.

2. Application of ufCOSY: Quantification of metabolites

analytical chemistry

Article

pubs.acs.org/ac

Fast Determination of Absolute Metabolite Concentrations by Spatially Encoded 2D NMR: Application to Breast Cancer Cell Extracts

Adrien Le Guennec, Illa Tea, Ingrid Antheaume, Estelle Martineau, Benoît Charrier, Meerakhan Pathan, Serge Akoka, and Patrick Giraudeau*

Université de Nantes, CNRS, CEISAM UMR 6230, B.P. 92208, 2 rue de la Houssinière, F-44322 Nantes Cedex 03, France

ABSTRACT: Two-dimensional nuclear magnetic resonance (2D NMR) forms a powerful tool for the quantitative analysis of complex mixtures such as samples of metabolic relevance. However, its use for quantitative purposes is far from being trivial, not only because of the associated experiment time, but also due to its subsequent high sensitivity to hardware instabilities affecting its precision. In this paper, an alternative approach is considered to measure absolute metabolite concentrations in complex mixtures with a high precision in a reasonable time. It is based on a "multi-scan single shot" (M3S) strategy, which is derived from the ultrafast 2D NMR methodology. First, the analytical performance of this methodology is compared to the one of conventional 2D NMR. 2D correlation spectroscopy (COSY) spectra are obtained in 10 min on model metabolic mixtures, with a precision in the 1−4% range (versus 5−18% for the conventional approach). The M3S approach also shows a better linearity than its conventional counterpart. It ensures that accurate quantitative results can be obtained provided that a calibration procedure is carried out. The M3S COSY approach is then applied to measure the absolute metabolite concentration in three breast cancer cell line extracts, relying on a standard addition protocol. M3S COSY spectra of such extracts are recorded in 20 min and give access to the absolute concentration of 14 major metabolites, showing significant differences between cell lines.

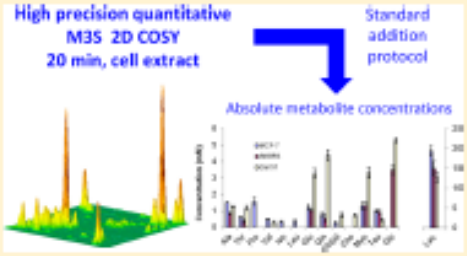

Nuclear magnetic resonance (NMR) is widely used in metabolomic studies, thanks to its capacity to provide nonambiguous site-specific information while being nondestructive. NMR metabolomic approaches are increasingly employed in a variety of applications such as disease diagnosis, toxicology, plant sciences, and nutrition.[1−6] In the vast majority of studies reported so far, a very standardized 1D proton NMR protocol has been employed for data acquisition, associated with multivariate statistical analysis to perform an efficient separation between samples of various origins.[5−7] Whereas this metabolomic approach offers a high degree of discrimination, the quantitative access to precise and accurate metabolite concentrations is made difficult by the high degree of overlap characterizing ^{1}H NMR spectra of biological samples. Measuring metabolite concentrations, however, can help in determining characteristic biomarkers and then in fully understanding metabolic complexities. As a consequence of the growing interest for such a quantitative approach,[8] recent years have witnessed the development of new analytical tools to overcome the current limitations of the usual metabolomic strategy. Targeted approaches have been designed to quantify individual metabolites by fitting the 1D spectra of complex samples by the sum of individual metabolite 1D spectra.[9] However, their precision is still limited by the complexity of spectral patterns when addressing complex biological samples.[10,11] On the other hand, recent studies have suggested the use of two-dimensional spectroscopy[12,13] for quantitative purposes in order to take advantage of the much lower degree of overlap characterizing two-dimensional (2D) NMR.[14−20] These approaches generally rely on a calibration procedure to overcome the apparent nonquantitativeness of 2D experiments, i.e., the dependence of peak volumes on a variety of factors, mainly relaxation times, J-couplings, and pulse sequence delays. Another strategy consists of measuring peak volumes and correcting them by a factor accounting for their dependence on J-couplings, relaxation times, etc.[17] This approach, however, requires that all coupling constants and relaxation times are previously determined with a good precision. The precited studies have also devoted large efforts to the reduction of the relatively long experiment duration characterizing 2D NMR experiments, not only for evident time-saving reasons, but also because long experiments are more likely to be affected by spectrometer instabilities in the course of time, which strongly affect their repeatability.[19]

On the other hand, the NMR community has developed a number of approaches departing from the classical parametric incrementation scheme of 2D NMR, in order to drastically reduce the duration of 2D NMR experiments.[21−27] In particular, the last 10 years have witnessed large efforts geared

Received: October 15, 2012
Accepted: November 21, 2012
Published: November 21, 2012

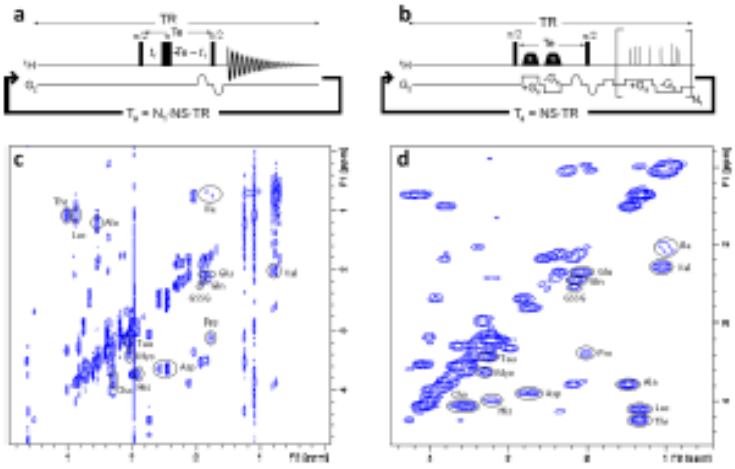

Figure 1. Strategies for recording quantitative 2D NMR constant-time COSY spectra, (a) by accumulating NS scans for each N_1 increment of a conventional 2D pulse sequence or (b) by accumulating NS ultrafast experiments in a multiscan single shot approach. The corresponding spectra are shown in (c) and (d) for the conventional and M3S approaches, respectively, acquired from a 6 mM metabolic mixture, in 10 min on a 500 MHz Avance III Bruker spectrometer with a cryoprobe. The experimental parameters are indicated in the Experimental Section. The metabolite peaks used for the analytical evaluation of the methods are indicated using the standard international code.

at developing the so-called "ultrafast 2D NMR" methodology,[22,28,29] capable of providing a complete 2D correlation in a single scan, i.e., in a fraction of a second. It relies on a spatial-encoding procedure over the sample length which has been described in detail in recent papers.[30−32] This methodology initially suffered from important limitations in terms of resolution and sensitivity,[32−35] but over the past few years, several significant improvements have increased its analytical performance,[36−38] making it suitable for the quantitative analysis of complex mixtures.[39,40] These first quantitative applications of ultrafast 2D NMR naturally raised the question of how such spatially encoded approaches would compare to conventional 2D NMR in terms of analytical performance. Sensitivity issues should be particularly taken into consideration when dealing with biological mixtures such as those involved in metabolomic studies. While it seemed evident that single-scan experiments performed in a fraction of a second were far less sensitive than minutes-long conventional approaches, it also turned out that accumulating transients from ultrafast experiments, a "multi-scan single shot" (M3S) approach, was potentially competitive with conventional 2D NMR.[41] By working on model metabolic mixtures, we showed that the sensitivity per unit of time of M3S experiments was higher than the one of conventional 2D NMR. This somewhat surprising result was mainly attributed to the absence of t_1 noise in spatially encoded experiments, highlighting their inherent higher immunity to hardware instabilities in the course of the experiment.

A consequence of this higher performance is that a better precision and accuracy could, in principle, be expected from the spatially encoded approach. The purpose of the present Article is to evaluate, in the case of homonuclear 2D NMR, the analytical performance of spatially encoded 2D NMR and to compare it to its conventional counterpart. The quantitative potentialities of the M3S strategy are first assessed on model mixtures; then, the application to the measurement of absolute metabolite concentration in breast cancer cell line extracts is presented and discussed.

EXPERIMENTAL SECTION

Model Metabolic Samples. Model metabolite samples were prepared for evaluating the analytical performance of the NMR methods. A reference sample containing 14 metabolites (alanine (Ala), threonine (Thr), valine (Val), isoleucine (Ile), lactate (Lac), glutamate (Glu), glutamine (Gln), glutathione (GSH), choline (Cho), histidine (His), myo-inositol (Myo), taurine (Tau), proline (Pro), and aspartate (Asp)) was dissolved in a phosphate buffer solution (0.1 M, pH = 7.4) to obtain a concentration of 20 mM for each metabolite. Then, five samples were prepared by dilution with the following metabolite concentrations: 2, 4, 6, 8, and 10 mM. All samples were filtered and analyzed in 5 mm tubes.

Chemicals for Cell Cultures. Culture media Dulbecco's Modified Eagle medium (D-MEM), antibiotics (penicillin–streptomycin), fetal bovine serum (FBS), and Dulbecco's phosphate buffered saline (D-PBS) were purchased from Invitrogen (www.invitrogen.com). Insulin from bovine pancreas was purchased from Sigma-Aldrich (www.sigmaaldrich.com). Chloroform (grade Rectapur) and methanol (HPLC grade VWR) were purchased from VWR International (www.vwr.com). Deuterium oxide (D_2O; 99.9%D) was obtained from EURISO-TOP (www.eurisotop.com).

Protocol for Cell Cultures. Three different lines of human breast cancer cells were used: Cal 51, SKBR3, and MCF-7. The cells were grown as monolayer cultures (between 9×10^6 and 1.6×10^7 cells/75 cm^2 flask in two identical flasks) in D-MEM supplemented with 10% of FBS, 1% of 10000 units/m: penicillin−10 000 μg/mL streptomycin, and 0.1 mg/mL of bovine insulin (except for MCF-7) at 37 °C in a humidified atmosphere of 5% CO_2. When cells were confluent, the culture

medium was removed from the culture flask (75 cm^2) and the cells were washed twice with D-PBS (apparent pH = 7.4, measured with a pH electrode). Afterward, the cells were quenched using 3 mL of methanol as described by Teng et al.[42] and detached from the culture flask using a cell lifter.

Extraction Procedure. The quenched cells were lyophilized, and the extraction was performed on 100 mg of lyophilized cells in 23.2 mL of a MeOH/$CHCl_3$/H_2O solution (6:6:5.4), according to the optimized procedure that we recently described[43] to extract intracellular metabolites. The aqueous phase contained water-soluble low-molecular weight endogenous metabolites, while nonpolar metabolites such as lipid molecules were in the organic phase. Proteins and other biological macromolecules were precipitated by the addition of methanol and chloroform and trapped in the solvent layer between the aqueous and organic phases. After centrifugation during 15 min at 4500*g*, only the upper aqueous phase was kept for analysis. The samples were dried by evaporation under a gentle flow of N_2 gas at 40 °C and were used for NMR analysis. Prior to NMR analysis, each sample was reconstituted in 0.65 mL of a 0.1 M phosphate buffer solution prepared in D_2O (pH = 7.4), containing NaN_3 to prevent bacteria contamination. The samples were homogenized, adjusted to pH = 7.40 ± 0.05, filtered, and analyzed using a 5 mm NMR tube.

NMR Acquisition Parameters. The NMR spectra of the metabolic mixtures were recorded at 293 K on a Bruker Avance III 500 spectrometer, at a frequency of 500.13 MHz with a cryogenically cooled probe including *z*-axis gradients and PW_{90} carefully calibrated for each sample. For all experiments, the water signal at 4.7 ppm was presaturated by continuous irradiation during the recovery delay. All experiments were performed under partial saturation conditions, with TR = 4.7 s.

The conventional CT correlation spectroscopy (COSY) 2D spectra[26] were recorded on the model metabolic mixtures with the pulse sequence described in Figure 1a, with a 5 ppm spectral width. The free induction decays (FIDs) were recorded with 10012 points and an acquisition time of 2.0 s. 64 t_1 increments were recorded with 2 scans and a recovery delay of 4.7 s, resulting in a total experiment time of approximately 10 min.

The ultrafast COSY experiments were recorded on the same mixtures using the pulse sequence represented in Figure 1b. The spatial encoding was performed using a constant-time spatial encoding scheme[29] with 15 ms smoothed chirp[45] encoding pulses. The sweep range for the encoding pulses (60 kHz) was set to be significantly larger than the chemical shift range. The amplitude of encoding gradients was set to 8.3 G/cm. The mixing period included opposite coherence-selection gradients (sin shape; 58.5 G/cm, 0.8 ms). For the acquisition, 128 acquisition gradient pairs were applied, with the following amplitude and duration: 58.5 G/cm and 256 μs. The amplitude and duration of the preacquisition gradient were adapted to adjust the peak position in the ultrafast dimension. This gradient adds an additional dephasing to the one obtained after spatial encoding, in order to center the chemical shift range of interest in the middle of the detection window in the spatially encoded dimension.[28] For the model metabolic samples, 128 scans were recorded with TR = 4.7 s, resulting in a 10 min total experiment time, and five successive experiments were recorded immediately one after the other, on each sample, for the purpose of evaluating the repeatability. For the application of ultrafast NMR to cancer cell line extracts, identical parameters were used, except that the experiment time was increased to 20 min (256 scans) in order to be able to detect the lower metabolite concentrations characterizing these samples. In this case, three successive experiments were recorded in order to calculate average values and standard deviations for the peak volumes.

NMR Processing Parameters. Before Fourier Transformation, 2D FIDs were weighed with apodization functions leading to the optimum sensitivity for the relevant peaks. For the conventional spectra, a sinebell function and a π/8 shifted sinebell function were applied in the direct and indirect dimensions, respectively. For the ultrafast spectra, a π/8 shifted sinebell function was applied in the conventional dimension. In the ultrafast dimension, an apodization was performed in the spatial dimension with optimized Gaussian apodization functions designed according to the procedure that we recently described.[46] The conventional spectra were zero-filled in both dimensions, and the ultrafast spectra were zero-filled in the conventional dimension.

All the spectra were processed in the magnitude mode, which is known to have an influence on the quantification of 2D peaks. As previously described, the integral of a Lorentzian peak diverges in magnitude mode. Still, accurate quantitative results can be obtained by carefully defining constant integration limits to obtain the same level of truncation for all peaks[47] and by accounting for potential intensity variations through a calibration procedure with high repeatability.

For all the ultrafast and conventional spectra, a zero order baseline correction was applied in both dimensions. Higher polynomial orders were evaluated but did not significantly improve the analytical performance.

The peak volumes were measured using the 2D integration tool in Topspin. The integration region limits were systematically optimized for each peak, on the highest concentrated mixture (i.e., the one with the highest peak volumes), with the following criteria: (i) integration regions centered on the peak of interest and (ii) integration region size chosen as large as possible to integrate the whole peak but small enough to avoid overlap with neighboring peaks and integration regions. As peak volumes are in arbitrary units, it is necessary to make sure that all the spectra have the same scaling factor.

All the spectra were acquired and analyzed using the Bruker program Topspin 2.1. The specific processing for the ultrafast spectra (as described in ref 28) was performed using our home-written routine in Topspin. All the pulse sequences, apodization functions, and processing programs described in this paper are available on demand.

Quantification of Metabolites in Cell Extract Samples. The concentrations of intracellular metabolites were calculated using a standard addition procedure. A model mixture for standard additions was prepared with 14 target metabolites (alanine, lactate, leucine, threonine, taurine, glutathione, glutamate, glutamine, choline, valine, isoleucine, myo inositol, proline, and glucose), dissolved in 2.5 mL of the phosphate buffer solution in order to reach a concentration of 4.10^{-2} mol/L for each metabolite. The constitution of this mixture was adapted compared to the one used for the analytical evaluation of the method, in order to obtain a mixture that reflected better the metabolic constitution of the breast cancer cell line extracts. Graded known volumes of this metabolite solution (four successive additions of 15 μL) were added to each cell extract, to obtain a range of added concentrations varying between 1.0 and 3.7 mmol/L for each metabolite, except for GSSG, whose added concentrations were between 0.5 and 1.8 mmol/L. Each

dx.doi.org/10.1021/ac203306t | Anal. Chem. 2011, 83, 10831–10837

sample was measured three times as described above. For each metabolite, a standard addition curve was fitted by the linear regression equation: $V = a[m] + b$, where V represents the 2D peak volume (a.u.) and $[m]$ is the concentration (in millimoles per liter) of the metabolite in the cell extract. The initial concentration of intracellular metabolites C_i was calculated by the b/a ratio, where a is the slope and b is the y-intercept of the linear regression curve.

RESULTS AND DISCUSSION

Ultrafast and Conventional COSY Experiments. The comparison described in this paper relies on the ultrafast and conventional COSY experiments described in Figure 1. As described in ref 41, the Ultrafast COSY pulse sequence (Figure 1b) is a constant-time experiment.[29] It is therefore compared to its conventional counterpart, constant-time (CT) COSY (Figure 1a), which offers a higher sensitivity than conventional COSY in the indirect domain.[44] Both experiments were previously optimized (see ref 41) to yield the highest sensitivity per unit of time. In Ultrafast 2D NMR (Figure 1b), the whole 2D FID is recorded in a single scan, but several FIDs are accumulated for the sake of sensitivity, resulting in the M3S approach described above.[41] Therefore, the total experiment duration T_a is given by NS × TR, where NS is the number of accumulations and TR is the duration of the pulse sequence, mainly dictated by the recovery delay. In conventional 2D NMR (Figure 1a), the experiment duration is $N_1 \times NS \times TR$, where N_1 is the number of increments in the indirect dimension.

The two acquisition strategies were compared on a series of model metabolic mixtures whose concentrations ranged from 2 to 10 mM. The spectra acquired in 10 min are represented in Figure 1c,d for the 6 mM sample, together with the corresponding pulse sequences. Both approaches were compared with parameters ensuring identical total experiment times (N_1 = 64 and NS = 2 for the conventional approach, NS = 128 for the M3S). In order to choose an appropriate repetition time TR, additional T_1 measurements were performed on the different mixtures (data not shown). They showed that the longitudinal relaxation times of the metabolites did not significantly change with concentration, which makes it possible to work under partial saturation conditions. Then, the TR value was optimized to 4.7 s to yield the maximum 2D peak intensity for the metabolite with the most limiting SNR on the 2D spectrum, i.e., proline.

From the spectra shown in Figure 1, one can easily notice the presence of t_1 noise on the conventional spectrum (Figure 1c), whereas this is not the case in the M3S approach (Figure 1d). As a consequence, the limiting SNR (i.e., the SNR in the less sensitive dimension of the 2D spectrum) is higher for the M3S approach, as discussed in ref 41. The resolution aspects are also worth discussing; they are fully described in the aforementioned reference, and the main conclusion is that the limiting resolution (i.e., the resolution in the dimension where it has the lowest value) is approximately identical for the two strategies.

Analytical Evaluation. The conventional and M3S approaches were compared from the analytical point of view with the experimental conditions described above. First, the repeatability was assessed on the 6 mM sample. For that, 15 spectra were recorded (three independent series of 5 spectra separated by 15 min intervals), and the peak volumes were measured from these spectra. The coefficients of variation on the 15 spectra were calculated for each metabolite signal shown in Figure 1. The results, plotted in Figure 2, show that the CV are between 1% and 4% for the M3S approach, whereas they

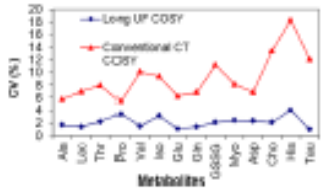

Figure 2. Coefficient of variation (CV) of the M3S and conventional 2D peak volumes for the various metabolites of the 6 mM model mixture. Each CV was determined from three series of five spectra, acquired in 10 min per spectrum on a 500 MHz Avance III Bruker spectrometer with a cryoprobe. The experimental parameters are indicated in the Experimental Section.

vary between 5.5% and 18.3% for the conventional one. This highlights the much higher repeatability of the M3S approach, a result that could be expected as the M3S was shown to be less sensitive to spectrometer instabilities in the course of time.[41]

In a second phase of the analytical evaluation, the linearity of the two approaches was assessed by recording five spectra for each of the five model samples, whose concentrations ranged from 2 to 10 mM. The linearity was evaluated by plotting calibration curves of 2D absolute peak volumes as a function of gravimetric concentration ratios. The very high coefficients of determination (r^2), shown in Table 1, show the excellent linearity of the two methods, thus proving that accurate measurements can be obtained after preliminary calibration. The r^2 values are higher for the M3S approach for 13 of the 14 metabolites, which can be correlated with the higher repeatability described above.

While the high linearity and repeatability ensure that accurate results can be obtained from the M3S approach, provided that a calibration procedure has been carried out, its accuracy was further assessed so that it can safely be used for quantitative analysis of metabolic samples. For that, additional experiments were performed for the M3S approach in order to calculate its recovery factor α.[45] An additional sample of known concentration (5 mM), and with the same composition as those used for evaluating the linearity, was prepared and analyzed by the M3S method. Its concentration was determined from its 2D NMR spectrum using the calibration curve obtained from the 5 other samples. The recovery factor was then calculated for each metabolite as the ratio between the NMR-based concentration and the gravimetric-based concentration. The recovery factor gives an estimate of the method accuracy: a value smaller than 100% indicates that the initial concentration is underestimated, while $\alpha > 100\%$ reveals an overestimated concentration. Here, the values obtained for the M3S method were between 97% and 102%, thus ensuring an accuracy better than 3% for this approach. The results of the analytical evaluation presented here highlight the good analytical performance of the M3S method, which can therefore be confidently used for the determination of concentrations in biological samples.

Determination of Absolute Intracellular Metabolite Concentrations. In order to illustrate its quantitative potentialities, the quantitative 2D COSY M3S protocol was applied to compare and contrast the metabolite contents from

dx.doi.org/10.1021/ac403308t | Anal. Chem. 2013, 85, 10831−10837

Table 1. Comparison of the Linearity of Conventional and M3S 2D COSY Experiments Recorded in 10 min per Spectrum on a Series of Five Model Metabolic Mixtures (with Concentrations of Individual Metabolites Equal to 2, 4, 6, 8, and 10 mM)[a]

metabolites	Ala	Lac	Thr	Pro	Val	Ile	Glu
r^2 (M3S)	0.999	0.996	0.999	0.995	0.999	0.999	0.998
r^2 (conventional)	0.999	0.978	0.997	0.998	0.994	0.994	0.997
metabolites	Gln	GSSG	Myo	Asp	Cho	Bta	Tau
r^2 (M3S)	0.999	0.990	0.998	1.000	0.997	0.999	0.999
r^2 (conventional)	0.988	0.989	0.998	0.995	0.996	0.997	0.998

[a]The correlation coefficients r^2 are obtained from calibration curves plotting the 2D NMR peak volume as a function of the gravimetric concentration. Each point of the correlation curve was the average of five experiments.

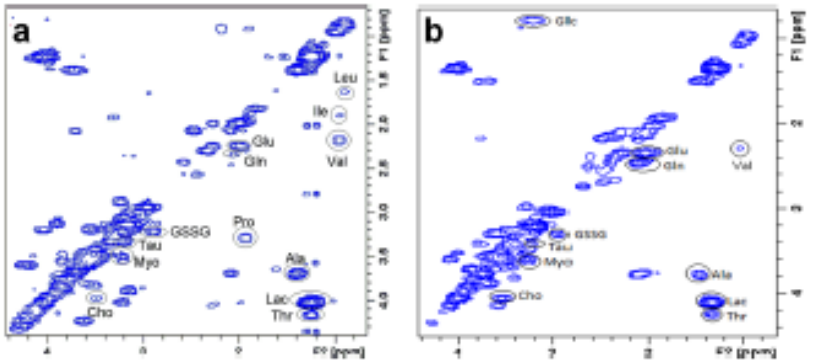

Figure 3. 2D ^{1}H M3S COSY spectrum of SKBR3 (a) and Cal 51 (b) breast cancer cell line extracts, obtained by $CHCl_3$/MeOH/H_2O extraction of breast cancer cells. The spectra were acquired in 20 min (256 transients) at 293 K on a 500 MHz Bruker Avance III spectrometer equipped with a cryoprobe. The relevant metabolite 2D peaks are indicated. On the Cal 51 sample (b), the glucose peak folded along the F_1 dimension is clearly visible on the top of the spectral window.

three different human breast cancer cell lines. Metabolites were extracted following a MeOH/$CHCl_3$/H_2O extraction procedure that was recently optimized for quantitative NMR-based metabolomics.[46] In order to obtain quantitative results from 2D NMR spectra, a calibration procedure is necessary to determine absolute metabolite concentrations, provided that the method shows a good linearity, which was ensured by the analytical evaluation described above. The most evident approach for obtaining a calibration curve consists of plotting, for several different samples of known metabolite concentrations, the relative peak volume ratio between the metabolite and an internal reference. However, such a procedure is associated with a number of drawbacks characterizing internal referencing. First, the reference compound should be soluble under particular pH and solvent conditions while avoiding chemical interactions with the metabolites. Moreover, it should exhibit at least one cross-peak on the 2D spectrum, while its signal should not overlap with those of the target metabolites. In order to circumvent these limitations and avoid matrix effects, we chose to rely on a standard addition procedure, similar to the one described in ref 20. A model solution was prepared, containing 14 target metabolites, previously identified on the M3S 2D spectrum of the cancer cell extracts, at a 4.10^{-2} mol L^{-1} concentration, and four additions were performed on each of the initial cell extracts as described in the Experimental Section. For the initial cell extracts, and after each addition, three ^{1}H COSY M3S spectra were recorded in order to calculate average values and standard deviations on NMR measurements. An experiment duration of 20 min was chosen, corresponding to NS = 256 scans and other parameters identical to those described above. It allowed a better sensitivity for the metabolite quantitation, while keeping the experiment time to a reasonable value. Figure 3 shows examples of M3S COSY spectra obtained in 20 min on MCF-7 and Cal 51 cell extracts, where the metabolite signals used for quantification are indicated. The signals arising from the 14 target metabolites are clearly visible, and differences between the two cell lines are clearly visible. The glucose peak is worth noticing: it is folded along the conventional F_1 dimension and appears on the top of the spectral window for the Cal 51 extract (Figure 3b). It is not visible in the MCF-7 extract because of its too low concentration in this sample. For each set of three spectra, the average peak volume was determined, and for each peak, this average volume was plotted as a function of the added concentration, resulting in 14 graphs (one per metabolite). This procedure was carried out for each cell extract. All curves were subjected to a linear regression, and the correlation coefficient r^2 was higher than 0.965 in all cases and superior to 0.99 in most cases, thus confirming the very high linearity of the method.

The concentration of each metabolite in each cell extract was determined from these results with the procedure described in the Experimental Section. All the concentrations were normalized to a 100 mg mass of lyophilized cells. The results are plotted in Figure 4, showing a large metabolite concentration range, from 10 to 20 mM for lactate to 0.3 mM for less abundant metabolites such as isoleucine, leucine, valine, GSSG, taurine, or threonine. Some metabolites are not

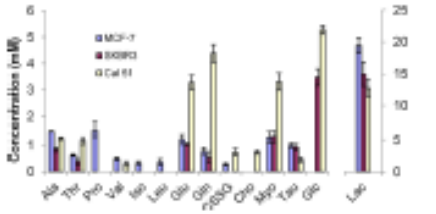

Figure 4. Metabolite concentrations of intracellular extracts obtained from three cell lines: SKBR3, MCF-7, and Cal 51 by a quantitative 2D M3S COSY protocol associated with a standard addition procedure. The concentrations are normalized to a 100 mg mass of lyophilized cells. The lactate concentration is plotted with a different vertical scale, as it is much more concentrated than the other metabolites.

present in certain extracts, particularly in SKBR3, because their concentration was probably too low to be detected within a 20 min experiment time. Also plotted in Figure 4 are the experimental errors (standard deviations) obtained, for each metabolite concentration, from the errors determined on the standard addition linear regression curve.

These results point out the capacity of the M3S approach to yield quantitative results in a reasonable amount of time. The biological interpretation of these results is out of the scope of this Article and would require comparing a high number of samples for more than three cell lines. Still, we can already observe significant differences between cell lines, which are often higher than the experimental error. It shows the potential usefulness of the M3S NMR strategy for discriminating cell lines and, more generally, biological samples from various origins.

One last point worth discussing is the sensitivity of the M3S approach. While the sensitivity aspects of ultrafast NMR have been widely addressed in ref 41, a practical question is the limit of concentration that can be quantified with such an approach. The answer is not unique, as the limit of detection depends both on the hardware (spectrometer and probe) and on the experiment time chosen by the user. Moreover, it is different for each metabolite because the amplitude of 2D peaks depends on J-couplings, T_2, and pulse sequence delays but also on the number of spins giving rise to the signal. With the hardware configuration and experimental parameters used in this study, the lower concentration that was quantified was close to 0.3 mM (Figure 4), which demonstrates that the actual limit of quantification is lower. Furthermore, this limit could be lowered, if necessary, by simply increasing the number of scans.

■ CONCLUSION

The results described in this study show the high analytical potential of the M3S approach compared to its conventional counterpart, particularly in terms of precision. This high precision is indispensable to detect and quantify small variations in metabolite concentrations, which is of the highest importance to analyze and understand metabolic pathways. The protocol described in this study offers a powerful tool to determine absolute metabolite concentrations in cell extracts and, more generally, in complex biological mixtures. More generally speaking, the development of precise and accurate quantitative 2D approaches such as the one described here is highly important in the field of metabolomics. First, because they allow, with a minimal sample preparation, the unambiguous, precise, and simultaneous quantification of targeted metabolites in complex samples but also because at the same time they make it possible to easily identify these metabolites, a task which is very difficult in complex mixtures. Therefore, the combination of structural identification and quantification forms a unique combination for the metabolomics community. In this context, the work presented in this paper demonstrates for the first time the interest of an "ultrafast 2D metabolomics" approach, showing an unequaled precision compared to conventional approaches, moreover in a relatively short duration.

While these different cell lines were analyzed here, our protocol will need to be applied to a variety of cell lines in order to obtain reliable biological information. From the NMR side, the use of an ultrafast-based version of the quantitative heteronuclear $^1H-^{13}C$ NMR proposed by Markley and coworkers[15] would also be an appealing option, as it offers a better discrimination between metabolite signals. In addition to the analytical potential of ultrafast-based methods demonstrated here, this paper, together with other recent studies,[40,49−51] demonstrates that ultrafast NMR has moved on from the stage of method development to the one of application to systems of increasing complexity.

■ AUTHOR INFORMATION

Corresponding Author

*Tel.: +33(0)2 51 12 57 09. Fax: +33(0)2 51 12 57 12. E-mail: patrick.giraudeau@univ-nantes.fr.

Notes

The authors declare no competing financial interest.

■ ACKNOWLEDGMENTS

We are grateful to Dr. Sophie Bazille-Nion for providing human breast cancer cell lines and for helpful discussions. We also acknowledge Michel Giraudeau for linguistic assistance. This research was supported by a young investigator starting grant from the "Agence Nationale de la Recherche" (ANR Grant 2010-JCJC-0804-01).

■ REFERENCES

(1) Rapid, S.; Salvev, V. *Trends Anal. Chem.* **2007**, *26*, 625−636.
(2) Wishart, D. S. *Am. J. Transplant.* **2008**, *8*, 2814−2820.
(3) Coen, M.; Holmes, E.; Lindon, J. C.; Nicholson, J. K. *Chem. Res. Toxicol.* **2008**, *21*, 9−27.
(4) Holmes, E.; Foxall, P. J. D.; Spraul, M.; Duncan Farrant, R.; Nicholson, J. K.; Lindon, J. C. *J. Pharm. Biomed. Anal.* **1997**, *15*, 1647−1659.
(5) Zhang, S.; Nagana Gowda, G. A.; Asiago, V.; Shanaiah, N.; Barbas, C.; Raftery, D. *Anal. Biochem.* **2008**, *383*, 76−84.
(6) Ludwig, C.; Ward, D. G.; Martin, A.; Viant, M. R.; Ismail, T.; Johnson, P. J.; Wakelam, M. J. O.; Günther, U. L. *Magn. Reson. Chem.* **2009**, *47*, S68−S73.
(7) Beckonert, O.; Keun, H. C.; Ebbels, T. M. D.; Bundy, J.; Holmes, E.; Lindon, J. C.; Nicholson, J. K. *Nat. Protoc.* **2007**, *2*, 2692−2703.
(8) Lindon, J. C.; Nicholson, J. K.; Holmes, E.; Everett, J. R. *Concepts Magn. Reson.* **2000**, *12*, 289−320.
(9) Weljie, A. M.; Newton, J.; Mercier, P.; Carlson, E.; Slupsky, C. M. *Anal. Chem.* **2006**, *78*, 4430−4442.
(10) Slupsky, C. M.; Rankin, K. N.; Wagner, J.; Fu, H.; Chang, D.; Weljie, A. M.; Saude, E.; Lix, B.; Adamko, D. J.; Shah, S.; Greiner, R.; Sykes, B. D.; Marrie, T. J. *Anal. Chem.* **2007**, *79*, 6995−7004.
(11) Tredwell, G. D.; Behrends, V.; Geier, F. M.; Liebeke, M.; Bundy, J. G. *Anal. Chem.* **2011**, *83*, 8683−8687.
(12) Ane, W. P.; Bartholdi, E.; Ernst, R. R. *J. Chem. Phys.* **1976**, *64*, 2229−2246.

(13) Jeener, J. Lecture presented at Ampere International Summer School II, Basko Polje, Yugoslavia, 1971.
(14) Giraudeau, P.; Guignard, N.; Hillion, H.; Bugaut, E.; Akoka, S. *J. Pharm. Biomed. Anal.* **2007**, *43*, 1243–1248.
(15) Lewis, I. A.; Schommer, S. C.; Hodis, B.; Robb, K. A.; Tonelli, M.; Westler, W.; Sussman, M.; Markley, J. L. *Anal. Chem.* **2007**, *79*, 9385–9390.
(16) Gronwald, W.; Klein, M. S.; Kaspar, H.; Fagerer, S. R.; Nurnberger, N.; Dettmer, K.; Bertsch, T.; Oefner, P. J. *Anal. Chem.* **2008**, *80*, 9288–9297.
(17) Rai, R. K.; Tripathi, P.; Sinha, N. *Anal. Chem.* **2009**, *81*, 10232–10238.
(18) Chylla, R. A.; Hu, K.; Ellinger, J. J.; Markley, J. L. *Anal. Chem.* **2011**, *83*, 4871–4880.
(19) Martineau, E.; Giraudeau, P.; Tea, I.; Akoka, S. *J. Pharm. Biomed. Anal.* **2011**, *54*, 252–257.
(20) Martineau, E.; Tea, I.; Akoka, S.; Giraudeau, P. *NMR Biomed.* **2012**, *25*, 985–992.
(21) Bretschneider, R.; Zhang, F. *J. Chem. Phys.* **2004**, *120*, 5253–5260.
(22) Frydman, L.; Scherf, T.; Lupulescu, A. *Proc. Natl. Acad. Sci. U.S.A.* **2002**, *99*, 15858–15862.
(23) Kupce, E.; Freeman, R. *J. Magn. Reson.* **2003**, *162*, 300–310.
(24) Kupce, E.; Freeman, R. *J. Am. Chem. Soc.* **2004**, *126*, 6429–6440.
(25) Mandelshtam, V. A.; Taylor, H. S.; Shaka, A. J. *J. Magn. Reson.* **1998**, *133*, 304–312.
(26) Schanda, P.; Brutscher, B. *J. Am. Chem. Soc.* **2005**, *127*, 8014–8015.
(27) Vitorge, B.; Bodenhausen, G.; Pelupessy, P. *J. Magn. Reson.* **2010**, *207*, 149–152.
(28) Frydman, L.; Lupulescu, A.; Scherf, T. *J. Am. Chem. Soc.* **2003**, *125*, 9204–9217.
(29) Pelupessy, P. *J. Am. Chem. Soc.* **2003**, *125*, 12345–12350.
(30) Gal, M.; Frydman, L. In *Encyclopedia of NMR*; Grant, D. M., Harris, R. K., Eds.; Wiley: New York, 2009; Vol. *10*.
(31) Mishkovsky, M.; Frydman, L. *Annu. Rev. Phys. Chem.* **2009**, *60*, 429–448.
(32) Tal, A.; Frydman, L. *Prog. Nucl. Magn. Reson. Spectrosc.* **2010**, *57*, 241–292.
(33) Giraudeau, P.; Akoka, S. *J. Magn. Reson.* **2008**, *192*, 151–158.
(34) Giraudeau, P.; Akoka, S. *J. Magn. Reson.* **2008**, *195*, 9–16.
(35) Pelupessy, P.; Duma, L.; Bodenhausen, G. *J. Magn. Reson.* **2008**, *194*, 169–174.
(36) Giraudeau, P.; Akoka, S. *J. Magn. Reson.* **2008**, *190*, 339–345.
(37) Giraudeau, P.; Akoka, S. *J. Magn. Reson.* **2010**, *205*, 171–176.
(38) Shrot, Y.; Frydman, L. *J. Chem. Phys.* **2009**, *131*, 224516.
(39) Giraudeau, P.; Remaud, G. S.; Akoka, S. *Anal. Chem.* **2009**, *81*, 479–484.
(40) Giraudeau, P.; Massou, S.; Robin, Y.; Cahoreau, E.; Portais, J.-C.; Akoka, S. *Anal. Chem.* **2011**, *83*, 3112–3119.
(41) Parhan, M.; Akoka, S.; Tea, I.; Charrier, B.; Giraudeau, P. *Analyst* **2011**, *136*, 3157–3163.
(42) Teng, Q.; Huang, W.; Collette, T. W.; Ekman, D. R.; Tan, C. *Metabolomics* **2009**, *5*, 199–208.
(43) Martineau, E.; Tea, I.; Loudet, G.; Giraudeau, P.; Akoka, S. *Anal. Bioanal. Chem.* **2011**, *401*, 2133–2142.
(44) Gerwin, M. E. *J. Magn. Reson. A* **1994**, *108*, 99–102.
(45) Böhlen, J. M.; Bodenhausen, G. *J. Magn. Reson. A* **1992**, *102*, 293–301.
(46) Giraudeau, P.; Akoka, S. *Magn. Reson. Chem.* **2011**, *49*, 307–313.
(47) Giraudeau, P.; Massou, S.; Robin, Y.; Cahoreau, E.; Portais, J.-C.; Akoka, S. *Anal. Chem.* **2011**, *83*, 3112–3119.
(48) McNaught, A. D.; Wilkinson, A. *Compendium of Chemical Terminology*, 2nd ed.; Blackwell: Oxford, 1997.
(49) Comuzzo, A.; Rennella, E.; Schanda, P.; Mimmi, M. C.; Cutral, T.; Raimondi, S.; Giorgetti, S.; Fogolari, F.; Viglino, P.; Frydman, L.; Gal, M.; Bellotti, V.; Brutscher, B.; Esposito, G. *J. Biol. Chem.* **2010**, *285*, 5827–5835.
(50) Lee, M.-K.; Gal, M.; Frydman, L.; Varani, G. *Proc. Natl. Acad. Sci. U.S.A.* **2010**, *107*, 9192–9197.
(51) Pardo, Z. D.; Olsen, G. L.; Fernández-Valle, M. E.; Frydman, L.; Martínez-Álvarez, R.; Herrero, A. *J. Am. Chem. Soc.* **2012**, *134*, 2706–2715.

3. Multi-Scan-Single-Shot ufHSQC

As described above (Paragraph 2.6) ultrafast 2D NMR is a highly convenient tool for quantitative analysis, and it also becomes a tool of high importance in areas where conventional 2D NMR is fruitless because of its high experimental duration [17-19]. However, not much is known about the effectiveness of ultrafast hetero-nuclear 2D NMR in quantitative analysis. HSQC is one of the most widespread used hetero nuclear techniques for analyzing complex biological samples. In this chapter, we aim to provide the quantitative evaluation of ufHSQC, by evaluating the repeatability of relative peak volumes on a model metabolite mixture by comparison to conventional 2D HSQC. A systematic comparison between accumulated-ultrafast experiments and conventional acquisitions for a given experimental time has been done. For the purpose of accumulated ultrafast experiments we chose "Multi-Scan-Single-Shot" (M3S) strategy derived from ultrafast NMR methodology (Chapter 1). We successfully evaluated the analytical performance of the M3S strategy in homo-nuclear experiments which is explained in previous chapters. In this chapter we implemented M3S strategy in ufHSQC to evalutate its analytical performance.

Many different parameters affect normal 2D methods prohibiting their use for quantification. One of them is *J*-modulation, which is due to the evolution of $J_{H\text{-}H}$ coupling during the two INEPT periods in HSQC. The evolution of homo-nuclear couplings will reduce the correlation peak intensity which affects the relative standard deviation. In this chapter we studied these *J*-modulation effects by implementing the CPMG experiment in ufHSQC.
One more parameter that affects the quantification is rf pulse miscalibration. This effect is potentially higher in multipulse sequences like HSQC. In order to overcome this problem we employed either adiabatic, and compsite adiabatic or Fantastic-four pulses in M3S-ufHSQC. Fantastic-four pulses which are designed by optimal control theory in ufHSQC [156]. We evaluated the robustness of these special pulses by comparing with hard pulses in ufHSQC.

3.1 Preliminary studies

The comparison described in this section relies on the ultrafast and conventional HSQC experiments shown in Figure 35. The pulse sequence chosen for this study is represented in Figure 35A. It is a standard HSQC pulse sequence, where a small number of gradient and rf pulses have been added for coherence-selection purposes. In ultrafast 2D NMR (Figure 35B), the

whole 2D FID is recorded in a single scan, however several FIDs are accumulated for the sake of sensitivity, according to the M3S approach described above. Therefore, the total experiment duration T_a is given by NS × TR, where NS is the number of accumulations and TR is the duration of the pulse sequence, mainly dictated by the recovery delay. In conventional 2D NMR, the experiment duration is N_1 × NS × TR, where N_1 is the number of increments in the indirect dimension. The two acquisition strategies were compared on a model metabolic mixture. The spectra acquired in 20 min 19 sec are represented in Figure 35C, D, together with the corresponding pulse sequences.

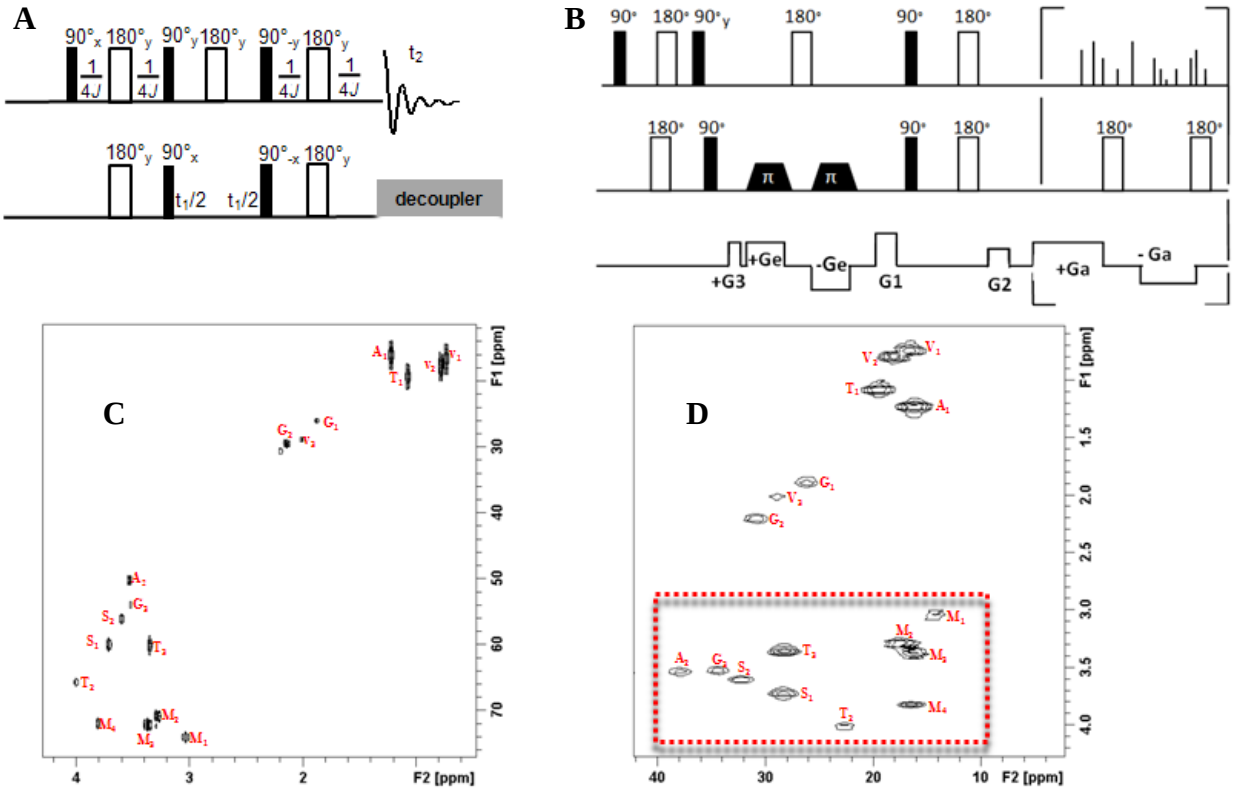

Figure 35: Strategies for recording quantitative 2D HSQC spectra, (A) by accumulating NS scans for each N_1 increment of a conventional 2D pulse sequence or (B) by accumulating NS ultrafast experiments in a multiscan single shot approach. The corresponding spectra are shown in (C) and (D) for the conventional and M3S approaches, respectively, acquired from a 500 mM metabolic mixture, in 20 min 19 sec on a 400 MHz Avance I Bruker spectrometer with a 5 mm dual+ probe. The experimental parameters are indicated in the Experimental Section. Folded peaks are highlighted with a red colour box.

Both approaches were compared with parameters ensuring identical total experiment times (N_1 = 128) and NS = 2 for the conventional approach, NS = 256 for the M3S). The ^{13}C NMR spectrum shows that the corresponding resonances cover a 70-ppm range, which is too big to

obtain a uf spectrum in a single scan without losing resolution. Therefore, we recorded the folded spectrum [147]. In the prelimary study, we evaluated the relative standard deviation (RSD) for the two approaches. The results are shown in Figure 36 and clearly highlight the superiority of the conventional HSQC. A possible explanation is that, unlike conventional homonuclear experiments where diagonal signals create a high level of t_1 noise, conventional HSQC experiments are not hampered by diagonal signals and are therefore less affected by hardware instabilities in the course of the experiment. Another possibility is that uf HSQC experiments are not fully optimized yet. As a consequence of this preliminary study, we chose to continue our quest for an optimum precision on the ufHSQC pulse sequence.

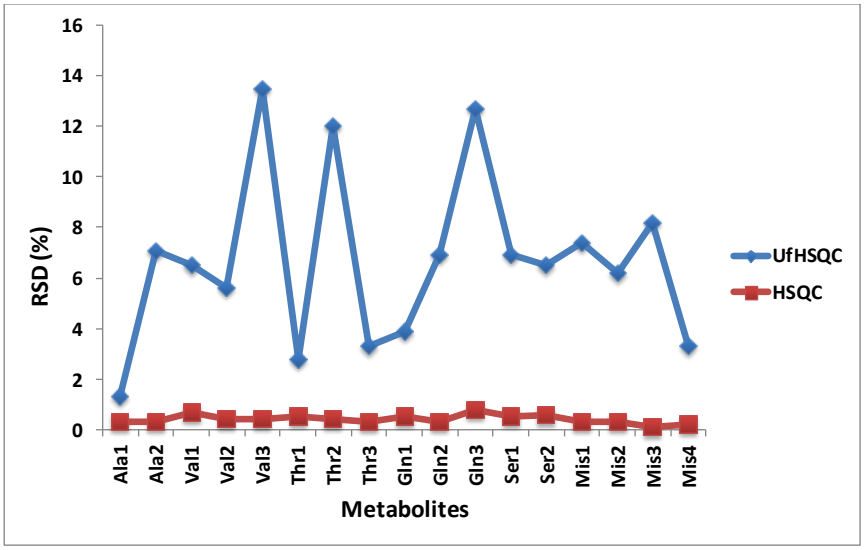

Figure 36: Relative Standard Deviation (RSD) of the M3S and conventional 2D peak volumes for the various metabolites of the 500 mM model mixture. Each RSD was determined from series of five spectra, acquired in 20 min 19 sec per spectrum on a 400 MHz Avance I Bruker spectrometer with a dual+ probe.

3.2 Strategies for improving precision

3.2.1 Study of *J*-modulation effect

For pulse sequences that incorporate a spin echo (e.g., a 180° pulse for refocusing, INEPT), an undesirable consequence is that while the chemical shift is refocused, the homo-nuclear scalar coupling (*J*) is not. The resulting perturbation of the observed signals is referred to as *J*-modulation. The manner in which *J*-modulation manifests itself will be dependent on various factors such as the magnitude of *J* and the spin echo time, and so the signal perturbation will not

always be clearly comprehensible. When a CPMG-sequence [157] is conducted simultaneously on two hetero-spins (CPMG–INEPT), the hetero-nuclear couplings will evolve, but the homo-nuclear coupling (J_{HH}) evolution is suppressed. We have adapted a CPMG-sequence to replace the INEPT periods of ufHSQC (Figure 37A) [16, 53]. The CPMG–INEPT period consists of 16 number of XY-16 sequences with total duration of $1/(2J_{CH})$. For a successful suppression of the J_{HH} evolution, the delay τ is optimized.

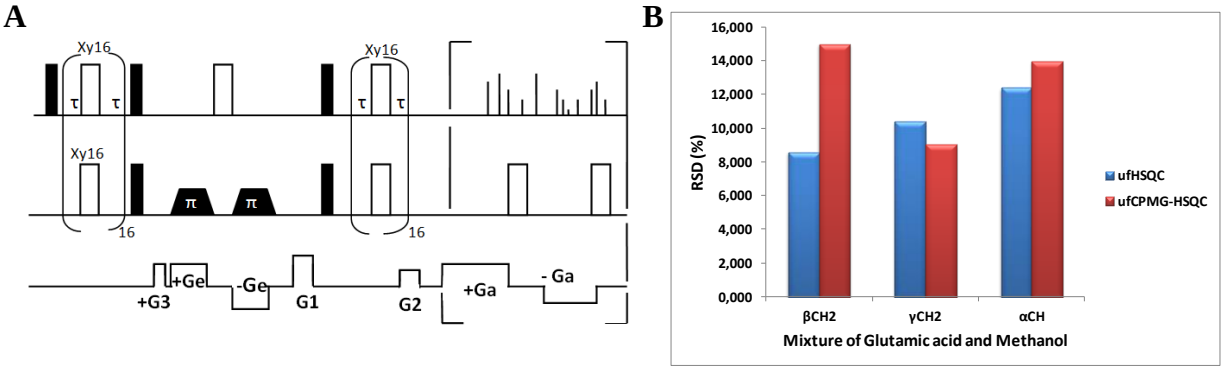

Figure 37: Pulse sequence of uf-CPMG-HSQC experiment (A). Narrow (filled) and wide (open) rectangles represent 90° and 180° respectively. τ =140 us was chosen such that the total length of the XY-16 spin echo pulse train equaled 5.55 ms. Relative Standard Deviation (RSD) of the ufHSQC and uf-CPMG-HSQC of the glutamic acid αCH, βCH_2 and γCH2 peak areas (or volumes) were measured relatively to the methanol CH_3 signal. Repeatability was evaluated for each method by repeating five experiments successively (B). Each CV was determined from series of five spectra, acquired in 10 min per spectrum on a 400 MHz Avance I Bruker spectrometer with a dual+ probe.

A mixture of glutamic acid and methanol was chosen for studying of *J*-modulation effects in ufHSQC. Glutamic aicd was chosen for the study of *J*-modulation due to its complex $J_{H\text{-}H}$ coupling network. The ufHSQC and uf-CPMG-HSQC spectra of glutamic acid and methanol mixture were recorded with 128 scans to estimate the effect of J_{HH} couplings on peaks volumes. We evaluated both ultrafast 2D methods for precise and accurate quantitative analysis. For ufHSQC and uf-CPMG-HSQC, the glutamic acid αCH, βCH_2 and γCH_2 peak areas (or volumes) were measured relatively to the methanol CH_3 signal. The repeatability was evaluated for each method by repeating five experiments successively. The results are presented in Figure 37B. The values of RSD obtained for uf-CPMG-HSQC are of the same order of magnitude as the values obtained for ufHSQC. This results highlight there is no significant effect of *J*-modulation on the repeatability of ufHSQC.

3.2.2 Adiabatic and Fantastic-4 pulses

RF inhomogeneity/miscalibration on ^{1}H and ^{13}C pulses deteriorates the signal intensity [158]. This shows a great effect on the precision of quantitative studies. The above issues can be solved or mitigated using adiabatic rf pulses. Adiabatic pulses offer large bandwidths and produce a uniform flip angle, provided that the B_1 field strength is above a certain threshold. Our group successfully reached a good precision by using adiabatic pulses in conventional 2D NMR [40].

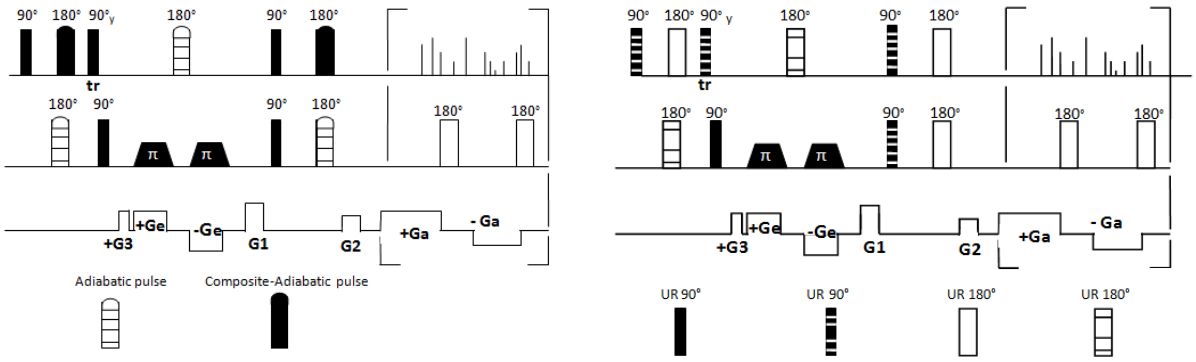

Figure 38: Pulse sequences of ufHSQC with adiabatic (A) and fantastic-four (B) pulses respectively. In the adiabatic pulse sequence narrow (filled) rectangular boxes represents 90° hard pulse. In the fantastic-four sequence UR 90°, PP 90°, UR 180° and PP 180° are represented by solid black bars, black bars with white horizontal stripes, white bars and white bars with black horizontal stripes, respectively. 'tr' is a time reverse shaped pulse. Both pulse sequences are practically of identical lengths. UR and PP indicate universal rotation and Point to Point pulses, respectively.

In order to study the repeatability, we measured the RSD for the peaks C_1, C_2, C_3 and C_4 of ibuprofen (Table 2) for the five successive experiments with hard, adiabatic and fantastic-four pulses. However the introduction of adiabatic and fantastic-four pulses did not significantly improve the repeatability.

In a second step, we investigated the potential effect of adiabatic and fantastic-four pulses on the robustness of the uf HSQC pulse sequence vis-a-vis rf pulse miscalibrations. A graph depicting the average of relative peak volumes versus the percentage of rf pulse miscalibration was plotted (Figure 39B). For peak C_1 we observed the same type of plot for adiabatic and fantastic-four pulses whereas for the hard pulse a slight deviation was observed. In the case of C_2 and C_3,

Table 2: Relative standard deviations (RSD) of the peaks of ibuprofen measured with hard, adiabatic and fantastic-four pulses respectively. Each value is average of five experiments.

Pulses	**Peaks**			
	1	**2**	**3**	**4**
Hard	1.5%	1.5%	2.8%	6.6%
Adiabatic	1.6%	1.5%	0.8%	7.8%
Fantastic four	1.8%	5.6%	1.1%	4.5%

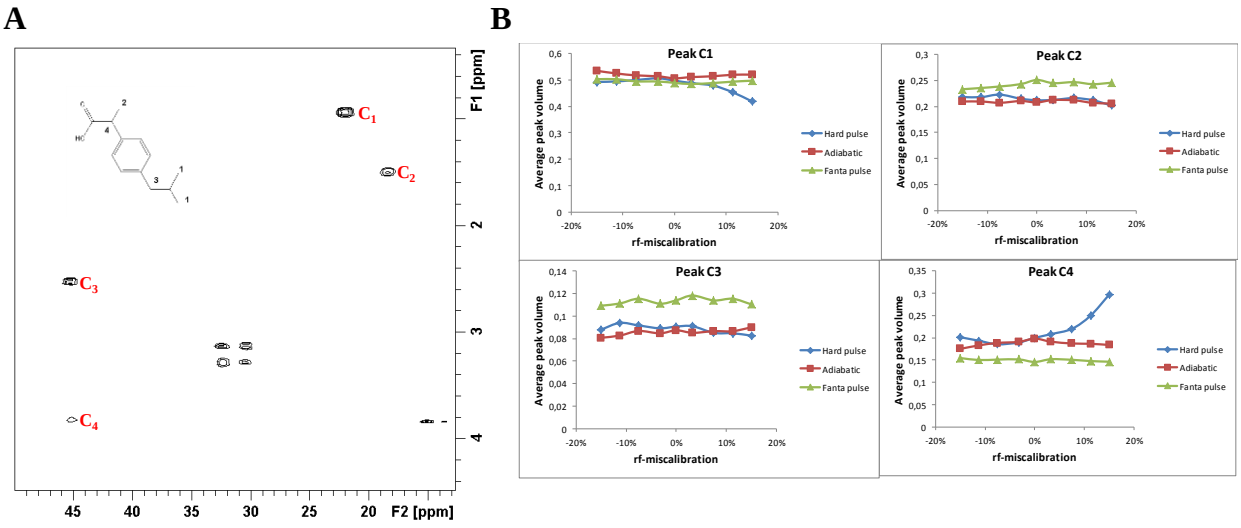

Figure 39: Uf HSQC spectrum (A) of Ibuprofen acquired in 1.7 minutes on a 400 MHz spectrometer. Peak volumes versus rf miscalibration (B). Each point in the graph is average of five successive experiments.

although we got similar plots for the three types of pulses, but the average peak volume for fantastic-four pulse was higher. Finally, in the case of C_4, the plots of hard and adiabatic pulses deviated from the fantastic-four pulse plot. Therefore, from this observation we can conclude that though rf is miscalibrated it does not affect the peak volumes in the case of fantastic-four or adiabatic pulses whereas in the case of the hard pulses it results in the deviation of the average peak volumes. Furthermore, these results highlight the interest of using fantastic-four or adiabatic pulses to increase the robustness of uf pulse sequences.

3.3 Materials and methods

3.3.1 Sample preparation

Three samples were used for this study. A mixture of 6 metabolites containing alanine (Ala), threonine (Thr), valine (Val), glutamine (Gln), myo-inositol (Myo), and Serine (Ser) was prepared by dissolving them in a phosphate buffer solution (0.1 M, pH = 7.4) to obtain a concentration of 500 mM for each metabolite.

A glutamic acid-methanol mixture in D_2O was also prepared by dissolving 100 mg in 1ml of 1M HCL to study *J*-modulation effects on peak volumes.

Ibuprofen was dissolved with acetone-d_6 in order to obtain a concentration of 100 mg mL^{-1} (0.49 mol L^{-1}). All the samples were analyzed in 5-mm NMR tubes.

3.3.2 NMR Acquisition Parameters

The NMR spectra were recorded at 298 K on a Bruker AVANCE I 400 spectrometer, equipped with a 5-mm dual probe and z-axis gradients at a ^1H frequency of 400.13 MHz. PW_{90} for ^1H and ^{13}C were carefully calibrated for each sample. The conventional HSQC spectra were recorded on the model metabolic mixture with the pulse sequence described in Figure 35A, with a 4 ppm spectral width in ^1H-dimension and 70 ppm in ^{13}C dimension. The free induction decays (FIDs) were recorded with 2048 points and an acquisition time of 0.6 s. The ^{13}C decoupling was performed with a garp-4 composite decoupling pulse sequence. 128 t_1 increments were recorded with 2 scans and a recovery delay of 4.55 s, resulting in a total experiment time of 22 min 19 sec. The ultrafast HSQC experiments were recorded using the pulse sequence represented in Figure 35B. The spatial encoding was performed using a constant-time spatial encoding scheme with 15 ms smoothed chirp encoding pulses. The uf specific parameters were set from the user-defined spectral widths and offsets, according to our Webpage [159]. The INEPT delay Δ was optimized to $1/4 \bullet {}^1J_{CH}$, with $^1J_{CH}$ = 130 Hz, corresponding to the average of the $^1H–^{13}C$ one-bond coupling constants.

The ^{13}C NMR spectra of the different samples show that the corresponding resonances cover spectral ranges which are too big to obtain a uf spectrum in a single scan without losing resolution. Therefore, we chose to use the folding option.

For the model metabolic mixture, 256 scans were recorded with TR = 5 s, resulting in a 20 min 19 sec total experiment time and five successive experiments were recorded, on each sample, for the purpose of evaluating the repeatability of relative peak volumes.

Uf-CPMG-HSQC experiments were recorded on a mixture of glutamic acid and methanol using the pulse sequence of Figure 37A. The INEPT and reverse- INEPT periods for coherence transfer through scalar coupling were modified by CPMG-INEPT in ufHSQC (Figure 37A). In our experiments XY-16 pulse trains are used on proton and carbon channels [88, 160]. The INEPT delay Δ was optimized for the $^1J_{CH}$-range of 115–190 Hz and the best value was 5.55 ms. Based on this value we chose τ = 140 μs so that the total length of the XY-16 spin echo pulse train equaled 5.55 ms.

Adiabatic full passage pulses were generated using Mathcad 8 (Math Soft, Inc.). They were designed with a cosine amplitude modulation of the rf field (ω_2 max 157.1 kHz and 93.89 kHz for ^{13}C and ^{1}H, respectively) and an offset independent adiabaticity (OIA) by optimizing the frequency sweep $\Delta\upsilon$ ($\Delta\upsilon$ = 72 kHz and 32 kHz for ^{13}C and ^{1}H, respectively) of length 106 ms each. For inversion pulses, adiabatic full passage pulses were used. For refocusing pulses, composite adiabatic pulses were used (Figure 38A) [40].

Hard pulses were replaced by corresponding Fantastic-four pulses in the ufHSQC sequence. For obtaining the most efficient replacement, the task of each hard pulse in Figure 35B is analyzed and classified according to the following four pulse types: UR 90°, PP 90°, UR 180° and PP 180° (represented in Figure 38B) by solid black bars, black bars with white horizontal stripes, white bars and white bars with black horizontal stripes, respectively). For example, the first ^{1}H $90°_x$-pulse acts on initial z magnetization and hence can be replaced by a PP $90°_y$ pulse that transfers I_z to $-I_y$. In the HSQC experiment, the following ^{1}H-180° pulse is a refocusing element that needs to be implemented as a UR 180° pulse, whereas, the simultaneously applied ^{13}C-180° pulse only needs to invert ^{13}C spins and can be replaced by a PP 180° pulse. Pulse bandwidths are 20 kHz for ^{1}H and 35 kHz for ^{13}C. The maximum rf amplitude for ^{13}C and ^{1}H spins were RF_{max} = 10 kHz and 18 kHz of length 1ms respectively [156].

3.3.3 NMR Processing and Integration Parameters

All the spectra were acquired and analyzed using the Bruker program Topspin 2.1. Before Fourier Transform, the HSQC raw data were weighed with a $\pi/2$-shifted sine-bell function and a

Lorentzian−Gaussian apodization in F_1 and F_2 dimensions, respectively. The data matrices were zero-filled to 8192 points in F_2 and to 1024 points in F_1. The specific processing and calibration for the uf spectra was performed using our home-written routine in Topspin, including apodization and zero filling as described in Ref [148]. The integration of 2D peak volumes was performed using the integration routine in the Bruker software. All the integration results are the average of five experiments. As described in the Results and Discussion, we chose to rely on the direct integration of 2D signals. The integration box widths were carefully adjusted for each series of experiments so as to obtain the same level of truncation for all peaks. Peak volumes were exported to Microsoft Excel 2010 for statistical analysis. The reduced peak volume ratios were calculated by dividing the volume of a given peak by the sum of all the integrated volumes. Then, the repeatability was assessed by calculating the relative standard deviation (RSD) on five successive experiments on the same sample.

3.4 Conclusion

Pertaining to this chapter, we evaluated the analytical performance of ufHSQC and compared it to its conventional counterpart. Although our initial examinations were not highly rewarding, we studied the *J*-modulations effects on relative standard deviations of the peak volumes. In addition to improving the pulse imperfection problems we also proposed adiabatic and fantastic-four pulses instead of hard pulses. We assessed the robustness of these pulses. Fantastic-four and adiabatic pulses are superior to the hard pulses. In the future we are also interested to study the off-resonances effects on the peak volumes. In HSQC experiments sensitivity is a huge problem. When highly concentrated samples are studied (which is not always of the case for metabolic mixtures) or by connecting with DNP, the experimental time in ultrafast can be reduced, which then leads to better improvement. Finally, it should be noted that we tried to implement a sensitivity-enhanced version of uf HSQC (see paragraph 1.6.4), but it did neither improve the repeatability nor the sensitivity.

Part D

Site-specific ^{13}C enrichment studies

Chimie Et Interdisciplinarité
Synthèse, Analyse,
Modélisation
CEISAM
UMR CNRS 6230
UNIVERSITÉ DE NANTES

1. Fluxomics studies by site specific ^{13}C enrichment measurements

In the previous part we introduced "Multi-Scan-Single-Shot" (M3S) starategy in the ultrafast homo-nuclear (COSY) and hetero-nuclear (HSQC) experiments. We evaluated their analytical performance. We used ufCOSY for the quantification of real breast cancer cells. This last part describes the development of quantitative uf methods in the context of fluxomics, *ie.* the study of metabolic fluxes in living organisms.

The work was done in collaboration with the group of Pr. J. C. Portais (INRA, UMR792 Ingénierie des Systèmes Biologiques et des Procédés, F-31400 Toulouse, France). By using ^{13}C-labelling experiments, the distribution of carbon fluxes in complex metabolic networks can be estimated from the labeling pattern of metabolites. The size of the network that can be investigated in a labeling experiment, as well as the accuracy on flux measurements, depends on the number and nature of the labeling data that are made available.

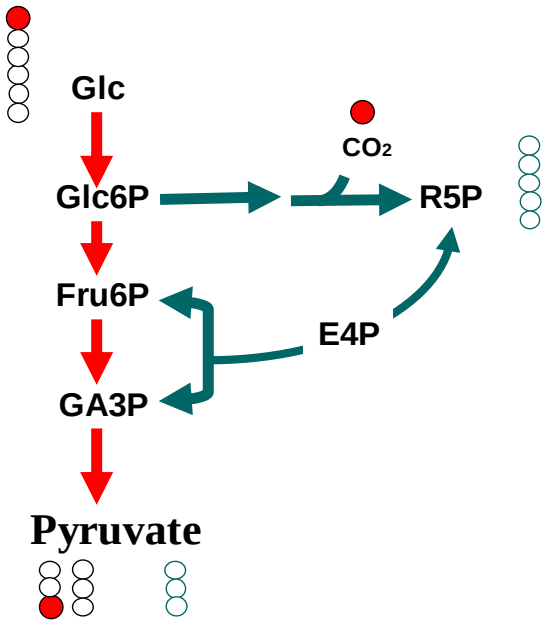

Figure 40: Principle of fluxomics: Organism are fed with glucose enriched in ^{13}C, after degradation of the organism; a complex mixture of labeled metabolites specific site ^{13}C is obtained. From the determination of site-specific ^{13}C enrichments, it is possible to determine metabolic pathways [161].

^{1}H NMR is a powerful tool for the study of ^{13}C isotopic enrichments (IE) i.e. the percentage of ^{13}C label incorporated in an individual carbon position of a metabolite, and isotopomers, i.e.

the various isotopic isomers that can be generated for the same metabolite (Figure 40). In a ^{1}H NMR spectrum, the signals from protons bound to a ^{12}C appear as center lines while the signal from protons attached to a ^{13}C nucleus appear as satellite lines due to the effects of hetero-nuclear scalar couplings (J_{CH}). The relative ^{13}C content in the considered carbon position can be calculated from the intensity of the satellite lines compared to the total intensity of the peak (Figure 41) [13].

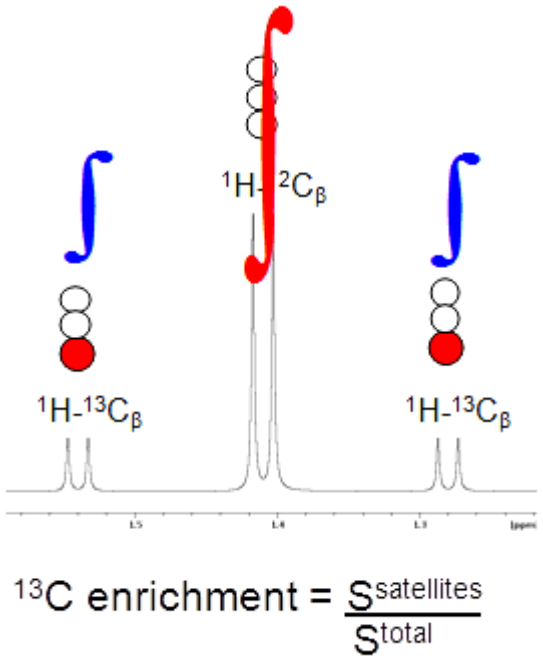

Figure 41: A simple case of 1D ^{1}H NMR spectrum, with the presence of intense satellite signals due to the ^{13}C-enrichment. To measure the isotopic enrichment, the area corresponding to the ^{13}C satellite is measured and this value is divided by the total area.

However this method is limited due to the overlapping of peaks in case of biological samples. To obtain good spectral resolution, an alternative is the application of 2D ^{1}H–^{1}H NMR experiments where the ^{1}H signals are dispersed (see Figure 8). However, these methods suffer from long acquisition times, thus limiting their use as a quantitative tool for fluxomics. We designed an ensemble of methods for measuring specific ^{13}C-enrichments in a very fast and accurate way, by using experiments based on ultrafast 2D NMR. A new ultrafast hetero-nuclear *J*-resolved spectroscopy strategy is presented. It is characterized by excellent analytical performances. However, ultrafast and conventional 2D methods are still limited by overlaps due

to ^{1}H-^{13}C splittings, thus limiting the metabolic information accessible for complex biological mixtures. To bypass this limitation, we also propose a fast 3D NMR method, UFJCOSY, which gives unambiguous access to isotopic enrichments in biological mixtures in a few minutes. We evaluated the analytical performance of these methods. The site – specific ^{13}C enrichments measurement on a model sample were found identical to those measured by 1D NMR. These methods are applied to the measurement of ^{13}C-enrichments on a biomass hydrolyzate obtained from *E. Coli* cells.

2. Hetero-nuclear *J*-resolved experiments

Journal of Magnetic Resonance 214 (2012) 335–339

Contents lists available at SciVerse ScienceDirect

Journal of Magnetic Resonance

journal homepage: www.elsevier.com/locate/jmr

Communication

Ultrafast hetero-nuclear 2D J-resolved spectroscopy

Meerakhan Pathan, Serge Akoka, Patrick Giraudeau*

Université de Nantes, CNRS, Chimie et Interdisciplinarité: Synthèse, Analyse, Modélisation (CEISAM), UMR 6230, BP 92208, 2 rue de la Houssinière, F-44322 Nantes Cedex 03, France

ARTICLE INFO

Article history:
Received 11 October 2011
Revised 8 November 2011
Available online 20 November 2011

Keywords:
Ultrafast 2D NMR
Hetero-nuclear J-resolved spectroscopy
Spatial encoding
$^{13}C-^{1}H$ couplings
^{13}C-enrichments

ABSTRACT

Ultrafast techniques enable the acquisition of 2D NMR spectra in a single scan. In this study, we propose a new ultrafast experiment designed to record hetero-nuclear $^{1}H-^{13}C$ J-resolved spectra in a fraction of a second. The approach is based on continuous constant-time phase modulated spatial encoding followed by a J-resolved detection scheme. An optional isotopic filter is implemented to remove the signal arising from ^{1}H bound to ^{12}C. While the most evident application of the technique proposed in this paper is the direct measurement of one bond scalar $^{13}C-^{1}H$ couplings for structural elucidation purposes, it also offers interesting potentialities for measuring ^{13}C isotopic enrichments in metabolic samples. The main features of this methodology are presented, and the analytical performances of the ultrafast hetero-nuclear J-resolved pulse sequence are evaluated on model samples.

1. Introduction

Two-dimensional nuclear magnetic resonance spectroscopy (2D NMR) has revolutionized the utility of NMR as an analytical technique [1,2]. One of the first 2D NMR experiments was the ^{1}H J-resolved (J-res) NMR proposed by Aue et al. [3], which allows the separation of chemical shifts and coupling interactions into two separate dimensions, greatly simplifying data analysis and resolution assignment, while also furnishing information about the homo-nuclear bonds in the sample through the J-couplings. Apart from being a powerful structural elucidation tool, this technique has found applications in bio-chemical studies, including metabolomics [4–6].

In 1976, the hetero-nuclear version of J-res NMR was proposed by Bodenhausen et al. [7]. Analogous to the homo-nuclear case, carbon-proton couplings are observed in the F_1 dimension while carbon chemical shifts are reflected in the F_2 dimension. The ability to probe scalar couplings or Residual Dipolar Couplings (RDCs) between ^{13}C and ^{1}H nuclei is highly helpful for numerous applications, such as molecular identifications or conformational analysis [8–10]. Despite its utility, one of the major disadvantages of this experiment, shared by all multi-dimensional NMR sequences, is the long experiment duration due to the t_1 incremental procedure necessary to sample the indirect F_1 dimension.

Various approaches to shorten the acquisition time of multi-dimensional NMR spectra have been developed [11–16]. The most efficient among these approaches is probably the so-called "ultrafast 2D NMR" approach proposed by Frydman and co-workers [17,18], where the acquisition of 2D NMR data is carried out in a single scan. The usual t_1 encoding is replaced by spatial encoding, followed by a conventional mixing period and by a detection block based on Echo Planar Imaging (EPI) [19]. The principles and features of ultrafast 2D NMR experiments have been described in details in recent literature [20–22]. One of the main advances in ultrafast 2D NMR methods is probably the replacement of the discrete spatial encoding scheme initially proposed by a continuous encoding pattern [23–26], relying on the combination of continuously frequency swept pulses applied during a bipolar gradient. The constant-time phase modulated encoding scheme proposed by Pelupessy [23] was shown to yield an optimal compromise between sensitivity and resolution [27,28], and it progressively became the method of choice to perform spatial encoding necessary for ultrafast experiments [29,30].

Despite its high potential, ultrafast 2D NMR still presents limitations in terms of sensitivity, resolution and spectral width, which have been described in recent papers [27,31–33]. Fortunately, several recent improvements have contributed to increase significantly the performances of ultrafast experiments, such as the introduction of a multi-echo excitation scheme to deal with sensitivity losses caused by molecular diffusion [28,34], or the implementation of various strategies to overcome spectral width and lineshape limitations [31,33,35–37].

In the present study we propose a new ultrafast experiment to record ultrafast hetero-nuclear J-resolved experiments. Its principles and features are described and potential applications are discussed and evaluated.

* Corresponding author. Address: Chimie et Interdisciplinarité: Synthèse, Analyse, Modélisation (CEISAM), UMR 6230, Faculté des Sciences, BP 92208, 2 rue de la Houssinière, F-44322 Nantes Cedex 03, France. Fax: +33 (0)2 51 12 57 12.
E-mail address: patrick.giraudeau@univ-nantes.fr (P. Giraudeau).

1090-7807/$ – see front matter © 2011 Elsevier Inc. All rights reserved.
doi:10.1016/j.jmr.2011.11.008

336 Communication / Journal of Magnetic Resonance 214 (2012) 335–339

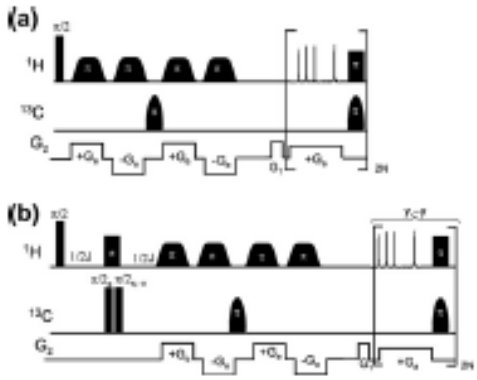

Fig. 1. Pulse sequences for ultrafast hetero-nuclear J-res without (a) and with isotopic filter (b), with ^{13}C decoupling in the ultrafast dimension, using a phase-modulated encoding scheme followed by a J-resolved detection scheme. The π hard pulses on the carbon channel are adiabatic cosine pulses with offset-independent-adiabaticity. The π pulse phase is alternated (y, y, −y, −y) to avoid undesirable stimulated echoes during detection. For the isotopic filter, two scans are necessary, with the indicated phase cycling on the second π/2 ^{13}C pulse and on the receiver, as indicated.

2. Method

The ultrafast hetero-nuclear J-resolved pulse sequence is presented in Fig. 1a. The excitation scheme proposed by Pelupessy [23], with a multiecho excitation designed to minimize molecular diffusion effects is employed [34]. A π adiabatic pulse is applied at the ^{13}C frequency in the middle of the excitation period to perform ^{13}C decoupling in the ultrafast dimension. The detection block, initially proposed by Giraudeau and Akoka [38], is modified by separating acquisition gradients with non-selective π pulses applied simultaneously on proton and carbon channels to refocus the effect of internal chemical shifts and proton–proton couplings. However the cumulated effects of the π hard pulse imperfections induce the formation of spurious stimulated echoes [39] for a series of three successive pulses, giving rise to undesirable signals at $\nu_2 = 0$ Hz. To compensate for it we introduce a y, y, −y, −y phase variation on the ^1H and ^{13}C π pulses applied during the acquisition. Its effect is to move the artefacts towards the edge of the ν_2 coupling range [38].

A notable difference with the homo-nuclear ultrafast J-resolved experiment is the large ^{13}C spectral range which needs to be decoupled. In order to perform homogeneous decoupling of the whole ^{13}C range, all the π hard pulses on the carbon channel are replaced by offset-independent-adiabaticity cosine adiabatic pulses optimized to obtain uniform decoupling [40].

In order to remove the signal arising from ^1H bound to ^{12}C, we also propose a modified version of the initial pulse sequence, based on an isotopic filter that can be introduced prior to spatial encoding, as shown on Fig. 1b. Provided that two scans are recorded with appropriate phase cycling on the second ^{13}C π/2 pulse and the receiver, the unwanted signal is completely filtered out for all protons.

3. Results and discussion

The ultrafast hetero-nuclear J-resolved experiment described in the previous section is first tested on a model mixture of labelled and unlabelled alanine (Fig. 2a). The spectrum is recorded with one scan in 190 ms. Proton-carbon couplings and ^1H chemical shifts are observed in the F_1 and the F_2 dimensions, respectively. The spectrum shows signals of ^1H attached to ^{13}C (central peaks) and ^{13}C (satellites), respectively. It is important to note that the spectrum is ^1H–^1H and ^1H–^{13}C decoupled in the spatially encoded dimension, with no need to perform the "tilt" operation commonly used in conventional J-resolved experiments.

In addition to the very short experimental duration, the ultrafast hetero-nuclear J-resolved experiment takes advantage of the high sensitivity of ^1H detection, which is not the case with the conventional hetero-nuclear J-resolved experiment. Another fundamental difference lies in the capacity of the conventional ^{13}C-detected experiment to detect only the signals arising from ^1H–^{13}C pairs, while the ultrafast experiment presented in Fig. 1a also detects resonances arising from ^1H bound to ^{12}C. This result can be viewed both as an advantage and a drawback. On the one hand, the possibility of detecting all protons provides an efficient way of measuring specific ^{13}C enrichments when working with partially labelled compounds. For the model alanine mixture, the site-specific ^{13}C enrichments were found identical to those measured by 1D NMR, i.e. 49.6% and 49.3% for the CH and the CH_3, respectively.

On the other hand, when working with complex mixtures and/or at low ^{13}C enrichments or natural abundance, the ^1H–^{12}C resonances may disturb the precise measurement of $^1J_{CH}$ coupling constants, which constitutes one of the main expected applications of the method. The modified version shown in Fig. 1b overcomes this drawback by removing the signal arising from ^1H bound to ^{12}C.

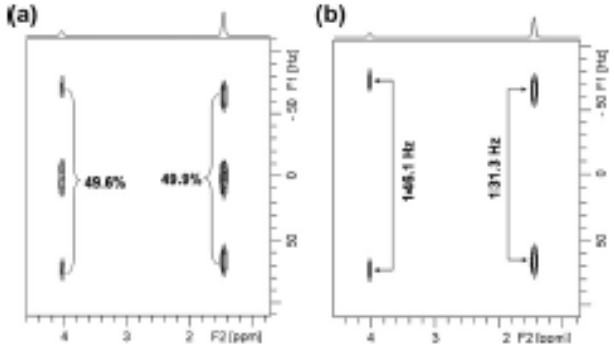

Fig. 2. Ultrafast hetero-nuclear J-res spectra, recorded without (a) and with isotopic filter (b), on a model mixture of labelled and unlabelled alanine. The spectra were acquired with the pulse sequences described in Fig. 1a and b respectively. The isotopic enrichments measured from Fig. 2a and the $^1J_{CH}$ couplings measured from Fig. 2b are indicated.

Communication / Journal of Magnetic Resonance 214 (2012) 335–339 337

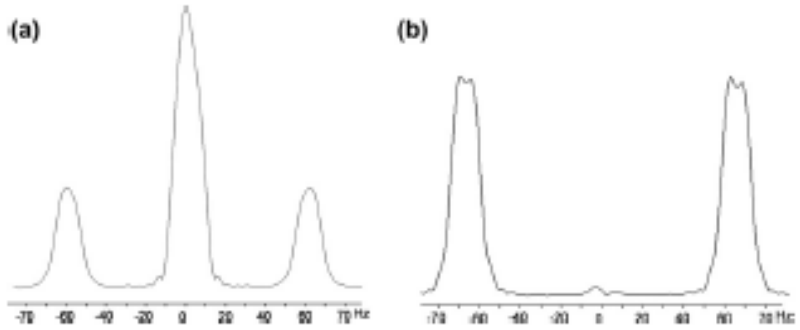

Fig. 3. Projection of columns corresponding to the alanine CH_3 peak at 1.47 ppm, obtained from the 2D spectra in Fig. 2, recorded without (a) and with isotopic filter (b).

This scheme was tested on the same model mixture (Fig. 2b). The spectrum was recorded with two scans. The 2D spectrum (Fig. 2b) shows the ^{12}C–^{1}H one bond couplings in the F_1 dimension. To evaluate the efficiency of the isotopic filter, we projected the columns of the alanine CH_3 peak at 1.4 ppm (Fig. 3) obtained from the spectra acquired with the two pulse sequences. The perfect suppression of the central peak shows the efficiency of the filter. The $^{1}J_{CH}$ coupling constants measured from the alanine sample (131.3 and 146.1 Hz) do not differ by more than 0.2% than those measured by 1D NMR (131.1 and 146.4 Hz). Moreover, in order to assess the precision of these measurements, ten successive experiments were performed, and the standard deviations on these values were found 0.1 Hz for both sites, indicating the high repeatability of the pulse sequence.

Prospective applications of this experiment include the measurement of coupling constants in non-enriched samples, a situation which is much more challenging regarding the filtering of ^{1}H–^{12}C signals. In order to assess the capacity of our pulse sequence to deal with such a situation, we applied it to a natural abundance ethyl bromopropionate sample. The corresponding spectra are represented in Fig. 4. The spectrum recorded without isotopic filter (Fig. 4a) clearly shows the impossibility to detect signals arising from ^{1}H bound to ^{13}C and to measure the corresponding coupling constants. When the filter is applied (Fig. 4b), these couplings become easily measurable even though the central signal is not totally suppressed. The residual central signal actually depends on the adequacy between the ^{1}H–^{13}C coupling constant of each signal and the delay chosen for the filter from the average coupling constant. Here, coupling constants were between 128 and 155 Hz, and an average J_{CH} of 140.4 Hz was chosen to calculate the filter delay. The resulting relative intensity of the central peak was between 0.4 and 1.7 relatively to the satellites, as a result of the scalar coupling mismatch. Still, the central peak does not affect the precision of the coupling constant measurement, as shown on the vertical projection of the peak at 2.9 ppm. If necessary, additional experiments may be performed while adapting the delay to a particular coupling constant, which could be necessary when the J_{CH} values are spread over a wide range.

While the capacity of the ultrafast method to measure coupling constants is relatively straightforward, its capacity to determine correctly isotopic enrichments in a wide range of values with good accuracy and precision needs to be evaluated. For that, we assessed the analytical performance of the experiment described in Fig. 1a on a series of [1-13C]-glucose mixtures with various isotopic enrichments ranging from 5% to 90%. The corresponding ultrafast 2D spectrum recorded in a single scan is represented in Fig. 5 for the 50% isotopic enrichment mixture. In aqueous solution, glucose undergoes a fast mutarotation reaction leading to a stable equilibrium between α- and β-glucopyranose [41], which explains the number of resonances observed. The isotopic enrichments are measured from the C_1^{β} resonance. For each sample, five 1D NMR and five 2D ultrafast hetero-nuclear J-res spectra are successively recorded to evaluate the precision of the method. For all samples, the isotopic enrichments measured by 2D NMR are plotted versus those obtained by quantitative 1D NMR. The accuracy is evaluated by the slope of the linear regression, and the determination coeffi-

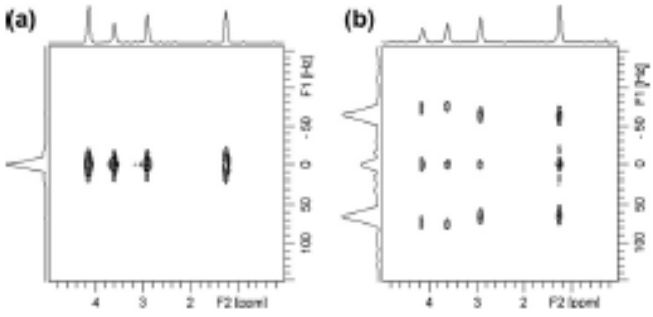

Fig. 4. Ultrafast hetero-nuclear J-res spectra, recorded without (a) and with isotopic filter (b), on a sample of ethyl(3-bromopropionate at natural abundance. The spectra were acquired with the pulse sequences described in Fig. 1a and b respectively. Two scans were necessary to record spectrum (b). The vertical projection of the column corresponding to the signal at 2.9 ppm is represented.

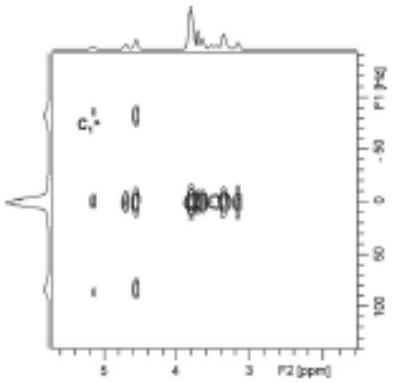

Fig. 5. Ultrafast hetero-nuclear J-resolved spectrum of a solution containing 50% of [1-^{13}C]-glucose and 50% of unlabelled glucose. The C_1^α peak was used for measuring ^{13}C isotopic enrichments.

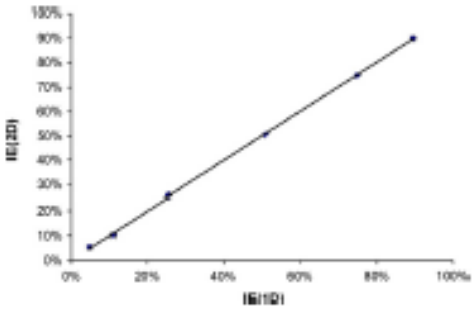

Fig. 6. ^{13}C-enrichments determined from ultrafast hetero-nuclear J-res spectra were plotted versus the values measured from 1D ^{1}H NMR. The [1-^{13}C]-glucose percentages were ranging from 5% to 90%. ^{13}C-enrichments in the C_1^α position of glucose were measured from the intensity of satellite signals relatively to the total intensity of the C_1^α signals.

cient r^2 is used to assess the linearity (Fig. 6). The values obtained highlight the excellent accuracy (slope close to unity, negligible intercept) and linearity (r^2 close to 1) of the method. Moreover, the small standard deviations (average 2%) highlight its very good repeatability. This high analytical performance opens new application perspectives of the ultrafast methodology as a tool for routine metabolic or fluxomic studies relying on specific ^{13}C-enrichment measurements [42]. The present study adds a new tool to the NMR-based metabolomics toolbox, an area where we had already proved the usefulness of ultrafast experiments [43].

A last point worth dwelling upon is the question of the sensitivity of the experiments described in this paper, especially when natural abundance samples are studied. The answer to this question is not unique, as sensitivity depends on the spectrometer and probe. However an estimation of the limit concentration that can be characterized for a given number of scans can be obtained from the Signal-to-Noise Ratio (SNR) values. For the 6.3 mol L^{-1} natural abundance ethyl bromopropionate sample studied in Fig. 4, an average SNR of 60 was obtained in the J_{CH} coupling dimension (the critical dimension from the SNR point of view) for a 2-scan experiment. Considering that a SNR of 3 corresponds to the limit of detection (LOD) [44], it means that the LOD would be around 0.3 mol L^{-1} with our hardware configuration. This value seems quite high, but lower concentrations are easily reached by signal averaging, a "multi-scan single shot" approach whose potentialities have been recently demonstrated [45]. Moreover, concentration is often not an issue for structural studies of small organic compounds where a sufficient amount of sample is available.

4. Conclusion

Ultrafast hetero-nuclear 2D J-resolved spectroscopy appears to be an efficient and versatile analytical tool to measure the proton-carbon couplings in a single scan or to access isotopic information. When an isotopic filter is employed, the most evident application of this technique is probably the direct measurement of one bond scalar ^{13}C–^{1}H couplings for structural elucidation purposes. Moreover, it should also form an interesting tool for measuring Residual Dipolar Couplings in oriented media [46]. When considering the non-filtered experiment, it opens the way towards applications in the field of metabolic and fluxomic studies by the measurement of isotopic enrichments in metabolic samples. The use of ultrafast J-resolved spectroscopy for such purposes would allow considerable time-saving that could significantly improve repeatability on successive measurements. Finally we are considering the extension of the ultrafast methodology to 3D NMR techniques in order to reach a higher level of discrimination between metabolite signals.

5. Experimental

A 1.16 mol L^{-1} mixture of various alanine isotopomers in D_2O was prepared as described in ref [42]. A 6.3 mol L^{-1} sample of ethyl 3-bromopromionate was prepared by adding 900 μL of this compound with 200 μL of acetone-d_6. Six samples containing unlabelled (natural abundance) and [1-^{13}C]-glucose in various ratios were prepared as described in Ref. [42]. The total amount of glucose was 50 mg, and the carbon-13 enrichment in position one was 5%, 10%, 25%, 50%, 75%, and 90%, respectively. The final glucose concentration was 0.46 mol L^{-1}. All the labelled compounds were purchased from Eurisotop (France).

All the NMR spectra were recorded at 298 K on a Bruker Avance III 500 spectrometer, at a frequency of 500.13 MHz with a cryogenically cooled probe including z-axis gradients and π/2 pulse of duration (PW_{90}) = 9.9 μs (except for the glucose sample where PW_{90} = 6.6 μs).

For all the ultrafast experiments, spatial encoding was performed using a constant-time spatial encoding scheme with four successive 1.5 ms smoothed chirp encoding pulses. The sweep range for the encoding pulses (60 kHz) was set to be significantly larger than the chemical shift range, and the amplitude of the encoding gradients was adapted to obtain a frequency dispersion equivalent to the frequency range of the pulses (G_e = 8.2 G/cm). A cosine adiabatic pulse with offset independent adiabaticity [40] of 300 μs with a sweep range of 60 kHz was applied at the ^{13}C frequency in the middle of the excitation period to perform ^{13}C decoupling in the ultrafast dimension.

The J-resolved detection block was formed of 128 detection gradients of duration T_e = 1.3 ms each. The acquisition gradient amplitude G_e was 40 G/cm. A non-selective π pulse and a cosine adiabatic pulse were applied simultaneously on proton and carbon channels, respectively.

The amplitude and duration of the pre-acquisition gradient were adapted to adjust the peak position in the ultrafast dimension. All the spectra were acquired and analyzed using the Bruker program Topspin 2.1. The specific processing for the ultrafast spectra was performed using our home-written routine in Topspin. The processing included an optimized gaussian apodization in the

ultrafast dimension to improve the line width and sensitivity, while conventional processing ($\pi/8$ shifted sinebell function and zero-filling) was performed in the conventional dimension. An automatic polynomial ($n = 5$) base line correction was applied in the conventional dimension.

Acknowledgments

The authors would like to thank Michel Giraudeau for linguistic assistance. This research was supported by funding from the "Agence Nationale de la Recherche" for young researchers (ANR Grant 2010-JCJC-0804-01).

References

[1] J. Jeener, Lecture Presented at Ampere International Summer School II, Basko Polje, Yugoslavia, 1971.
[2] W.P. Aue, E. Bartholdi, R.R. Ernst, Two-dimensional spectroscopy. Application to nuclear magnetic resonance, J. Chem. Phys. 64 (1976) 2229–2246.
[3] W.P. Aue, J. Karhan, R.R. Ernst, Homonuclear broad band decoupling and two-dimensional J-resolved NMR spectroscopy, J. Chem. Phys. 64 (1976) 4226–4227.
[4] F. Rastrelli, A. Bagno, Selective J-resolved spectra: a double pulsed field gradient spin-echo approach, J. Magn. Reson. 182 (2006) 29–37.
[5] C. Ludwig, M.R. Viant, Two-dimensional J-resolved NMR spectroscopy: review of a key methodology in the metabolomics toolbox, Phytochem. Anal. 21 (2010) 22–32.
[6] A. Khatib, E.C. Wilson, H.K. Kim, A.W.M. Lefeber, C. Erkelens, Y.H. Choi, R. Verpoorte, Application of two-dimensional J-resolved nuclear magnetic resonance spectroscopy to differentiation of beer, Anal. Chim. Acta 559 (2006) 264–270.
[7] C. Bodenhausen, R. Freeman, D.L. Turner, Two-dimensional J spectroscopy: proton-coupled Carbon-13 NMR, J. Chem. Phys. 65 (1976) 839–840.
[8] J.S. Taylor, D.S. Garrett, M.P. Cohen, Solution-state structure of the Dewar pyrimidinone photoproduct of thymidylyl-(3′ .5′)-thymidine, Biochemistry 27 (1988) 7206–7215.
[9] U.R. Prabhu, S.R. Chaudhuri, N. Suryaprakash, Visualization of enantiomers and determination of homo- and hetero-nuclear residual dipolar and scalar couplings: the natural abundant 13C edited J/D-resolved NMR techniques, Chem. Phys. Lett. 500 (2010) 334–341.
[10] J. Farjon, J.-P. Baltaze, P. Lesot, D. Merlet, J. Courtieu, Heteronuclear selective refocusing 2D NMR experiments for the spectral analysis of enantiomers in chiral oriented solvents, Magn. Reson. Chem. 42 (2004) 594–599.
[11] V.A. Mandelshtam, H.S. Taylor, A.J. Shaka, Application of the filter diagonalization method to one- and two-dimensional NMR spectra, J. Magn. Reson. 133 (1998) 304–312.
[12] R. Brüschweiler, F. Zhang, Covariance nuclear magnetic resonance spectroscopy, J. Chem. Phys. 120 (2004) 5253–5260.
[13] E. Kupce, R. Freeman, Two-dimensional Hadamard spectroscopy, J. Magn. Reson. 162 (2003) 300–310.
[14] E. Kupce, R. Freeman, Projection-reconstruction technique for speeding up multidimensional NMR spectroscopy, J. Am. Chem. Soc. 126 (2004) 6429–6440.
[15] P. Schanda, B. Brutscher, Very fast two-dimensional NMR spectroscopy for real-time investigation of dynamic events in proteins on the time scale of seconds, J. Am. Chem. Soc. 127 (2005) 8014–8015.
[16] B. Vitorge, C. Bodenhausen, P. Pelupessy, Speeding up nuclear magnetic resonance spectroscopy by the use of SMART Recovery Times – SMART NMR, J. Magn. Reson. 207 (2010) 149–152.
[17] L. Frydman, A. Lupulescu, T. Scherf, Principles and features of single-scan two-dimensional NMR spectroscopy, J. Am. Chem. Soc. 125 (2003) 9204–9217.
[18] L. Frydman, T. Scherf, A. Lupulescu, The acquisition of multidimensional NMR spectra within a single scan, Proc. Natl. Acad. Sci. USA 99 (2002) 15858–15862.
[19] P. Mansfield, Spatial mapping of the chemical shift in NMR, Magn. Reson. Med. 1 (1984) 370–386.
[20] M. Gal, L. Frydman, Ultrafast multidimensional NMR: principles and practice of single-scan methods, in: D.M. Grant, R.K. Harris (Eds.), Encyclopedia of NMR, Wiley, New-York, 2009.
[21] M. Mishkovsky, L. Frydman, Principles and progress in ultrafast multidimensional nuclear magnetic resonance, Annu. Rev. Phys. Chem. 60 (2009) 429–448.
[22] A. Tal, L. Frydman, Single-scan multidimensional magnetic resonance, Prog. Nucl. Magn. Reson. Spectrosc. 57 (2010) 241–292.
[23] P. Pelupessy, Adiabatic single scan two-dimensional NMR spectroscopy, J. Am. Chem. Soc. 125 (2003) 12345–12350.
[24] B. Shapira, Y. Shrot, L. Frydman, Symmetric spatial encoding in ultrafast 2D NMR spectroscopy, J. Magn. Reson 178 (2006) 33–41.
[25] Y. Shrot, L. Frydman, Spatial encoding strategies for ultrafast multidimensional nuclear magnetic resonance, J. Chem. Phys. 128 (2008) 052209.
[26] Y. Shrot, B. Shapira, L. Frydman, Ultrafast 2D NMR spectroscopy using a continuous spatial encoding of the spin interactions, J. Magn. Reson 171 (2004) 163–170.
[27] P. Giraudeau, S. Akoka, Sources of sensitivity losses in ultrafast 2D NMR, J. Magn. Reson. 192 (2008) 151–158.
[28] P. Giraudeau, S. Akoka, Sensitivity losses and line shape modifications due to molecular diffusion in continuous encoding ultrafast 2D NMR experiments, J. Magn. Reson. 195 (2008) 9–16.
[29] P. Giraudeau, G.S. Remaud, S. Akoka, Evaluation of Ultrafast 2D NMR for Quantitative Analysis, Anal. Chem. 81 (2009) 479–484.
[30] C. Wu, M. Zhao, S. Cai, Y. Lin, Z. Chen, Ultrafast 2D COSY with constant-time phase-modulated spatial encoding, J. Magn. Reson. 204 (2010) 82–90.
[31] P. Pelupessy, L. Duma, G. Bodenhausen, Improving resolution in single-scan 2D spectroscopy, J. Magn. Reson. 194 (2008) 169–174.
[32] Y. Shrot, L. Frydman, The effects of molecular diffusion in ultrafast two-dimensional nuclear magnetic resonance, J. Chem. Phys. 128 (2008) 164513.
[33] Y. Shrot, L. Frydman, Spatial/spectral encoding of the spin interactions in ultrafast multidimensional NMR, J. Chem. Phys. 131 (2009) 224516.
[34] P. Giraudeau, S. Akoka, Resolution and sensitivity aspects of ultrafast J-resolved 2D NMR spectra, J. Magn. Reson. 190 (2008) 339–345.
[35] P. Giraudeau, S. Akoka, A new gradient-controlled method for improving the spectral width of ultrafast 2D NMR experiments, J. Magn. Reson. 205 (2010) 171–176.
[36] P. Giraudeau, Y. Shrot, L. Frydman, Multiple Ultrafast, Broadband 2D NMR spectra of hyperpolarized natural products, J. Am. Chem. Soc. 131 (2009) 13902–13903.
[37] P. Giraudeau, S. Akoka, Sensitivity and lineshape improvement in ultrafast 2D NMR by optimized apodization in the spatially encoded dimension, Magn. Reson. Chem. 49 (2011) 307–313.
[38] P. Giraudeau, S. Akoka, A new detection scheme for ultrafast J-resolved spectroscopy, J. Magn. Reson 186 (2007) 352–357.
[39] E.L. Hahn, Spin echoes, Phys. Rev. 80 (1950) 580–594.
[40] E. Tenailleau, S. Akoka, Adiabatic 1H decoupling scheme for very accurate intensity measurements in 13C NMR, J. Magne. Reson. 185 (2007) 50–58.
[41] N. Le Barc'h, J.M. Crosnel, P. Looten, M. Mathlouthi, Kinetic study of the mutarotation of α-glucose in concentrated aqueous solution by gas–liquid chromatography, Food Chem. 74 (2001) 119–124.
[42] S. Mareau, C. Nicolai, F. Lelièvre, J.-C. Portais, NMR-based flavonomics: quantitative 2D NMR methods for isotopomers analysis, Phytochemistry 68 (2007) 2330–2340.
[43] P. Giraudeau, S. Mareau, Y. Robin, E. Cahoreau, J.-C. Portais, S. Akoka, Ultrafast quantitative 2D NMR: an efficient tool for the measurement of specific isotopic enrichments in complex biological mixtures, Anal. Chem. 83 (2011) 3112–3119.
[44] ICH-Q2B, Validation of analytical procedures: methodology, 1995. <http://www.fda.gov/downloads/Drugs/GuidanceComplianceRegulatoryInformation/Guidances/ucm073384.pdf>.
[45] M. Pathan, S. Akoka, I. Tea, B. Charrier, P. Giraudeau, Multi-scan single shot quantitative 2D NMR: a valuable alternative to fast conventional quantitative 2D NMR, Analyst 136 (2011) 3157–3163.
[46] C.M. Thiele, Residual dipolar couplings (RDCs) in organic structure determination, Eur. J. Org. Chem. 34 (2008) 5673–5695.

3. Fast 3D experiments

CHEMPHYSCHEM

ChemPubSoc Europe

DOI: 10.1002/cphc.201200255

UFJCOSY: A Fast 3D NMR Method for Measuring Isotopic Enrichments in Complex Samples**

Patrick Giraudeau,*[a] Edern Cahoreau,[b, c, d] Stéphane Massou,[b, c, d] Meerakhan Pathan,[a] Jean-Charles Portais,[b, c, d] and Serge Akoka[a]

Methods based on ^{13}C isotopic enrichment are common procedures for metabolite quantification and metabolic flux analysis in complex biological samples.[1–4] 2D NMR spectroscopy is a powerful tool in this field,[5–11] as it offers the capacity of measuring site-specific ^{13}C enrichments in complex samples. However, existing methods relying on 2D NMR are hampered by numerous overlaps when complex mixtures are studied. Here, we propose a fast 3D NMR method, based on ultrafast spatially-encoded NMR, which gives unambiguous access to isotopic enrichments (IEs) in biological mixtures in a few minutes, an experiment duration roughly 60 times shorter than a conventional 3D NMR approach.

The combination of NMR with ^{13}C-labeling strategies is a powerful tool for studying metabolic fluxes in living systems.[5–11] Biological samples are generally incubated with ^{13}C-labeled substrates, and the metabolic fluxes in complex networks can be estimated from the labeling pattern of metabolites. As the isotope distribution is generally not uniform over a given molecule, analytical methods must be able to measure site-specific ^{13}C enrichments (i.e. the ^{13}C enrichment for each position of each molecule). The simplest procedure consists of integrating the ^{13}C-satellite peaks on ^1H NMR spectra,[8,12,13] however this approach is impractical due to the large overlap between peaks in complex mixtures. Several approaches based on 2D ^1H NMR have been designed to circumvent this drawback.[7–9] Homonuclear 2D spectra are recorded, where ^1H–^{13}C couplings are expressed in one dimension only which reduces overlaps while permitting the determination of site-specific isotopic enrichments by extracting rows (parallel to the F_2 dimension) from the 2D spectrum. Whereas this approach initially suffered from long experiment durations, we recently proposed a strategy to reduce the experiment time by several orders of magnitude, based on the ultrafast 2D NMR methodology.[14] This acquisition strategy, relying on spatial encoding, makes it possible to record 2D NMR spectra in a single scan—or a few scans when signal averaging is necessary for sensitivity purposes.[15–17]

However, both conventional and ultrafast 2D NMR methods are still affected by signal overlaps due to the ^1H–^{13}C splitting (typically 100–200 Hz) in one of the two dimensions. Consequently, many isotopomers cannot be resolved by these methods, thus limiting the metabolic information accessible for complex biological mixtures.[8,14] In order to bypass this limitation, it would be interesting to tilt the ^1H–^{13}C splittings in a third dimension, thus avoiding overlaps caused by heteronuclear couplings while preserving the information on ^{13}C enrichments. Such an acquisition strategy, however, would require the sampling of an additional spectral dimension, thus increasing the acquisition duration to several tens of hours, which would be highly impractical.

This communication presents a new NMR acquisition strategy permitting the acquisition of 3D data in a few minutes, based on the ultrafast 2D NMR strategy developed by Frydman[17] and described in recent papers.[17–19] In the corresponding NMR pulse sequence (Figure 1), two dimensions are recorded in an ultrafast fashion, while the third one is recorded in a conventional way. Therefore, a full 3D spectrum can be recorded in the time generally required to obtain a conventional 2D spectrum.

The pulse sequence starts like a conventional correlation spectroscopy (COSY) experiment, with a linear time incrementation to sample the ^1H chemical shifts in the first dimension, including a 180° ^{13}C pulse in the middle of this period to refocus the heteronuclear couplings. The 90° coherence transfer pulse is then followed by a constant-time spatial encoding scheme,[20] while the heteronuclear couplings are again refocused by a 180° pulse. Finally, the information is decoded in an echo-planar-imaging fashion (EPI),[21] and 180° pulses are applied during the detection to refocus chemical shift interactions.[22] Therefore, the ^1H–^{13}C splittings are detected in the third dimension, similarly to the ultrafast heteronuclear *J*-resolved strategy that we have described recently.[23] Following the acquisition, a processing specific to ultrafast acquisitions is applied (see Experimental Section).

Figure 2a presents the 3D NMR spectrum obtained in 11 min on a model alanine sample with this pulse sequence. The ^1H chemical shifts are expressed in dimensions F_1 and F_3, the conventionally sampled and spatially encoded dimensions, respectively. A F_1F_3 plane read from the 3D spectrum gives rise to a COSY-type correlation (Figure 2b), where the peaks are not broadened by heteronuclear couplings in spite of the ^{13}C enrichment, contrary to the 2D methods previously published.[7,9,10] The heteronuclear couplings are obtained in di-

[a] Dr. P. Giraudeau, M. Pathan, Prof. S. Akoka
EBSI team, CEISAM UMR 6230, Université de Nantes, CNRS
B.P. 92208, 2 rue de la Houssinière, 44322 Nantes Cedex 03 (France)
E-mail: patrick.giraudeau@univ-nantes.fr

[b] E. Cahoreau, Dr. S. Massou, Prof. J.-C. Portais
Université de Toulouse; INSA, UPS, INP
135 Avenue de Rangueil, 31077 Toulouse (France)

[c] E. Cahoreau, Dr. S. Massou, Prof. J.-C. Portais
INRA, UMR792 Ingénierie des Systèmes Biologiques et des Procédés
31400 Toulouse (France)

[d] E. Cahoreau, Dr. S. Massou, Prof. J.-C. Portais
CNRS, UMR5504, 31400 Toulouse (France)

[**] UFJCOSY: Ultrafast *J*-Resolved Correlation Spectroscopy

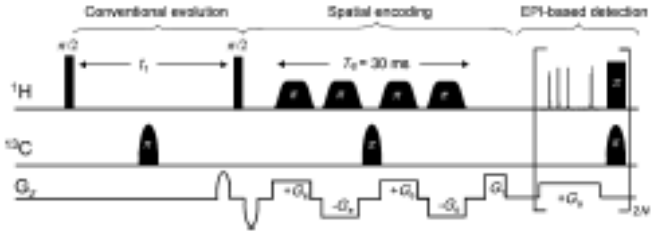

Figure 1. 3D UFJCOSY NMR pulse sequence for the fast measurement of site-specific ^{13}C isotopic enrichments in complex mixtures. The ^1H homonuclear correlations are obtained through the conventional (F_1) and spatially encoded (F_2) dimensions, while the third dimension (F_3), based on an echo-planar imaging detection, which give access to ^1H–^{13}C heteronuclear couplings.

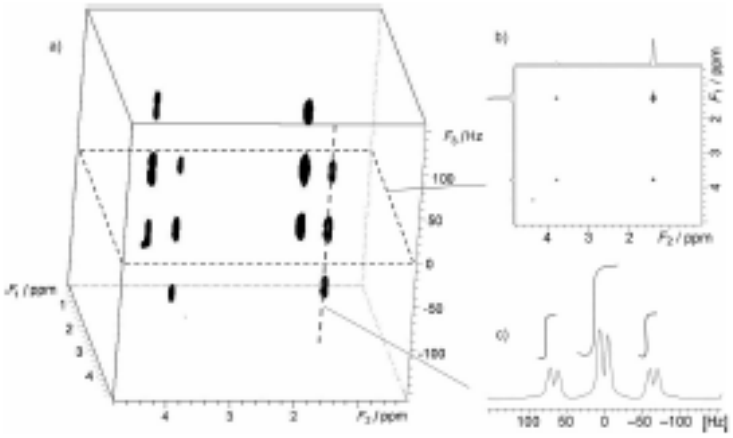

Figure 2. a) 3D UFJCOSY NMR spectrum recorded with the pulse sequence of Figure 1 on a model, partially labeled alanine sample. b) F_1/F_2 COSY plane and c) column extracted from the 3D spectrum. 128 conventional time increments were recorded in the F_1 dimension, resulting in a total acquisition time of about 11 min. The ultrafast dimension (F_3) was spatially-encoded during 30 ms, a value chosen to optimize sensitivity and resolution. The echo-planar-imaging (F_3) dimension was recorded with $2N = 128$ acquisition gradients, resulting in 64 acquisition points in the F_3 dimension. Recording a conventional 3D spectrum equivalent to this dataset would have required approximately 12 h acquisition time. The spectra were recorded on a 500 MHz Bruker spectrometer with a cryoprobe. The data were processed with our home-written routine in Topspin.

mension F_3, and the ^{13}C isotopic enrichments (IEs) are measured by reading a column perpendicular to the COSY plane (Figure 2 c). The IE values are then obtained by dividing the surface under the ^{13}C satellites by the total area. For this model sample, ^{13}C enrichments of 49% and 46% were obtained on the alanine CH and CH_3 peaks. These values were very similar to those recently measured by ultrafast 2D NMR on the same sample[24] (49.0% and 48.8%, respectively).

In order to illustrate the potentialities of the UFJCOSY (ultrafast *J*-resolved correlation spectroscopy) approach on a real sample, we applied it to a biomass extract obtained from *E. coli* cells grown on a mixture of 50% [U-^{13}C]-glucose and 50% nonlabeled glucose. Figure 3 presents the 2D COSY plane extracted from the corresponding 3D UFJCOSY spectrum, and a few columns parallel to the F_1 dimension are also represented. The 2D COSY plane illustrates the high resolution gain obtained compared to the conventional and to the ultrafast 2D spectra as shown in ref. [14]. The columns perpendicular to this COSY plane contain all the information needed to determine the site-specific ^{13}C isotopic enrichments.

The results presented above illustrate the potentialities of the 3D UFJCOSY pulse sequence for the fast measurement of ^{13}C IEs in biological samples. The full analytical evaluation (accuracy, precision, linearity) of this method on a variety of samples is the subject of current research and will be described in future papers. Sensitivity issues are far from being trivial and will also need to be evaluated. Still, we believe that this method will allow the measurement of a higher number of IEs than the 2D approaches previously described, and with a greater analytical performance. Variants of the pulse sequence presented in Figure 1 are also under investigation, based on double-quantum filtered COSY (DQF-COSY) or total correlation spectroscopy (TOCSY).

These results also highlight the potentialities of the hybrid conventional/ultrafast 3D approach. A similar strategy was suggested by Mishkovsky et al. in a biomolecular context,[14] but was never applied in practice, to the best of our knowledge. Of course, this kind of experiments exhibits the same characteristics as ultrafast 2D NMR, such as limitations in terms of spectral width, sensitivity and resolution.[24–38] However, solutions have been recently proposed which have greatly enhanced the performance of ultrafast 2D spectroscopy.[24,26,29–31] Some of them have been applied here, such as a multiecho spatial encoding[24] (Figure 1) to limit the influence of molecular diffusion effects, or the application of a spatial apodization procedure in the spatially-encoded dimension[32] to improve line shape and sensitivity. Moreover, the overall sensitivity is improved by the data accumulation performed in the conventional dimension. We hope that the research presented in this paper will open numerous development perspectives towards hybrid acquisition strategies mixing ultrafast, conventional or other fast sampling methods.

CHEMPHYSCHEM

ChemPubSoc Europe

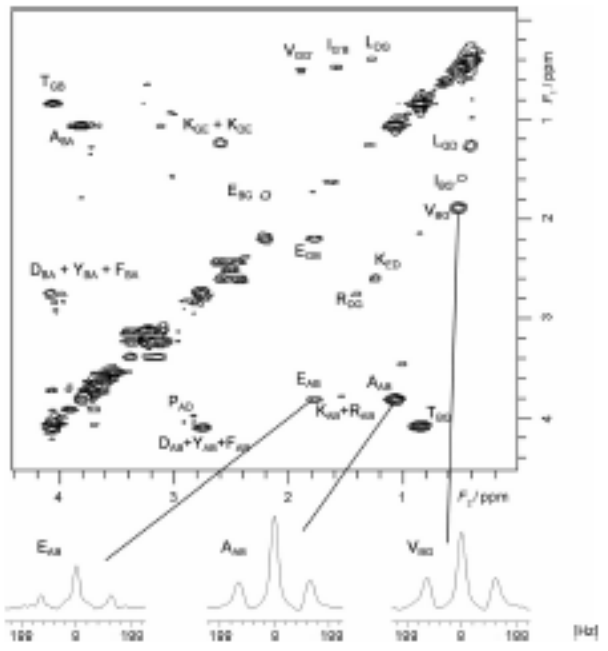

Figure 2. F_1/F_2 COSY plane from a 3D UF/COSY NMR spectrum recorded with the pulse sequence of Figure 1 on a biomass extract from *E. coli* cells grown on 30% of [U-^{13}C]-glucose and 50% of natural abundance glucose. Columns perpendicular to the COSY plane are represented on the bottom. Cross peaks are annotated as described in ref. [14]. 256 conventional time increments were recorded in the t_1 dimension, resulting in a total acquisition time of about 22 min. The ultrafast dimension was spatially-encoded during 30 ms, a value chosen to optimize sensitivity and resolution. The echo-planar-imaging (F_2) dimension was recorded with $2N=128$ acquisition gradients, resulting in 64 acquisition points in the F_2 dimension. Recording a conventional 3D spectrum equivalent to this dataset would have required approximately 24 h acquisition time. The spectra were recorded on a 500 MHz Bruker spectrometer with a cryoprobe. The data were processed with our home-written routine in Topspin.

Experimental Section

The model alanine and the *E. Coli* biomass samples were identical to those described in ref [14], where the complete sample preparation is described. All NMR spectra were recorded at 300 K on a Bruker Avance III 500 spectrometer working under Topspin 2.1, at a ^{1}H frequency of 500.13 MHz with a cryogenically cooled probe including z-axis gradients. For ultrafast 3D experiments (pulse sequence shown in Figure 1), 128 t_1 increments were recorded in the conventional dimension for Figure 2, and 256 increments were recorded for Figure 3, as a better resolution was required to characterize the complex mixture. The spatial encoding was performed using a multi-echo constant-time spatial encoding scheme[29] formed of four 7.5 ms smoothed chirp pulses[30] with 10% smoothing. The sweep range for the encoding pulses (60 kHz) was set to be significantly larger than the ^{1}H chemical shift range, and the amplitude of the encoding gradients was adapted to obtain a frequency dispersion equivalent to the frequency range of the pulses ($G_e = 5.3$ G cm^{-1}). Acquisition gradient parameters were set as follows: $G_a = 23.4$ G cm^{-1}, $T_a = 1.6$ ms (experiment of Figure 2) and $T_a = 1.1$ ms (experiment of Figure 3). 128 detection gradients were applied in both cases. In the ultrafast dimension, 1024 points were recorded during each acquisition gradient.

The specific processing for ultrafast spectra was performed using our home-written routine in Topspin. The processing included a $\pi/8$-shifted sine window function in the conventional dimension, a $\pi/8$-shifted sine-squared window function in the EPI dimension, and a zero-filling to 512 points in the conventional dimension and to 256 points in the EPI dimension. In the ultrafast dimension, zero filling by a factor of 1 was applied and an optimized apodization function was applied as recently described[31] in order to obtain optimum line shapes while improving sensitivity at no cost in terms of resolution. Ultrafast data were processed in magnitude mode to correct phase distortions induced by spatial encoding.[14]

Acknowledgements

The authors acknowledge funding from the French National Research Agency (ANR starting grant QUANTUM 2010-JCJC-0804-01 and ANR 08-BIOE-002). The authors are grateful to Michel Giraudeau for linguistic assistance.

Keywords: 3D NMR spectroscopy · isotopic labeling · metabolism · spatial encoding · ultrafast NMR spectroscopy

[1] J. K. Kelleher, *Metab. Eng.* **2001**, *3*, 100–110.
[2] R. G. Ratcliffe, Y. Shachar-Hill, *Biol. Rev. Cambridge Philos. Soc.* **2005**, *80*, 27–43.
[3] R. G. Shulman, D. L. Rothman, *Annu. Rev. Physiol.* **2001**, *63*, 15–48.
[4] W. Wiechert, *Metab. Eng.* **2001**, *3*, 195–206.
[5] R. A. Carvalho, F. M. Jeffrey, A. D. Sherry, C. R. Malloy, *FEBS Lett.* **1998**, *440*, 382–386.
[6] W. Eisenreich, J. Slaghuis, R. Laupitz, J. Bussemer, J. Stritzker, C. Schwarz, R. Schwarz, T. Dandekar, W. Goebel, A. Bacher, *Proc. Natl. Acad. Sci. USA* **2006**, *103*, 2040–2045.
[7] L. A. Lewis, R. H. Karsten, M. E. Norton, M. Tonelli, W. M. Westler, J. L. Markley, *Anal. Chem.* **2010**, *82*, 4558–4563.
[8] S. Massou, C. Nicolas, F. Letisse, J.-C. Portais, *Phytochemistry* **2007**, *68*, 2330–2340.
[9] S. Massou, C. Nicolas, F. Letisse, J.-C. Portais, *Metab. Eng.* **2007**, *9*, 252–257.
[10] T. Szyperski, *Eur. J. Biochem.* **1995**, *232*, 433–448.
[11] T. Szyperski, *Q. Rev. Biophys.* **1998**, *31*, 41–106.
[12] A. P. Alonso, H. Vigeolas, P. Raymond, D. Rolin, M. Dieuaide-Noubhani, *Plant Physiol.* **2005**, *138*, 2220–2232.
[13] D. Ronnen, M. Dieuaide-Noubhani, E. J. Dufour, P. Raymond, D. Rolin, *J. Biol. Chem.* **2002**, *277*, 43948–43960.
[14] P. Giraudeau, S. Massou, Y. Robin, E. Cahoreau, J.-C. Portais, S. Akoka, *Anal. Chem.* **2011**, *83*, 3112–3119.

[15] M. Mishkovsky L. Frydman, *Annu. Rev. Phys. Chem.* **2009**, *60*, 429 – 448.
[16] L. Frydman, A. Lupulescu, T. Scherf, *J. Am. Chem. Soc.* **2003**, *125*, 9204 – 9217.
[17] L. Frydman, T. Scherf, A. Lupulescu, *Proc. Natl. Acad. Sci. USA* **2002**, *99*, 15858 – 15862.
[18] M. Mishkovsky M. Gal, L. Frydman, *J. Biomol. NMR* **2007**, *39*, 291 – 301.
[19] A. Tal, L. Frydman, *Prog. Nucl. Magn. Reson. Spectrosc.* **2010**, *57*, 241 – 292.
[20] P. Pelupessy, *J. Am. Chem. Soc.* **2003**, *125*, 12345 – 12350.
[21] P. Mansfield, *J. Phys. C: Solid State Phys.* **1977**, *10*, 55 – 58.
[22] P. Giraudeau, S. Akoka, *J. Magn. Reson.* **2007**, *186*, 352 – 357.
[23] M. Pathan, S. Akoka, P. Giraudeau, *J. Magn. Reson.* **2012**, *214*, 335 – 339.
[24] P. Giraudeau, S. Akoka, *J. Magn. Reson.* **2008**, *190*, 339 – 345.
[25] Y. Shrot, L. Frydman, *J. Chem. Phys.* **2008**, *128*, 164513.
[26] Y. Shrot, L. Frydman, *J. Chem. Phys.* **2009**, *131*, 224516.
[27] P. Giraudeau, S. Akoka, *J. Magn. Reson.* **2008**, *192*, 151 – 158.
[28] P. Giraudeau, S. Akoka, *J. Magn. Reson.* **2008**, *195*, 9 – 16.
[29] P. Giraudeau, S. Akoka, *J. Magn. Reson.* **2010**, *205*, 171 – 176.
[30] P. Giraudeau, S. Akoka, *Magn. Reson. Chem.* **2011**, *49*, 307 – 313.
[31] P. Pelupessy, L. Duma, G. Bodenhausen, *J. Magn. Reson.* **2008**, *194*, 169 – 174.
[32] J. M. Böhlen, G. Bodenhausen, *J. Magn. Reson. Ser. A* **1993**, *102*, 293 – 301.

Received: March 28, 2012
Published online on June 26, 2012

Conclusion and Perspectives

Chimie Et Interdisciplinarité
Synthèse, Analyse,
Modélisation
CEISAM
UMR CNRS 6230
UNIVERSITÉ DE NANTES

Conclusion and Perspectives

My work in this thesis was to develop ultrafast quantitative NMR methods specifically in the context of metabolic studies. In the first chapter I describe a routine made to facilitate the implementation of ultrafast NMR in order to increase the application range of this promising technique. We hope that these developments will help increasing the number of groups using uf NMR, and to initiate new collaborations.

In a second part, the Multi-Shot-Single-Scan strategy has been used and compared with its conventional counterpart in terms of sensitivity and resolution. This strategy has been applied applied to measure the absolute metabolite concentration in breast cancer cell line extracts, relying on a standard addition protocol. The main conclusion of this part is that homo-nuclear uf 2D NMR gives a higher level of precision and linearity than the corresponding conventional 2D NMR experiments. Then we introduced the M3S strategy in hetero-nuclear experiments (HSQC). The precision of this method still needs to be improved, and for the moment conventional experiments remain more sensitive and repeatable. Finally in order to study the site specific ^{13}C-enrichments in fluxomics, we have proposed an ultrafast hetero-nuclear *J*-resolved experiment. The ability to differentiate the $J_{C\text{-}H}$ couplings and ^{1}H chemical shifts in two orthogonal dimensions within a single transient opens up many other interesting applications. As an example, this approach could be pivotal in studying the residual dipolar couplings (RDC) in liquid crystals. Another significant development presented in this thesis is the 3D*J*COSY for the site specific ^{13}C-enrichment in complex biological mixtures. In this scheme, the conventional COSY experiment has been mixed with ultrafast hetero-nuclear *J*-resolved experiment to create a new Hybrid experiment. Very recently our group evaluated the analytical performance of this method in case of complex biological mixtures [162]. These hybrid 3D strategies could open new development and application perspectives in fields where 3D NMR is employed, such as protein NMR.

The ability of uf NMR spectroscopy to acquire multidimensional NMR spectra is mainly limited by the inherent low sensitivity of this technique. In recent years many methods have been developed to enhance the nuclear polarization, such as dynamic nuclear polarization (DNP), Para-hydrogen and optical pumping. By coupling DNP with uf NMR, L. Frydman and his group demonstrated the high possibility to record single-scan 2D spectra following the

hyperpolarization of analytes in low concentration [145, 153]. However, the DNP-NMR coupling has not so far been evaluated for quantitative analysis. In addition, the peak volumes of the spectra obtained by this method depend on a number of additional parameters specific to the DNP, which means that many methodological developments will be necessary in order to use this approach for quantitative purposes. One of the promising applications is to implement the DNP-ultrafast strategy on *in vivo* systems to study the metabolic pathways in real time. This will require the development of localized uf spectroscopy methods, such as those recently proposed by T. Roussel et al. [136].

References

Chimie Et Interdisciplinarité
Synthèse, Analyse,
Modélisation
CEISAM
UMR CNRS 6230
UNIVERSITÉ DE NANTES

References

1. J.K. Kwakye, *Use of NMR for quantitative analysis of pharmaceuticals.* Talanta, 1985. **32**: p. 1069-1071.

2. U. Holzgrabe, *Quantitative NMR spectroscopy in pharmaceutical applications.* Progress in Nuclear Magnetic Resonance Spectroscopy, 2010. **57**(2): p. 229-240.

3. D.S. Wishart, *Quantitative metabolomics using NMR.* Trac-Trend. Anal. Chem., 2008. **27**(3): p. 228-237.

4. J.C. Lindon, et al., *Metabonomics: Metabolic processes studied by NMR spectroscopy of biofluids.* Concepts in Magnetic Resonance, 2000. **12**(5): p. 289-320.

5. S. Zhang, et al., *Correlative and quantitative 1H NMR-based metabolomics reveals specific metabolic pathway disturbances in diabetic rats.* Anal. Biochem., 2008. **383**(1): p. 76-84.

6. G.F. Pauli, B.U. Jaki, and D.C. Lankin, *Quantitative 1H NMR: Developpement and potential of a method for natural products analysis.* J. Nat. Prod., 2005. **68**: p. 133-149.

7. E. Tenailleau, et al., *Authentication of the origin of vanillin using quantitative natural abundance ^{13}C NMR.* J. Agric. Food Chem., 2004. **52**: p. 7782-7787.

8. F. Le Grand, G. George, and S. Akoka, *Natural abundance 2H-ERETIC-NMR authentication of the origin of methyl salicylate.* Journal of Agricultural and Food Chemistry, 2005. **53**(13): p. 5125-5129.

9. E. Caytan, et al., *Precise and accurate quantitative ^{13}C NMR with reduced experimental time.* Talanta, 2007. **71**: p. 1016-1021.

10. R. Peyraud, et al., *Demonstration of the ethylmalonyl-CoA pathway by using 13C metabolomics.* Proc. Natl. Acad. Sci. U. S. A., 2009. **106**(12): p. 4846-4851.

11. H. Koskela, *Quantitative 2D NMR studies.* Annu. Rep. NMR Spectrosc., 2009. **66**: p. 1-31.

12. E. Martineau, et al., *Absolute quantification of metabolites in breast cancer cell extracts by quantitative 2D 1H INADEQUATE NMR.* NMR Biomed., 2012. 25(8): p. 985-992.

13. S. Massou, et al., *NMR-based fluoxomics: Quantitative 2D NMR methods for isotopomers analysis.* Phytochemistry, 2007. **68**: p. 2330-2340.

14. L. Zhang and G. Gellerstedt, *Quantitative 2D HSQC NMR determination of polymer structures by selecting suitable internal standard references.* Magn. Reson. Chem., 2007. **45**: p. 37-45.

15. I.A. Lewis, et al., *Method for determining molar concentrations of metabolites in complex solutions from two-dimensional ^{1}H-^{13}C NMR spectra.* Anal. Chem., 2007. **79**: p. 9385-9390.

16. S. Heikkinen, et al., *Quantitative 2D HSQC (Q-HSQC) via suppression of J-Dependence of polarization transfer in NMR spectroscopy: application to wood lignin.* J. Am. Chem. Soc, 2003. **125**: p. 4362-4367.

17. P. Giraudeau, G.S. Remaud, and S. Akoka, *Evaluation of Ultrafast 2D NMR for Quantitative Analysis.* Anal. Chem., 2009. **81**(1): p. 479-484.

18. P. Giraudeau, et al., *Ultrafast 2D NMR applied to the kinetic study of D-glucose mutarotation in solution.* J. Spectrosc. Dyn., 2011. **1**: p. 2.

19. P. Giraudeau, et al., *Ultrafast Quantitative 2D NMR: An Efficient Tool for the Measurement of Specific Isotopic Enrichments in Complex Biological Mixtures.* Anal. Chem., 2011. **83**(8): p. 3112-3119.

20. J.L. Jungnickel and J.W. Forbes, *Quantitative Measurement of Hydrogen Types by Integrated Nuclear Magnetic Resonance Intensities.* Anal. Chem., 1963. **35**: p. 938-942.

21. D.P. Hollis, *Quantitative Analysis of Aspirin, Phenacetin, and Caffeine Mixtures by Nuclear Magnetic Resonance Spectrometry.* Anal. Chem., 1963. **35**: p. 1682-1684.

22. V. Rizzo and V. Pinciroli, *Quantitative NMR in synthetic and combinatorial chemistry.* J. Pharm. Biomed. Anal., 2005. **38**: p. 851-857.

23. F. Malz and H. Jancke, *Validation of quantitative NMR.* J. Pharmaceut. Biomed. Anal., 2005. **38**: p. 813-823.

24. S.K. Bharti and R. Roy, *Quantitative 1H NMR spectroscopy.* TrAC Trends in Analytical Chemistry, 2012. **35**(0): p. 5-26.

25. F. Podo, et al., *Absolute metabolite quantification by in vivo NMR spectroscopy: I. Introduction, objectives and activities of a concerted action in biomedical research.* Magnetic Resonance Imaging, 1998. **16**: p. 1085-1092.

26. M.A. Farag, A. Porzel, and L.A. Wessjohann, *Comparative metabolite profiling and fingerprinting of medicinal licorice roots using a multiplex approach of GC–MS, LC–MS and 1D NMR techniques.* Phytochemistry, 2012. **76**(0): p. 60-72.

27. D.J. Cookson and B.E. Smith, *Optimal conditions for obtaining quantitative 13C NMR data.* J. Magn. Reson., 1984. **57**: p. 355-368.

28. T.H. Mareci and K.N. Scott, *Quantitative analysis of mixtures by carbon-13 nuclear magnetic resonance spectroscopy.* Anal. Chem., 1977. **49**(14): p. 2130-2136.

29. J.N. Shoolery, *Some quantitative applications of ^{13}C NMR spectroscopy.* Prog. Nucl. Magn. Reson. Spectrosc., 1977. **11**: p. 79-93.

30. T. Mavromoustakos, et al., *13C NMR analysis of the triacylglycerol composition of greek virgin olive oils.* Magn. Reson. Chem., 1997. **35**: p. S3-S7.

31. G. Vlahov, *Application of NMR to the study of olive oils.* Prog. NMR Spectrosc., 1999. **35**: p. 341-357.

32. M. Aursand, L. Jorgensen, and H. Grasdalen, *Quantitative high-resolution 13C Nuclear Magnetic Resonance of anserine and lactate in white muscle of Atlantic salmon (salmo salar).* Comp. Biochem. Physiol., 1995. **112B**: p. 315-321.

33. U. Bussy, et al., *Isotopic finger-printing of active pharmaceutical ingredients by 13C NMR and polarization transfer techniques as a tool to fight against counterfeiting.* Talanta, 2011. **85**: p. 1909-1914.

34. E. Tenailleau, *Développement de la RMN quantitative du ^{13}C en abondance naturelle*, 2005, Thèse de doctorat, Université de Nantes: Nantes.

35. P. Dais and A. Spyros, *31P NMR spectroscopy in the quality control and authentication of extra-virgin olive oil: A review of recent progress.* Magn. Reson. Chem., 2007. **45**: p. 367-377.

36. G.C. Levy, T. Pehk, and P.R. Srinivasan, *Quantitative ^{15}N NMR spectroscopy.* Org. Magn. Reson., 1980. **14**: p. 129-132.

37. D.G. Lonnon and J.M. Hook, *^{17}O Quantitative Nuclear Magnetic Resonance Spectroscopy of Gasoline and Oxygenated Additives.* Anal. Chem., 2003. **75**: p. 4659-4666.

38. W. He, et al., *Quantitative 19F NMR method validation and application to the quantitative analysis of a fluoro-polyphosphates mixture.* Journal of Fluorine Chemistry, 2006. **127**(6): p. 809-815.

39. P. Giraudeau, J.L. Wang, and E. Baguet, *Improvement of the inverse-gated decoupling sequence for a faster quantitative analysis by ^{13}C NMR.* C.R. Chimie, 2006. **9**: p. 525-529.

40. C. Thibaudeau, et al., *Performance Evaluation of Quantitative Adiabatic ^{13}C NMR Pulse Sequences for Site-specific Isotopic Measurements.* Anal. Chem., 2010. **2010**: p. 5582-5590.

41. E. Martineau, *Etude de profils métaboliques dans les cellules de culture humaines par spectroscopie isotopique: application pour la découverte de nouvelles cibles thérapeutiques*, 2011, Thèse de doctorat, Université de Nantes: Nantes.

42. R.K. Rai, P. Tripathi, and N. Sinha, *Quantification of metabolites from two-dimensional Nuclear MAgnetic Resonance spectroscopy: Application to human urine samples.* Anal. Chem., 2009. **81**: p. 10232-10238.

43. P. Giraudeau, et al., *Optimization of homonuclear 2D NMR for fast quantitative analysis: Application to tropine-nortropine mixtures.* J. Pharmaceut. Biomed. Anal., 2007. **43**: p. 1243-1248.

44. R. Freeman, S.P. Kempsell, and M.H. Levitt, *Radiofrequency pulse sequences which compensate their own imperfections.* J. Magn. Reson., 1980. **38**: p. 453-479.

45. T. Fujirawa and K. Nagayama, *Composite inversion pulses with frequency switching and their application to broadband decoupling.* J. Magn. Reson., 1988. **77**: p. 55-63.

46. M.H. Levitt and R. Freeman, *NMR population inversion using a composite pulse.* J. Magn. Reson., 1979. **33**: p. 473-476.

47. M.H. Levitt and R. Freeman, *Compensation for pulse imperfections in NMR spin-echo experiments.* J. Magn. Reson., 1981. **43**: p. 65-80.

48. E.C. Cano, M.A. Smith, and A.J. Shaka, *Adjustable, Broadband, Selective Excitation with Uniform Phase.* J. Magn. Reson, 2002. **155**: p. 131-139.

49. T.-L. Hwang, P.C.M. Van Zijl, and M. Garwood, *Broadband adiabatic refocusing without phase distorsion.* J. Magn. Reson, 1997. **124**: p. 250-254.

50. E. Kupce and R. Freeman, *Adiabatic pulses for wideband inversion and broadband decoupling.* J. Magn. Reson. A, 1995. **115**: p. 273-276.

51. E. Kupce and R. Freeman, *Stretched adiabatic pulses for broadband decoupling spin inversion.* J. Magn. Reson. A, 1995. **117**: p. 246-256.

52. R.D. Boyer, R. Johnson, and K. Krishnamurthy, *Compensation of refocusing inefficiency with synchronized inversion sweep (CRISIS) in multiplicity-edited HSQC.* J. Magn. Reson., 2003. **165**: p. 253-259.

53. H. Koskela, I. Kilpeläinen, and S. Heikkinen, *Some aspects of quantitative 2D NMR.* J. Magn. Reson., 2005. **174**: p. 237-244.

54. E. Tenailleau and S. Akoka, *Adiabatic ^{1}H decoupling scheme for very accurate intensity measurements in ^{13}C NMR.* J. Magne. Reson., 2007. **185**(1): p. 50-58.

55. W. Gronwald, et al., *Urinary Metabolite Quantification Employing 2D NMR Spectroscopy.* Anal. Chem., 2008. **80**(23): p. 9288-9297.

56. F. Hu, et al., *Nondestructive Quantification of Organic Compounds in Whole Milk without Pretreatment by Two-Dimensional NMR Spectroscopy.* Journal of Agricultural and Food Chemistry, 2007. **55**(11): p. 4307-4311.

57. E. Martineau, et al., *Fast and precise quantitative analysis of metabolic mixtures by 2D ^{1}H INADEQUATE NMR.* J. Pharm. Biomed. Anal., 2011. **54**: p. 252-257.

58. K. Hu, et al., *Measurement of Absolute Concentrations of Individual Compounds in Metabolite Mixtures by Gradient-Selective Time-Zero 1H–13C HSQC with Two Concentration References and Fast Maximum Likelihood Reconstruction Analysis.* Analytical Chemistry, 2011. **83**(24): p. 9352-9360.

59. K. Hu, W.M. Westler, and J.L. Markley, *Simultaneous Quantification and Identification of Individual Chemicals in Metabolite Mixtures by Two-Dimensional Extrapolated Time-Zero 1H−13C HSQC (HSQC0).* Journal of the American Chemical Society, 2011. **133**(6): p. 1662-1665.

60. J. Jeener, Lecture presented at Ampere International Summer School II, Basko Polje, Yugoslavia, 1971.

61. W.P. Aue, E. Bartholdi, and R.R. Ernst, *Two-dimensional spectroscopy. Application to nuclear magnetic resonance.* J. Chem. Phys., 1976. **64**(5): p. 2229-2246.

62. R.R. Ernst, G. Bodenhausen, and A. Wokaun, *Principles of nuclear magnetic resonance in one and two dimensions*. Oxford Science Publications ed. 1987, Oxford.

63. W.P. Aue, et al., *Sensitivity of two-dimensional NMR spectroscopy.* J. Magn. Reson., 1978. **29**: p. 523-533.

64. A. Martinez, et al., *High-resolution and high-sensitivity 2D homonuclear J-resolved NMR spectroscopy.* Magnetic Resonance in Chemistry, 2012. **50**(1): p. 28-32.

65. W.P. Aue, J. Karhan, and R.R. Ernst, *Homonuclear broad band decoupling and two-dimensional J-resolved NMR spectroscopy.* J. Chem. Phys., 1976. **64**(10): p. 4226-4227.

66. M.R. Viant, *Improved methods for the acquisition and interpretation of NMR metabolomic data.* Biochemical and Biophysical Research Communications, 2003. **310**(3): p. 943-948.

67. Y. Wang, et al., *Spectral editing and pattern recognition methods applied to high-resolution magic-angle spinning 1H nuclear magnetic resonance spectroscopy of liver tissues.* Anal. Biochem., 2003. **323**: p. 26-32.

68. O. Hendrawati, et al., *Metabolic differentiation of Arabidopsis treated with methyl jasmonate using nuclear magnetic resonance spectroscopy.* Plant Science, 2006. **170**: p. 1118-1124.

69. A. Sanchez-Sampedro, et al., *Metabolomic alterations in elicitor treated Silybum marianum suspension cultures monitored by nuclear magnetic resonance spectroscopy.* Journal of Biotechnology, 2007. **130**: p. 133-142.

70. H. Widarto, et al., *Metabolomic Differentiation of Brassica rapa; Following Herbivory by Different Insect Instars using Two-Dimensional Nuclear Magnetic Resonance Spectroscopy.* Journal of Chemical Ecology, 2006. **32**: p. 2417-2428.

71. J. Alonso, et al., *Two-Dimensional correlated spectroscopy (COSY) of intact frog muscle: Spectral pattern characterization and lactate quantitation.* Magn. Reson. Med., 1989. **11**: p. 316-330.

72. M. Rance, et al., *Improved spectral resolution in COSY ^{1}H NMR spectra of proteins via double quantum filtering.* Biochem. Biophys. Res. Comm., 1983. **117**(2): p. 479-485.

73. U. Piantini, O.W. Sorensen, and R.R. Ernst, *Multiple quantum filters for elucidating NMR coupling networks.* J. Am. Chem. Soc, 1982. **104**: p. 6800-6801.

74. R. Nouaille, et al., *Production of maltodextrin 1-Phosphate by Fibrobacter succinogenes S85.* FEBS letters, 2004. **576**(1): p. 226-230.

75. M.E. Girvin, *Increased Sensitivity of COSY Spectra by Use of Constant Time t1 Periods.* J. Magn. Reson. Ser. A, 1994. **108**: p. 99-102.

76. S.R. Hartmann and E.L. Hahn, *Nuclear double resonance in the rotating frame.* Phys. Rev., 1962. **128**: p. 2042-2053.

77. A. Bax and D.G. Davis, *Practical aspects of two-dimensional transverse NOE spectroscopy.* J. Magn. Reson, 1985. **63**: p. 207-213.

78. D.G. Davis and A. Bax, *Assignment of complex ^{1}H NMR spectra via two-dimensional homonuclear Hartmann-Hahn spectroscopy.* J. Am. Chem. Soc, 1985. **107**: p. 2820-2821.

79. L. Braunschweiler and R.R. Ernst, *Coherence transfer by isotropic mixing: Application to proton correlation spectroscopy.* J. Magn. Reson, 1983. **53**: p. 521-528.

80. A. Bax and D.G. Davis, *MLEV-17-based two-dimensional homonuclear magnetization transfer spectroscopy.* J. Magn. Reson, 1985. **65**: p. 355-360.

81. M.J. Thrippleton and J. Keeler, *Elimination of Zero-Quantum Interference in two-dimensional spectra.* Angew. Chem. Int. Edit., 2003. **42**: p. 3938-3941.

82. S. Massou, et al., *Application of 2D-TOCSY NMR to the measurement of specific ^{13}C-enrichments in complex mixtures of ^{13}C-labeled metabolites.* Metab. Eng., 2007. **9**: p. 252-257.

83. G. Bodenhausen and D.J. Ruben, *Natural abundance nitrogen-15 NMR by enhanced heteronuclear spectroscopy.* Chem. Phys. Lett., 1980. **69**(1): p. 185-9.

84. L. Müller, *Sensitivity enhanced detection of weak nuclei using heteronuclear multiple quantum coherence.* J. Am. Chem. Soc., 1979. **101**: p. 4481-4484.

85. A. Richardson, et al., *Central carbon metabolism in the progression of mammary carcinoma.* Breast Cancer Research and Treatment, 2008. **110**: p. 297-307.

86. Y. Xi, et al., *Improved identification of metabolites in complex mixtures using HSQC NMR spectroscopy.* Analytica Chimica Acta, 2008. **614**: p. 127-133.

87. A.G. Palmer III, et al., *Sensitivity improvement in proton-detected two-dimensional heteronuclear correlation NMR spectroscopy.* J. Magn. Reson., 1991. **93**: p. 151-170.

88. H. Koskela, et al., *Quantitative two-dimensional HSQC experiment for high magnetic field NMR spectrometers.* Journal of Magnetic Resonance, 2010. **202**: p. 24-33.

89. A.F. Mehlkopf, et al., *Sources of t_1 noise in two-dimensional NMR.* J. Magn. Reson., 1984. **58**: p. 315-323.

90. G.A. Morris, *Systematic sources of signal irreproducibility and t1 noise in high field NMR spectrometers.* J. Magn. Reson., 1992. **100**: p. 316-328.

91. R. Baumann, et al., *Improvement of 2D NOE and 2D correlated spectra by triangular multiplication.* J. Magn. Reson., 1981. **44**: p. 76-83.

92. P. Giraudeau and S. Akoka, *Chapter Three - Fast and Ultrafast Quantitative 2D NMR: Vital Tools for Efficient Metabolomic Approaches*, in *Advances in Botanical Research*, R. Dominique, Editor. 2013, Academic Press. p. 99-158.

93. G.A.N. Gowda, et al., *Quantitative Analysis of Blood Plasma Metabolites Using Isotope Enhanced NMR Methods.* Analytical Chemistry, 2010. **82**: p. 8983-8990.

94. E. Martineau, et al., *Fast Quantitative 1H–13C Two-Dimensional NMR with Very High Precision.* Analytical Chemistry, 2013. **85**(9): p. 4777-4783.

95. P. Schanda and B. Brutscher, *Very fast two-dimensional NMR spectroscopy for real-time investigation of dynamic events in proteins on the time scale of seconds.* J. Am. Chem. Soc., 2005. **127**: p. 8014-8015.

96. A. Ross, M. Salzmann, and H. Senn, *Fast-HMQC using Ernst angle pulses: an efficient tool for screening of ligand binding to target proteins.* J-Bio NMR, 1997. **10**: p. 389-396.

97. K. Pervushin, B. Vögeli, and A. Eletsky, *Longitudinal 1H Relaxation Optimization in TROSY NMR Spectroscopy.* Journal of the American Chemical Society, 2002. **124**(43): p. 12898-12902.

98. E. Lescop, T. Kern, and B. Brutscher, *Guidelines for the use of band-selective radiofrequency pulses in hetero-nuclear NMR: Example of longitudinal-relaxation-enhanced BEST-type 1H–15N correlation experiments.* Journal of Magnetic Resonance, 2010. **203**(1): p. 190-198.

99. B. Vitorge, G. Bodenhausen, and P. Pelupessy, *Speeding up nuclear magnetic resonance spectroscopy by the use of SMAll Recovery Times – SMART NMR.* Journal of Magnetic Resonance, 2010. **207**(1): p. 149-152.

100. H.H.D.W. Freeman.R, *Phase and intensity anomalies in Fourier transform NMR* J. Magn. Reson, 1971. 4: p. 366-383.

101. H. Barkhuijsen, et al., *Retrieval of frequencies, amplitudes, damping factors, and phases from time-domain signals using a linear least-squares procedure.* J. Magn. Reson, 1985. **61**: p. 465-481.

102. P. Koehl, *Linear prediction spectral analysis of NMR data.* Progress in Nuclear Magnetic Resonance Spectroscopy, 1999. **34**(3): p. 257-299.

103. Y. Zeng, et al., *Enhanced spectral resolution in 2D NMR signal analysis using linear prediction extrapolation and apodization.* J. Magn. Reson., 1989. **89**: p. 473-483.

104. R. Brüschweiler and F. Zhang, *Covariance nuclear magnetic resonance spectroscopy.* J. Chem. Phys, 2004. **120**(11): p. 5253-5260.

105. R. Brüschweiler, *Theory of covariance nuclear magnetic resonance spectroscopy.* J. Chem. Phys., 2004. **121**(1): p. 409-414.

106. Y. Chen, et al., *Quantitative covariance NMR by regularization.* J. Biomol. NMR, 2007. **38**: p. 73-77.

107. D. Jeannerat, *Computer optimized spectral aliasing in the indirect dimension of ^{1}H-^{13}C heteronuclear 2D NMR experiments. A new algorithm and examples of applications to small molecules.* J. Magn. Reson, 2007. **186**: p. 112-122.

108. G. Bodenhausen and R.R. Ernst, *The accordion experiment, a simple approach to three-dimensional NMR spectroscopy.* Journal of Magnetic Resonance (1969), 1981. **45**(2): p. 367-373.

109. G. Bodenhausen and R.R. Ernst, *Direct determination of rate constants of slow dynamic processes by two-dimensional "accordion" spectroscopy in nuclear magnetic resonance.* Journal of the American Chemical Society, 1982. **104**(5): p. 1304-1309.

110. T. Szyperski, et al., *Reduced dimensionality in triple-resonance NMR experiments.* Journal of the American Chemical Society, 1993. **115**(20): p. 9307-9308.

111. T. Szyperski, et al., *3D 13C-15N-heteronuclear two-spin coherence spectroscopy for polypeptide backbone assignments in 13C-15N-double-labeled proteins.* Journal of Biomolecular NMR, 1993. **3**(1): p. 127-132.

112. J.C.H. Mehdi Mobli, Glenn F. King, *Fast acquisition methods in multidimensional NMR.* Biomolecular NMR spectroscopy, 2011. **3**: p. 305-337.

113. S. Kim and T. Szyperski, *GFT NMR, a New Approach To Rapidly Obtain Precise High-Dimensional NMR Spectral Information.* Journal of the American Chemical Society, 2003. **125**(5): p. 1385-1393.

114. J.C.J. Barna, et al., *Exponential sampling, an alternative method for sampling in two-dimensional NMR experiments.* J. Magn. Reson., 1987. **73**: p. 69-77.

115. B.E. Coggins, R.A. Venters, and P. Zhou, *Radial sampling for fast NMR: Concepts and practices over three decades.* Progress in Nuclear Magnetic Resonance Spectroscopy, 2010. **57**(4): p. 381-419.

116. E. Kupče and R. Freeman, *Reconstruction of the three-dimensional NMR spectrum of a protein from a set of plane projections.* Journal of Biomolecular NMR, 2003. **27**(4): p. 383-387.

117. M. Gal, *Methodological Developments in Ultrafast Multidimensional NMR for Monitoring Dynamic Biomolecular events*, in *Department of Chemical Physics*2009, Weizmann Institute of Science: Rehovot, Israel.

118. S. Sibisi, *Two-dimensional reconstructions from one-dimensional data by maximum entropy.* Nature, 1983. **301**(5896): p. 134.

119. P. Schmieder, et al., *Quantification of Maximum-Entropy Spectrum Reconstructions.* Journal of Magnetic Resonance, 1997. **125**(2): p. 332-339.

120. J.C. Hoch, *[12] Modern spectrum analysis in nuclear magnetic resonance: Alternatives to the fourier transform*, in *Methods in Enzymology*, J.O. Norman and L.J. Thomas, Editors. 1989, Academic Press. p. 216-241.

121. J.C. Hoch and A.S. Stern, *Maximum entropy reconstruction, spectrum analysis and deconvolution in multidimensional nuclear magnetic resonance*, in *Methods in Enzymology*, V.D.U.S. Thomas L. James, Editor. 2002, Academic Press. p. 159-178.

122. V. Orekhov, I. Ibraghimov, and M. Billeter, *MUNIN: A new approach to multi-dimensional NMR spectra interpretation.* Journal of Biomolecular NMR, 2001. **20**(1): p. 49-60.

123. E. Kupce and R. Freeman, *Two-dimensional Hadamard spectroscopy.* J. Magn. Reson, 2003. **162**: p. 300-310.

124. E. Kupce and R. Freeman, *Frequency-domain Hadamard spectroscopy.* J. Magn. Reson, 2003. **162**: p. 158-165.

125. L. Frydman, T. Scherf, and A. Lupulescu, *The acquisition of multidimensional NMR spectra within a single scan.* Proc. Natl. Acad. Sci. USA, 2002. **99**(25): p. 15858-15862.

126. L. Frydman, A. Lupulescu, and T. Scherf, *Principles and features of single-scan two-dimensional NMR spectroscopy.* J. Am. Chem. Soc., 2003. **125**: p. 9204-9217.

127. A. Tal and L. Frydman, *Single-scan multidimensional magnetic resonance* Prog. Nucl. Magn. Reson. Spectrosc., 2010. **57**: p. 241-292.

128. P. Mansfield, *Multi-planar image formation using NMR spin echoes.* J. Phys. C: Solid State Phys., 1977. **10**: p. 55-58.

129. L. Frydman, A. Lupulescu, and T. Scherf, *Principles and features of single-scan two-dimensional NMR spectroscopy.* J. Am. Chem. Soc., 2003. **125**(30): p. 9204-9217.

130. Y. Shrot and L. Frydman, *Ghost-peak suppression in ultrafast two-dimensional NMR spectroscopy.* J. Magn. Reson, 2003. **164**: p. 351-357.

131. Y. Shrot, A. Tal, and L. Frydman, *New developments in the spatial encoding of spin interactions for single-scan 2D NMR.* Magnetic Resonance in Chemistry, 2009. **47**(5): p. 415-422.

132. Y. Shrot, B. Shapira, and L. Frydman, *Ultrafast 2D NMR spectroscopy using a continuous spatial encoding of the spin interactions.* J. Magn. Reson, 2004. **171**: p. 163-170.

133. A. Tal, B. Shapira, and L. Frydman, *A continuous phase-modulated approach to spatial encoding in ultrafast 2D NMR spectroscopy.* J. Magn. Reson, 2005. **176**: p. 107-114.

134. N.S. Andersen and W. Köckenberger, *A simple approach for phase-modulated single-scan 2D NMR spectroscopy.* Magn. Reson. Chem., 2005. **43**: p. 791-794.

135. P. Pelupessy, *Adiabatic single scan two-dimensional NMR spectroscopy.* J. Am. Chem. Soc., 2003. **125**: p. 12345-12350.

136. T. Roussel, et al., *3D localized 2D ultrafast J-resolved magnetic resonance spectroscopy: In vitro study on a 7T imaging system.* J. Magn. Reson., 2012. **215**: p. 50-55.

137. P. Giraudeau and S. Akoka, *Resolution and sensitivity aspects of ultrafast J-resolved 2D NMR spectra.* J. Magn. Reson., 2008. **190**: p. 339-345.

138. P. Giraudeau and S. Akoka, *A new detection scheme for ultrafast J-resolved spectroscopy.* J. Magn. Reson, 2007. **186**: p. 352-357.

139. Y. Shrot and L. Frydman, *Compressed sensing and the reconstruction of ultrafast 2D NMR data: Principles and biomolecular applications* J. Magn. Reson., 2011. **209**: p. 352-358.

140. Y. Shrot and L. Frydman, *Spatial/spectral encoding of the spin interactions in ultrafast multidimensional NMR.* J. Chem. Phys., 2009. **131**: p. 224516.

141. P. Giraudeau and S. Akoka, *Sources of sensitivity losses in ultrafast 2D NMR.* J. Magn. Reson., 2008. **192**: p. 151-158.

142. P. Giraudeau and S. Akoka, *Sensitivity losses and line shape modifications due to molecular diffusion in continuous encoding ultrafast 2D NMR experiments.* J. Magn. Reson., 2008. **195**: p. 9-16.

143. Y. Shrot and L. Frydman, *The effects of molecular diffusion in ultrafast 2D NMR.* Journal of the American Chemical Society, 2008. **128**: p. 164513.

144. B. Shapira, et al., *Line shape considerations in ultrafast NMR.* J. Magn. Reson, 2004. **166**: p. 152-163.

145. P. Giraudeau, Y. Shrot, and L. Frydman, *Multiple Ultrafast, Broadband 2D NMR Spectra of Hyperpolarized Natural Products.* J. Am. Chem. Soc., 2009. **131**(39): p. 13902-13903.

146. P. Pelupessy, L. Duma, and G. Bodenhausen, *Improving resolution in single-scan 2D spectroscopy.* J. Magn. Reson., 2008. **194**(2): p. 169-174.

147. P. Giraudeau and S. Akoka, *A new gradient-controlled method for improving the spectral width of ultrafast 2D NMR experiments.* J. Magn. Reson., 2010. **205**: p. 171-176.

148. P. Giraudeau and S. Akoka, *Sensitivity and lineshape improvement in ultrafast 2D NMR by optimized apodization in the spatially encoded dimension.* Magn. Reson. Chem., 2011. **49**(6): p. 307-313.

149. L. Rouger, et al., *Limitation of Diffusion Effects in Ultrafast 2D Nuclear Magnetic Resonance by Encapsulation of Analytes in Phospholipidic Vesicles.* ChemPhysChem, 2012. **13**(18): p. 4124-4127.

150. A. Herrera, et al., *Real-Time Monitoring of Organic Reactions with Two-Dimensional Ultrafast TOCSY NMR Spectroscopy13.* Angew. Chem. Int. Ed., 2009. **48**(34): p. 6274-6277.

151. A. Herrera, et al., *2D Ultrafast HMBC : a valuable tool for monitoring organic reactions.* Org. Lett., 2010. **12**(1): p. 144-147.

152. L.H.K. Queiroz, et al., *Real-time mechanistic monitoring of an acetal hydrolysis using ultrafast 2D NMR.* Magnetic Resonance in Chemistry, 2012. **50**(7): p. 496-501.

153. L. Frydman and D. Blazina, *Ultrafast two-dimensional nuclear magnetic resonance spectroscopy of hyperpolarized solutions.* Nature Physics, 2007. **3**(6): p. 415-419.

154. B. Shapira, et al., *Real-time 2D NMR identification of analytes undergoing continuous chromatographic separation.* J. Am. Chem. Soc., 2004. **126**: p. 1262-1265.

155. L.H.K. Queiroz Junior, et al., *Real-time separation of natural products by ultrafast 2D NMR coupled to on-line HPLC.* Analyst, 2012. **137**(10): p. 2357-2361.

156. M. Nimbalkar, et al., *The Fantastic Four: A plug 'n' play set of optimal control pulses for enhancing NMR spectroscopy.* Journal of Magnetic Resonance, 2013. **228**(0): p. 16-31.

157. S. Meiboom and D. Gill, *Modified spin-echo method for measuring nuclear relaxation times.* Rev. Sci. Instrum., 1958. **29**: p. 688-691.

158. E. Tenailleau, et al., *NMR approach to the quantification of nonstatistical ^{13}C distribution in natural products: vanillin.* Anal. Chem., 2004. **76**: p. 3818-3825.

159. M. Pathan, et al., *New practical tools for the implementation and use of ultrafast 2D NMR experiments.* Magnetic Resonance in Chemistry, 2013. **51**(3): p. 168-175.

160. F.A. Mulder, et al., *Improved HSQC experiments for the observation of exchange broadened signals.* Journal of Biomolecular NMR, 1996. **8**(2): p. 223-228.

161. J.-C. Portais, *Cours de Métabolomique de Master 2*, 2007, Université Paul Sabatier, Toulouse.

162. R. Boisseau, et al., *Fast spatially-encoded 3D NMR strategies for 13C-based metabolic flux analysis.* Analytical Chemistry, 2013.

List of Illustrations

Chimie Et Interdisciplinarité
Synthèse, Analyse,
Modélisation
CEISAM
UMR CNRS 6230
UNIVERSITÉ DE NANTES

List of Tables

List of Figures

List of Scientific Production

Chimie Et Interdisciplinarité
Synthèse, Analyse,
Modélisation
CEISAM
UMR CNRS 6230
UNIVERSITÉ DE NANTES

List of Publications and Communications

Publications

- **Pathan, M.,** Akoka, S., Tea, I., Charrier, B., Giraudeau, P. "Multi-scan single shot" quantitative 2D NMR: A valuable alternative to fast conventional quantitative 2D NMR. Analyst (2011) *136, 3157-3163.*
- **Pathan, M**., Akoka, S., Giraudeau, P. "Ultrafast hetero-nuclear 2D J-resolved spectroscopy". J. Magn. Reson (2012) *214, 335-339.*
- Giraudeau, P., Cahoreau, E., Massou, S., **Pathan, M**., Akoka, S. "UFJCOSY: a fast 3D NMR method for measuring isotopic enrichments in complex samples" Chem Phys Chem (2012) *13, 3098-3101*.
- Le Guennec, A., Tea, I., Antheaume, I., Martineau, E., Charrier, B., **Pathan, M**., Akoka, S., Giraudeau, P. "Fast determination of absolute metabolite concentrations by spatially-encoded 2D NMR: application to breast cancer cell extracts" Anal. Chem (2012) *84, 10831-10837.*
- **Pathan, M**., Akoka, S., Tea, I., Charrier, B., Giraudeau, .P. "New practical tools for the implementation and use of ultrafast 2D NMR experiments". Magn. Reson in Chem (2013) *51, 3, 168-175.*
- Rouger, L, Charrier, B., **Pathan, M**., Akoka, S., Giraudeau, P. "Processing strategies to obtain clean interleaved ultrafast 2D NMR spectra" J. Magn. Reson (*Submitted*)

Oral Communications

- **Pathan M**., Akoka, S., Tea, I., Charrier, B., Giraudeau, P. Multi-scan Single Shot 2D NMR: a New Tool to Optimize Fast Quantitative Analysis. SMASH Conference, Chamonix, France, 18-21 September, 2011.
- **Pathan, M.**, Akoka, S., Giraudeau, P. Ultrafast multidimensional NMR methods for measuring isotopic enrichments in complex metabolic samples. 6èmes journées du RFMF, Nantes, France, 21-23 May, 2012.
- Giraudeau, P., Tea, I., Martineau, E., **Pathan, M**., Akoka S. Nouvelles approches en RMN 2D rapide et ultrarapide pour la quantification de metabolites. 6èmes journées du RFMF, Nantes, France, 21-23 May, 2012.
- Giraudeau, P., Cahoreau, E., Massou, S., **Pathan, M**., Portais, J.-C., Akoka, S. Fast 2D and 3D NMR tools for metabolic flux analysis in complex biological mixtures. EUROMAR conference, Dublin, Ireland, 1-5 July, 2012.
- **Pathan, M**., Mougel, J.-B., Charrier, B., Tea, I., Akoka, S., Giraudeau, P. Ultrafast NMR for dummies. SMASH conference, Providence, USA, 9-12 September, 2012.

- Giraudeau, P., Le Guennec, A., Martineau, E., **Pathan, M**., Charrier, B., Tea, I., Akoka, S. Spatially-encoded 2D NMR strategies for fast quantitative metabolomics. 54th ENC (Pacific Grove,USA).

- Tea, I., Le Guennec, A., Giraudeau, P., Tea, I., Martineau, E., **Pathan, M**., Akoka S. Spatially-encoded 2D NMR strategies for fast quantitative metabolomics. 7 journées du RFMF, Amiens, France, 10-13 June, 2013.

- Giraudeau, P., Le Guennec, A., Martineau, E., **Pathan, M**., Charrier, B., Tea, I., Akoka, S. New tools for the implementation and use of ultrafast 2D NMR, 7 journées du RFMF, Amiens, France, 10-13 June, 2013.

- Tea, I., Le Guennec, A., Giraudeau, P., Tea, I., Martineau, E., **Pathan, M**., Akoka S. Spatially-encoded 2D NMR Strategies for Fast Quantitative Metabolomics. Metabolomics Society Conference SECC, Glasgow, 1-4 July, 2013.

Posters

- Akoka, S., **Pathan, M**., Tea, I., Charrier, B., Giraudeau, P. Why slow ultrafast 2D can be more sensitive than conventional methods. GERM-GERMN Bi-national Conference, Sitges, Spain, 3-6 April 2011.

- **Pathan, M.**, Akoka, S., Tea, I., Charrier, B., Giraudeau, P. Quantitative "long ultrafast" NMR as a valuable alternative to conventional 2D NMR. EUROMAR 2011, Frankfurt, Germany, 21-25 August, 2011.

- **Pathan, M**., Akoka, S., Tea, I., Charrier, B., Giraudeau, P. Multi-scan Single Shot 2D NMR: a New Tool to Optimize Fast Quantitative Analysis. SMASH Conference, Chamonix, France, 18-21 September, 2011.

- **Pathan, M.**, Akoka, S., Giraudeau, P. Ultrafast multidimensional NMR methods for measuring isotopic enrichments in complex metabolic samples. 6èmes journées du RFMF, Nantes, France, 21-23 May, 2012.

- Giraudeau, P., Cahoreau, E., Massou, S., **Pathan, M**., Portais, J.-C., Akoka, S. Fast 2D and 3D NMR tools for metabolic flux analysis in complex biological mixtures. EUROMAR conference, Dublin, Ireland, 1-5 July, 2012.

- **Pathan, M.**, Mougel, J.-B., Charrier, B., Tea, I., Akoka, S., Giraudeau, P. Ultrafast NMR for dummies. SMASH conference, Providence, USA, 9-12 September, 2012.

- Giraudeau, P., Le Guennec, A., Martineau, E., **Pathan, M**., Charrier, B., Tea, I., Akoka, S. Spatially-encoded 2D NMR strategies for fast quantitative metabolomics. 54th ENC (Pacific Grove,USA).

- Akoka, S., Le Guennec, A., Martineau, E., **Pathan, M**., Charrier, B., Tea, I., Giraudeau, P. Fast determination of absolute metabolite concentrations by spatially-encoded 2D NMR:

application to breast cancer cell extracts. 21st annual meeting of ISMRM (Salt Lake City, USA).

- **Pathan, M**., Mougel, J.-B., Charrier, B., Tea, I., Akoka, S., Giraudeau, P. Ultrafast NMR with ease. EUROMAR 2013, Crete, Greece, 1-5 June, 2013.
- Giraudeau, P., Le Guennec, A., Martineau, E., **Pathan, M**., Charrier, B., Tea, I., Akoka, S. New tools for the implementation and use of ultrafast 2D NMR, 7 journées du RFMF, Amiens, France, 10-13 June, 2013.

Développements méthodologiques en RMN 2D ultrarapide pour l'étude de métabolismes

La RMN 2D ultrarapide (uf) est une méthodologie prometteuse permettant l'obtention de spectres RMN 2D en un seul scan. L'objectif principal de ce travail est de développer des méthodes quantitatives basées sur la RMN 2D uf, et de les appliquer à la quantification de métabolites dans des échantillons biologiques. Ainsi, en nous basant sur la RMN 2D uf, nous avons développé une stratégie multi-scan permettant de déterminer les concentrations absolues de métabolites dans des mélanges complexes, avec une précision élevée en un temps raisonnable. Les performances analytiques de cette approche sont nettement supérieures à celles de la RMN 2D conventionnelle. En particulier, les expériences ultrarapides sont mieux immunisées contre les instabilités temporelles de l'appareillage, d'où une meilleure précision. Une première application à la détermination des concentrations de métabolites dans des extraits cellulaires de cancer du sein est présentée. Une autre partie de ce travail consiste à développer et appliquer des méthodes uf pour la détermination d'enrichissements isotopiques ^{13}C site-spécifiques, dans le domaine de la fluxomique. Nous avons mis au point plusieurs méthodes ultrarapides (RMN *J*-résolue hétéronucléaire, ufJCOSY 3D) pour la mesure rapide, précise et juste de ces enrichissements. Enfin, le succès d'une méthode analytique dépend fortement de son exportabilité. Afin de faciliter son implémentation par d'autres utilisateurs, nous avons développé une interface permettant de convertir les paramètres d'acquisition RMN conventionnels (largeurs spectrales, fréquences RF) en paramètres spécifiques aux expériences ultrarapides (gradients et impulsions à fréquence variable).

Mots clé : RMN 2D, RMN ultrarapide, Métabolites, Analyse Quantitative, Enrichissements ^{13}C

Methodological developments in ultrafast 2D NMR for metabolic studies

Ultrafast (uf) 2D NMR is a very promising methodology enabling the acquisition of 2D NMR spectra in a single scan. The main goal of this work is to develop quantitative methods based on uf 2D NMR and to apply them to the quantification of metabolites in biological mixtures. Based on ultrafast 2D NMR, we developed a quantitative "Multi-Scan-Single-Shot" (M3S) strategy, capable of measuring absolute metabolite concentrations in complex mixtures with a high precision in a reasonable time. The analytical performance of this methodology appears much higher than the one of its conventional counterpart. In particular, uf experiments are more immune to hardware temporal instabilities, thus leading to a higher precision. A first application to the determination of metabolite concentrations in breast cancer cell extracts is presented. Another part of this thesis considers the application of such methods to the determination of ^{13}C site-specific enrichments in biological samples, an approach which is particularly useful in fluxomics. We have designed an ensemble of methods like uf hetero-nuclear *J*-resolved and 3D ufJCOSY for measuring specific ^{13}C-enrichments in a very fast and accurate way, by using experiments based on ultrafast 2D NMR. Finally, the success of an analytical method stands in its capacity to be applied by other researchers and users. Therefore, to make this methodology implementable and applicable by non-specialists, we developed a simple routine capable of translating the conventional NMR acquisition parameters (spectral widths, transmitter frequencies) into specific uf parameters (gradients and chirp pulse parameters).

Keywords: 2D NMR, ultrafast NMR, Metabolites, Quantitative Analysis, ^{13}C-enrichments.